DISSERTATION

DEVELOPMENT OF A CONTINUOUS FLOW ULTRASONIC HARVESTING

SYSTEM FOR MICROALGAE

Submitted by

Esteban Hincapié Gómez

Department of Mechanical Engineering

In partial fulfillment of the requirements

For the Degree of Doctor of Philosophy

Colorado State University

Fort Collins, Colorado

Fall 2014

Doctoral Committee:

    Advisor: Anthony J. Marchese

    Bryan D. Willson
    Lakshmi Prasad Dasi
    Graham Peers

ABSTRACT

DEVELOPMENT OF A CONTINUOUS FLOW ULTRASONIC HARVESTING

SYSTEM FOR MICROALGAE

Microalgae have vast potential as a sustainable source of biofuel. However, numerous

technoeconomic analyses have indicated that microalgae harvesting represents a critical

bottleneck in the microalgae value chain in terms of energy requirements, capital cost and

operating cost. This dissertation presents an approach that uses a combination of

acoustophoretic, fluid mechanical, and gravitational forces toward the development of a

continuous flow microalgae harvesting system. Ultrasonic Standing Waves have been widely

reported in the literature as an approach to manipulate particles in a fluid, a phenomena known as

acoustophoresis. These waves exert an acoustic force that agglomerate the cells in the wave

nodes or antinodes and the force is directly proportional to the cell acoustic contrast factor.

Ultrasonic microalgae harvesting is a promising low cost and low energy approach. However, a

better understanding of the acoustic properties of microalgae is essential for the development of

this technology. Accordingly, a major component of this work focused on accurately

quantifying the acoustic contrast factor of microalgae cells of *Nannochloropsis oculata*,

Nannochloropsis gaditana, Phaeodactylum tricornutum and *Chlamydomonas reinhardtii* by

measuring the average cell density and speed of sound using a vibrating tube densitometer. The

results indicate a linear correlation of *density* and *speed of sound* as a function of cell

concentration. Using this correlation, non-scattering volume average relationships were used to

compute density and speed of sound for the average algal cell. The acoustic contrast factor was estimated to be between 0.04 – 0.06 for microalgae cells in their corresponding growth media. Second, particle tracking velocimetry was used to determine the magnitude of the acoustophoretic force. In these studies, in addition to microalgae cells, polyamide seeding particles were used as a surrogate. The results obtained conclude that the maximum acoustophoretic forces are approximately 5 pN for *Chlamydomonas reinhardtii* cells and the results also show that there is change in the acoustic contrast factor from positive to negative with lipid accumulation.

This dissertation also presents a novel device for the acoustic harvesting of microalgae. The design is based on using the acoustophoretic force, acoustic transparent materials and inclined settling (Boycott effect). A filtration efficiency of 70% ± 5% and a concentration factor of 11.6 ± 2.2 were achieved at a flow rate of 25 mL · min^{-1} and an energy consumption of 3.6 ± 0.9 kWh · m^{-3}. The effects of the applied power, flow rate, inlet cell concentration and inclination were explored. It was found that the filtration efficiency of the device is proportional to the power applied. However, the filtration efficiency experienced a plateau at a 100 W · L^{-1} of power density applied. The filtration efficiency also increased with increasing inlet cell concentration and was inversely proportional to the throughput of the device as measured flow rate. It was also found that the optimum settling angle for maximum concentration factor occurred at an angle of 50° ± 5°. At these optimum conditions, the device had higher filtration efficiency in comparison to other similar devices reported in the previous literature.

ACKNOWLEDGEMENTS

DEDICATION

To my wife and my mother for their support.

TABLE OF CONTENTS

LIST OF TABLES

LIST OF FIGURES

LIST OF KEYWORDS

1. INTRODUCTION

1.1 Algae Biofuels and Bioproducts

Depletion of fossil fuels and climate change from anthropogenic greenhouse gas emissions arguably represent the first civilization-scale challenges ever faced by the human race [1,2]. Unfortunately, there is no single technological panacea for these omnipresent global challenges. Rather, these challenges can only be met by a comprehensive global energy policy that includes conservation, increased efficiency of energy conversion devices, wind energy, solar energy, biofuels, carbon sequestration, nuclear energy and responsible and strategic utilization of our finite fossil fuel reserves.

Although a myriad of technical and environmental challenges must be overcome to realize an economically viable algal biofuels industry, phototrophic microalgae are arguably the only biofuel feedstock that has the productivity required for production at a scale commensurate with global liquid fuel needs. If implemented sustainably into the global energy and food portfolio, microalgal products can reduce greenhouse gas emissions while simultaneously displacing a substantial percentage of our declining fossil fuel resources [3]. Microalgal feedstocks have several potential advantages when compared with current energy crops such as maize, sugarcane, and soybeans. These potential advantages include:

1)   Substantially higher productivity. Microalgae oil yield is between 10 to 100 times higher (gallons·acre^{-1}·year^{-1}) when compared with traditional oil crops. Thus, microalgae could be the only feedstock with the potential to displace world oil consumption [4].

2)   No direct competition with food production and the ability to grow in salt water. Some microalgae strains are able to grow in sea water, which accounts for 70% of surface area of earth. Furthermore, microalgae could potentially be cultivated in arid land using brackish water [5].

3)   Potential for carbon dioxide mitigation. Microalgae consume carbon dioxide at a ratio of 1.83 kg of CO_2 per kilogram of biomass. Thus, microalgal farms could be co-located with power plants as a means of recycling greenhouse CO_2 [6].

4)   Co-production of animal feed. Microalgae can accumulate up to 54% of dry weight as protein, with a similar amino acid profile to the Food and Agricultural Organization reference case for conventional foods [7].

1.2   Algae Dewatering

Despite the potential advantages described above, many challenges must be overcome if microalgae derived fuels are to achieve the scale required to displace a substantial percentage of fossil fuels. For example, two critical steps remain capital intensive and energy inefficient: the current cost of cultivation at scale and the need for expensive high-speed centrifuges to harvest microalgae [8]. The main results of a recent techno economic study on algal biofuels are shown in Figure 1. The authors assumed a combination of flocculation and centrifugation for the harvesting process. Figure 1 (*left*) shows the direct installed capital costs in millions of dollars excluding civil works and indicates that harvesting is the highest capital expense as a consequence of the centrifuges and settlers cost. Figure 1 (*right*) shows the gross operating costs in million dollars·yr^{-1} excluding maintenance and labor and concludes that flocculants for algae harvesting are the highest operating cost [9]. Algae dewatering, in particular, is a critical challenge that must be addressed. Because algae are typically cultivated at highly diluted concentrations (approx. 99.9% water), algae dewatering represents the most significant energy sink in the entire

microalgae to biofuels value chain. Accordingly, the development and demonstration of a scalable, low-energy, continuous-flow dewatering system such as the ultrasonic system proposed herein represents a critical need for the nascent algal biofuels industry.

Numerous lifecycle and techno-economic analyses indicate that algal biofuels are not presently economically (or energetically) favorable partly as consequence of the dewatering bottleneck described above. The waterborne algal cells are present in highly diluted concentrations ranging from 1 to 6 $g \cdot L^{-1}$ and a 100-fold concentration is required for the downstream oil extraction processes to operate effectively [10]. Microalgae cells of interest for biofuel production are very small (~ 10 microns or less) and their density is similar to water thereby imposing a challenging barrier for the use of conventional dewatering techniques. Traditional approaches for cell separation (e.g. centrifuge) are energy intensive and have high capital and operating costs [11].
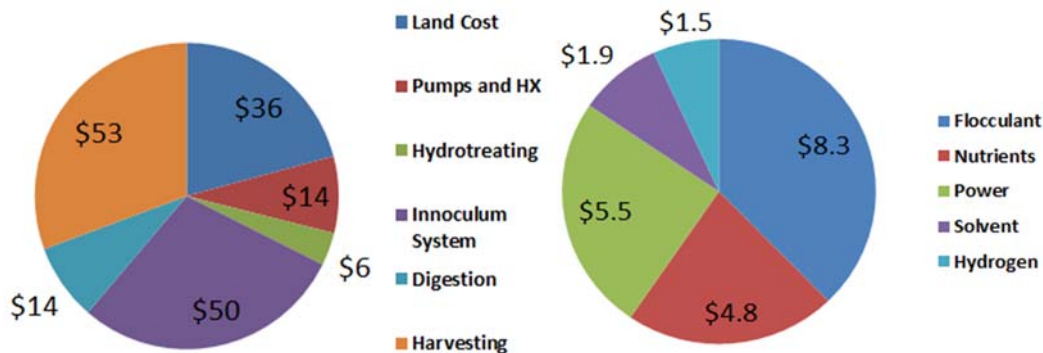
Figure 1. Installation and operating costs for a 5 billion gallon per year algae-to-biofuel plant.

Ultrasonic Standing Waves (USW) has been used in the past as a method to remove cells in suspension on a media. There are about eight different medium scale designs reported in the literature and discussed in detail in Chapter 2. Medium scale here refers to operational volumes

from 5 to 500 mL. The literature reports evenmore designs for Lab on a Chip applications where dimensions are ca. 300 microns. The use of acoustic waves for cell harvesting have the following advantages:

- Acoustic filters do not rely on centrifugal forces neither use filtration membranes, potentially yielding lower operating costs.

- Acoustic filters do not have moving parts and maintenance cost may be lower than rotative equipment such as centrifuge or belt presses.

- Acoustic filters do not require high kinetic energy or pressure, what could provide lower energy consumption per unit of volume processed.

1.3 Research Questions

This work has two major objectives. The first one is to develop a better understanding of the acoustic properties of microalgae by measuring the speed of sound and density of the cell. The second is the development of an acoustic harvester device. The main research questions are:

- What is the magnitude of the microalgae acoustic contrast factor and does it depend on the cultivation variables?

- Is it possible to create a continuous flow acoustic harvesting device?

- Could we utilize a combination of fluid mechanics drag force, gravity and acoustic force to separate algal cells?

- What would be the performance of this device under different operating conditions?

2. LITERATURE REVIEW

A disadvantage of acoustic harvesting are the lower superficial velocities required to maintain the laminar flow required for algae agglomeration as explained in the upcoming chapters. However, this issue might be offseted by understanding the different forces involved in the acoustic and flow fields. This chapter describes previous efforts in the development of acoustic harvesting devices of biological cells and also the existing state of the art regarding acoustic properties of particles.

2.1 Acoustophoresis

The nature of diluted microalgae cells in water is a benefit for the application of acoustic technologies. Water is an excellent material for the propagation of acoustic waves as indicated by its low attenuation coefficient in comparison to electromagnetic waves (Table 1). This characteristic is the main reason why acoustic waves are the preferred method for underwater communications [12].

Table 1. Attenuation for pressure and electromagnetic waves in water

Wave	Ultrasound	Electromagnetic	Light	γ ray
Attenuation	1 dB per 48 km	1 dB per 30 cm	1 dB per 10 cm	1 dB per 1.5 cm

Acoustic waves can be mathematically described by the so called "wave equation" in terms of the acoustic pressure [13]:

$$\frac{\partial^2 p}{\partial x^2} = \frac{1}{c^2}\frac{\partial^2 p}{\partial t^2} \qquad (1)$$

Here p is the acoustic pressure (Pa), x is the distance coordinate (m), c is the speed of sound (m·s⁻¹) and t is the time (s). There is a special case when a progressive wave ends in a hard termination, for example a reflecting surface. In this case, no power leaves the fluid and the wave is fully reflected creating a constructive interference. This case is called the Standing Wave.

The use of ultrasonic standing waves (USW) has been reported in the literature as an approach to manipulate particles in a fluid. A particle on suspension in the fluid becomes a scattering point for the acoustic wave. This scattering is responsible for the creation of a force on the particle [14]. The USW's exert the acoustic radiation force (F_{ac}) that collects the particles in acoustic nodes or antinodes according to the following equation:

$$F_{ac} = 4\pi R^3 k E_{ac} F \sin\langle 2kx \rangle \qquad (2)$$

where R is the radius of the cell, k the wavenumber, E_{ac} the acoustic energy density in the fluid, x the distance from a pressure node and F the acoustic contrast factor [15]. The acoustic contrast factor is defined as follows:

$$F = \frac{1}{3}\left[\frac{5\Lambda - 2}{1 + 2\Lambda} - \frac{1}{\sigma^2 \Lambda}\right] \qquad (3)$$

where Λ is the ratio of density of particle and the media ($\Lambda = \rho_p/\rho_m$) and σ is the ratio of the speed of sound in the particle and in the media ($\sigma = \rho_p/\rho_m$). This phenomenon of particle

6

migration with the sound pressure is known as acoustophoresis. Figure 2 (left) is a simulation of an acoustic wave showing the nodes (cyan) and the antinodes (red and blue). The acoustophoretic motion is simulated in the middle and right figures. Here, cells are in suspension in the middle before the acoustic wave is generated. Then the cells travel toward the nodes of the acoustic wave as a consequence of the acoustophoretic motion.
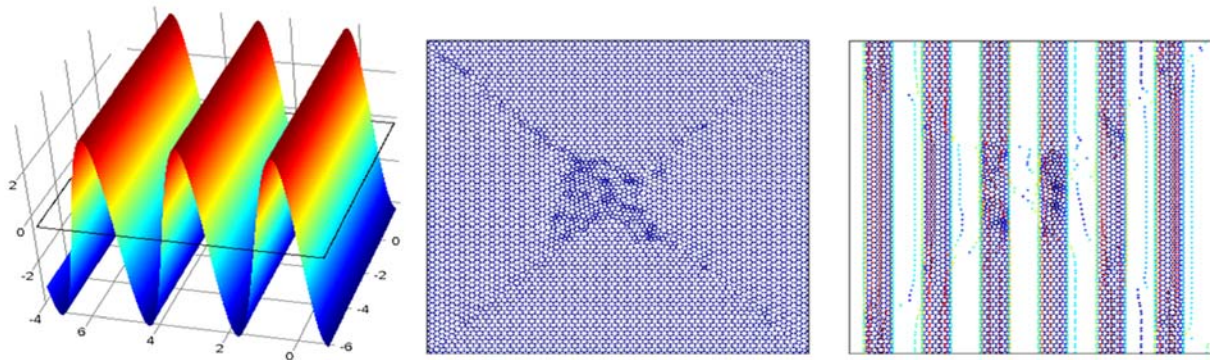
Figure 2. Simulation of an acoustic wave and the acoustophoretic motion of particles. The left graph shows the acoustic wave. The center is the particles at t=0 and right is the particles in the nodal planes after the acoustophoresis was applied.

The literature reports several attempts to concentrate different particles and cells using acoustophoresis, including: erythrocytes, lipid particles, yeast, bacteria, mammalian cells and, more recently, microalgae [16]. The main advantage is that ultrasonic filters have no complex structures which can become blocked. The filters are robust, have no moving mechanical parts and work over a wide range of conditions [17].

The literature reports that Kundt and Lehman first described the use of acoustophoresis. Such behavior of particles in ultrasound was known as "dust striations" at the time. Kundt experimented with tubes filled with spheres and was able to visualize resonance modes of acoustic waves in a famous set up known as the *Kundt tube*. However, a mathematical derivation was not published until 1934, when L.V. King presented the first acoustic force equation. King,

7

did his derivation under the assumption of an incompressible sphere under a plane standing wave (4) and a progressive wave (5):

$$\bar{P} = \pi\rho_0|A|^2\alpha^3 \sin 2kx \frac{\left\{1 + \frac{2}{3}(1 - \rho_0/\rho_1)\right\}}{2 + \rho_0/\rho_1} \tag{4}$$

$$\bar{P} = 2\pi\rho_0|A|^2\alpha^6 \sin 2kx \frac{\left\{1 + \frac{2}{9}(1 - \rho_0/\rho_1)^2\right\}}{(2 + \rho_0/\rho_1)^2} \tag{5}$$

Where $\bar{P}$ is the mean radiation pressure acting on the particle, ρ_0 and ρ_1 are the density of the medium and the particle respectively, A is the wave amplitude, $\alpha = ka$ where k is the wave number and a is the radius of the particle, and x is distance. One of the main results from King's work is that a standing wave field has a higher mean radiation pressure than a progressive wave. The former is proportional to radius of the particle to the power six while the first one is proportional to the cube of the radius.

King's equation described well the case of hard spheres such as a steel or glass under an acoustic field. However, the model was improved by K. Yosioka and Y. Kawasima to address more compressible materials such as cells, gas bubbles or oil dropplets [18]. The two authors developed a new equation that accounted for compressibility under a standing wave (6):

$$\bar{P} = 4\pi\rho_0\alpha^3 \sin 2kx \cdot F(\Lambda, \sigma) \tag{6}$$

Where F is the acoustic contrast factor, a term that averages the differences in density and speed of sound in the particle and the media:

$$F(\Lambda, \sigma) = \frac{\Lambda + [2\,(\Lambda - 1)/3]}{1 + 2\Lambda} - \frac{1}{3\Lambda\sigma^2} \qquad (7)$$

Where $\Lambda = \rho_1/\rho_0$ and $\sigma = c_1/c_0$.

The acoustic radiation force, $\boldsymbol{F}_{\mathbf{ac}}$, depends strongly on the density and the speed of sound in the particle as indicated by Equation 3. Accordingly, as described in detail in §5.4.1, a major objective of the proposed study is to accurately characterize these acoustic parameters for a variety of microalgae strains currently under consideration for large scale cultivation of biofuels and bioproducts.

2.1.1 Derivation of the primary radiation force

The velocity potential can be expressed as the sum of the incoming and scattered potentials (Barmatz & Collas, 1984), where the incoming field would be the case if the sphere was absent:

$$\Phi = \Phi_{in} + \Phi_{sc} \qquad (8)$$

Here Φ is the resulting velocity potential created by the incoming velocity potential (Φ_{in}) and the scattering velocity potential (Φ_{sc}) It is necessary to introduce the concept of the acoustic radiation stress tensor, with δ as the kronecker delta [19]:

$$S_{ij} = -\langle P - P_0\rangle\delta_{ij} - \rho_0\langle u_i u_j\rangle \qquad (9)$$

Where P is the original sound pressure and P_0 is the sound pressure at the new sound created by the scattering point. The stress tensor can be related to the velocity potential from a combination of the momentum and continuity equations by the following equation:

$$\langle P - P_0 \rangle = \frac{1}{2}\frac{\rho_0}{c_0^2}\langle \left(\frac{\partial\phi}{\partial t}\right)^2 \rangle - \frac{1}{2}\rho_0\langle |\nabla\phi|^2 \rangle \tag{10}$$

Considering that the radius of the particle is smaller than the wavelength ($R \ll \lambda$), the following expression for the time average potential can be derived [20]:

$$U^{rad} = \pi\kappa_0 a^3 p_a^2 \left[\frac{f_1}{3}\cos^2(kx) - \frac{f_2}{2}\sin^2(kx)\right] \tag{11}$$

Where κ_0 is the compressibility of the media and f_1 and f_2 are factors dependent on the compressibility of the particle and the media. Thus, the radiation force is found by differentiation:

$$F_x^{rad} = -\partial_x U^{rad} = 4\pi F(\Lambda, \sigma)ka^3 E_{ac}\sin(2kx) \tag{12}$$

2.1.2 Primary Radiation Force

The primary radiation force presented above is responsible for the longitudinal movement of the particles towards the pressure nodes or antinodes. The standing wave radiation force moves the cells into bands at or near pressure nodal planes which are separated by half the acoustic wavelength as indicated in the Equation 2. This force dominates the first few seconds

agglomerating the particles in planes [21]. This force is better understood as particle and acoustic field interaction [22].

2.1.2 Secondary Radiation Force

The secondary radiation force is a consequence of the particle-particle interaction due to localized scattering fields. This force is only relevant when the particles are separated about 4 diameters or less. However, this is also responsible for the formation of clumps that can overcome the critical radius of buoyancy [21]. The force becomes relevant when the average distance between particles significantly diminishes as a consequence of the primary radiation force. Once the particles are located in the planes they migrate to form clumps and they can trigger coagulation and sedimentation. This force is better understood as particle and particle field interaction [22].

1.3.3 Bernoulli Radiation Force

The Bernoulli radiation force is caused by non homogeneous wave propagation. As discussed before, one of the main assumptions of a standing wave is the longitudinal propagation of the wave in a small diameter cylinder. However, in real scale geometries the wave is not a one dimensional phenomenon but rather two. This force is perpendicular to the axis of wave propagation [21]. The Bernoulli or also know as Bjerknes Radiation Force is responsible for the lateral movement within the planes what forms relatively large discrete clumps [17].

2.1 Sedimentation - Ultrasonically Enhanced Settling (UES)

Enhanced sedimentation is reported in the literature as a method to effectively harvest different types of cells. The primary acoustic radiation force, the secondary radiation force and the Bernoulli force will agglomerate cells into clumps of various sizes which eventually will

11

achieve the critical radii. This concept has been successfully exploited in the development of continuous flow ultrasound enhanced sedimentation filters. The literature report designs to filter hybridoma cells and yeast [17].

Doblhoff et al. published one of the first approaches to acoustic cell separation [23]. The researchers proposed two designs of acoustic traps by using an acoustic transparent layer. The chambers are shown in Figure 3. The units were composed of a Piezoelectric Disc (PD), borosilicate or glass carrier (G), glass reflecting surface (R), Viton seals (S), laminar aperture plate (AP) and acoustic transparent layer made of 10 μm thick polyethylene foil (ATL). Both the single chamber (SC) and double chamber (DB) had an acoustic length (*l*) of 16.7 mm. The cell culture was pumped through the bottom outlet (*I*) and the exit was located in the top part of the chamber (*O*). An acoustic standing wave was generated and the culture was recirculated four times in the chamber. The pumps were stopped and a sample was taken from the top of the chamber and the efficiency calculated.
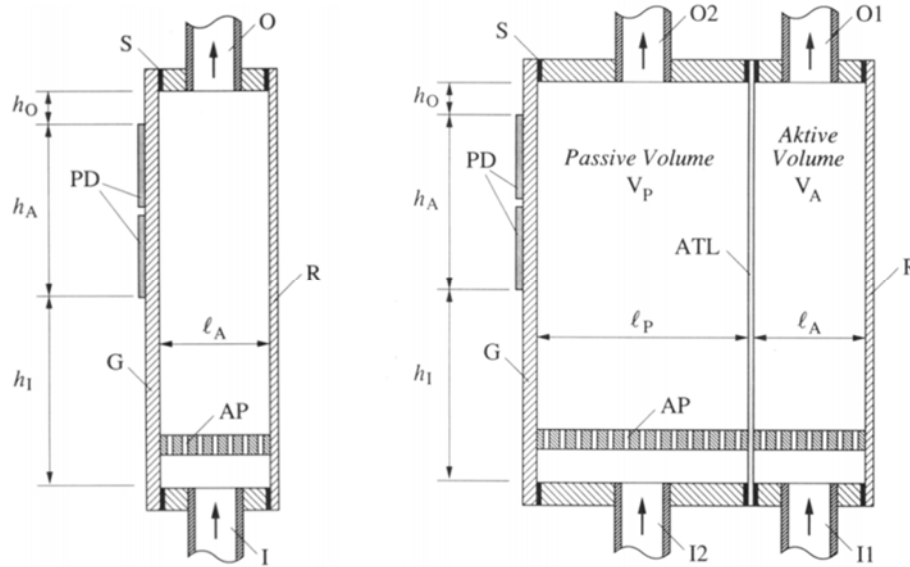
Figure 3. First generation acoustic filter with single and double chambers. The mixture of water and cells enters in the bottom. The acoustic standing wave is created in between the transducers PD. Reprinted with permission from John Wiley and Sons, Inc.

Doblhoff et al. found that the separation efficiency decreased with the power consumption for the single chamber design (Figure 4, white and black dots, with 16 mm thickness (SC1) and 32 mm thickness (SC2)). The decrease was reduced if the unit was air cooled with a fan. The researchers found that sonication causes a temperature gradient of the fluid in the flow direction. This heat input is a consequence of the resistive nature of the piezoelectric crystal. The PZT releases part of the electric energy as heat. This temperature increase causes local variations in sound velocity and thus spatial variations in the acoustic wave phase.

The inhomogeneous acoustic properties of the resonator resulted in a corresponding decrease in the resonator performance. The researchers then proposed the double chamber design where they recirculated water at a constant temperature to remove heat from the process.
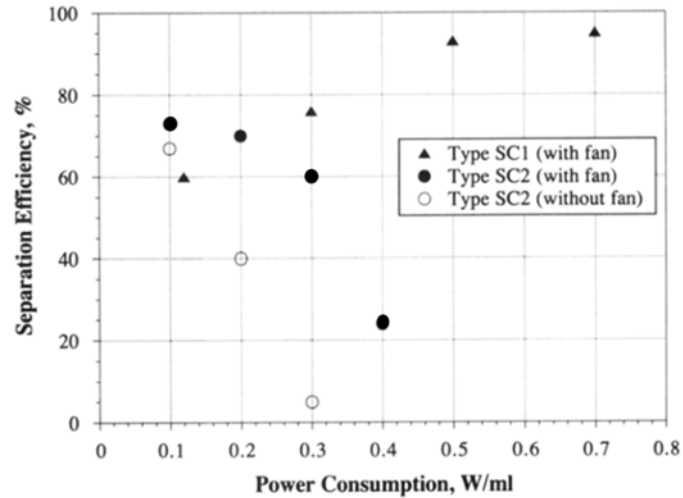
Figure 4. Separation efficiency for the single chamber design indicating the increase in separation efficiency when the cooling fan was used. Reprinted with permission from John Wiley and Sons, Inc.

Hawkes et al. improved the concept of the water cooled chamber [17]. The researchers modified the inlet and outlets of the acoustic filter. The first improvement consisted in separating the inlet from the concentrated outlet. The inlet was located in the lateral walls of the device while the outlet was located in the bottom to capture the concentrated cell clumps (Figure 5). The dark grey rectangular region represents the piezoelectric transducer. The total thickness was 3 cm. The clarified outlet remained in the top and the researchers also maintained the cooling circuit to remove the heat and make stable the acoustic field.
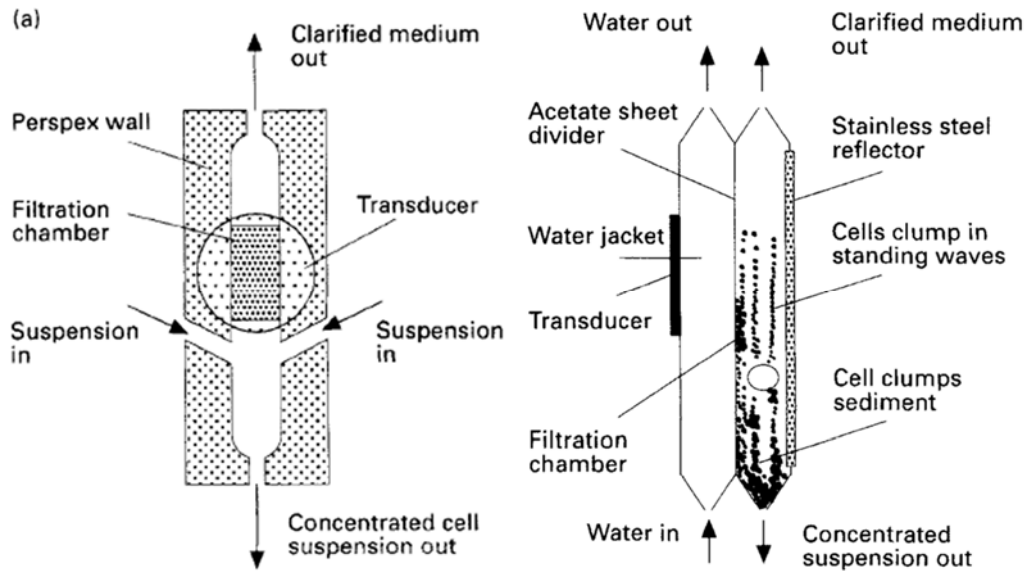
Figure 5. Front and lateral view of the ultrasound enhanced sedimentation chamber. There are different inlet, concentrated outlet and clarified outlet ports. Reprinted with permission from John Wiley and Sons, Inc.

Hawkes et al. achieved with this design a concentration efficiency of 95% for *E. Coli* and yeast operating at a frequency of 1 MHz. The cleared outlet flow rate was 4.8 mL · min^{-1} and an average superficial velocity of 0.8 mm · s^{-1}. The amplifier output voltages were between 45 and 72 Volts peak to peak (V$_{pp}$).

Bosma et al. did indeed use the algae strain *Monodus subterraneous* in a Applisens BioSep separation chamber [24]. The system is shown in Figure 6. The researchers used a statistical tool to analyze the correlation among the following five factors: biomass concentration, incoming flow rate, ratio between harvest and ingoing flow, time frequency before the field was switched off and power input. The model used data from 31 experiments and was able to predict the efficiency with an R^2 value of 0.88 indicating the validity of the analysis.
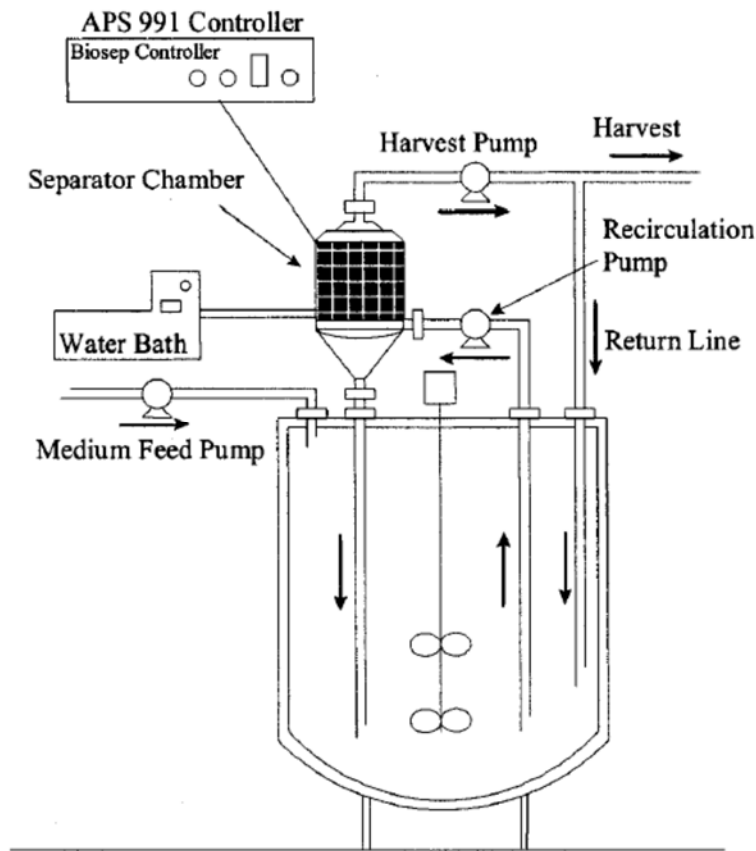
Figure 6. Schematic of the perfusion system operated in a bioreactor. Reprinted with permission from John Wiley and Sons, Inc.

2.2 Non-inertial acoustic field

Despite the advantages of enhanced sedimentation, all the previous proposed designs rely

on the density difference between the cells and the media to operate as indicated by Equation 17.

For example, if the cells of interest have exactly the same density of the media, the mentioned

designs will not work. That is the case with microalgae in which the cell density is close to

water. Therefore, the use of solely acoustic non – inertial force approach could introduce a new

separation criteria and allow more flexible designs [25]. In Figure 7, the scheme of the h-shape

resonator is introduced. On the left side the suspension is fed into the inlet I of the separator, on

the right side the upper outlet O1 is for the separated diluted media and the lower outlet O2 for

the cell concentrated suspension. In contrast to the ultrasonically enhanced sedimentation based

separators, the h-shape resonator utilizes the acoustic radiation force directly for separating the

liquid flow lines into cleared and concentrated outlets. Therefore, the direct ultrasonic separation

concept of the h-resonator is not relying on gravity [22].
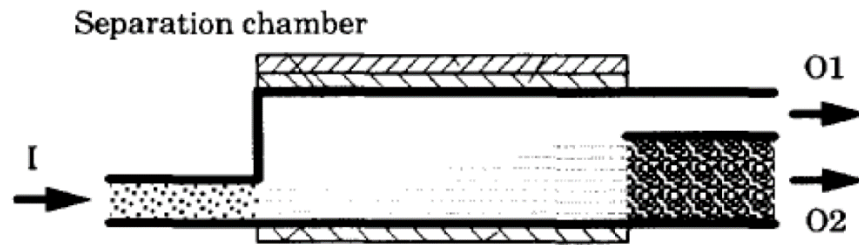
Figure 7. Scheme of the h-shape separator. The cells are trapped in the bottom half and harvested
through the bottom port. Reprinted with permission from IEEE®

Bohm et al. designed a h – shaped particle separation as indicated in Figure 8 for

microgravity conditions. The pictures compare the performance of the separator under non –

gravity and gravity conditions. The resonator had 15 cm in length with a piezoelectric driven at

2 MHz. The input power was 60 W and the cyanobacterium *Spirulina platensis* was used as the

model microorganism [26].
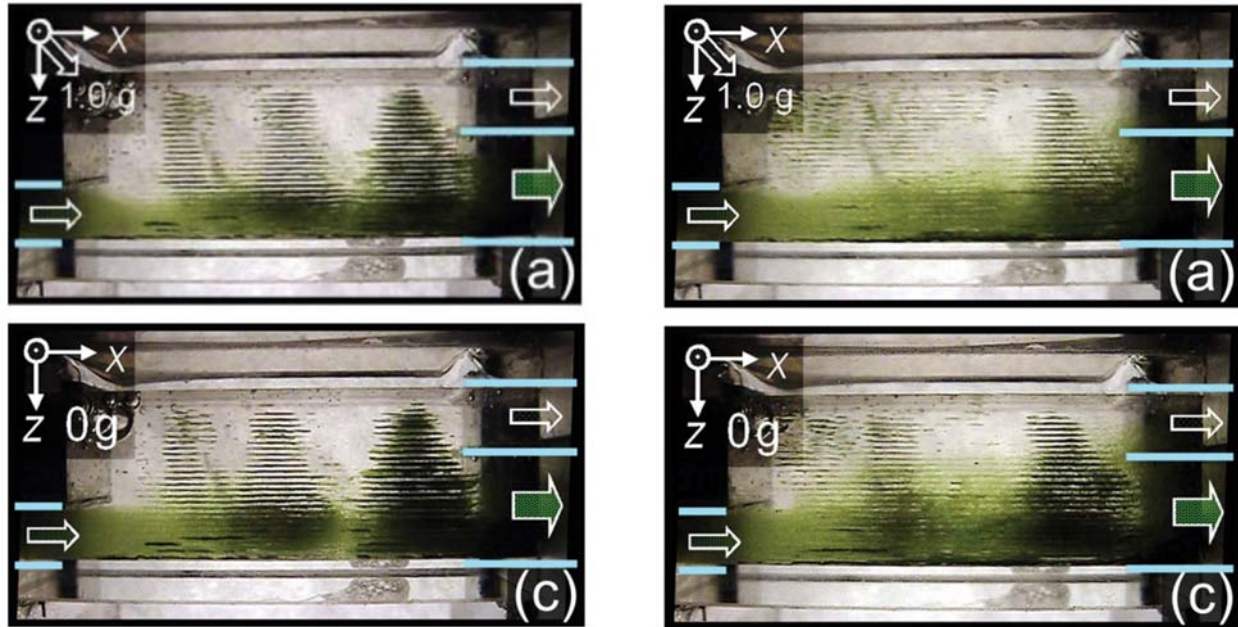
Figure 8. Pictures of the h – shaped resonator. The microalgae cells were trapped in the bottom half. Reprinted with permission from John Wiley and Sons, Inc

The researchers determined the separation efficiency for the Spirulina cells and microbeads of Polystyrene for flow rates between 0 to 90 L·d⁻¹ as indicated in Figure 9. The *S. plantesis* separation and the 5 μm behave similarly presenting a steep decrease with increasing flow rate. The separation efficiency was also determined as indicated in the figure. The cells remained attached to the walls of the separator at flat angles reducing the filtration efficiency. The best angle identified was at -45º.
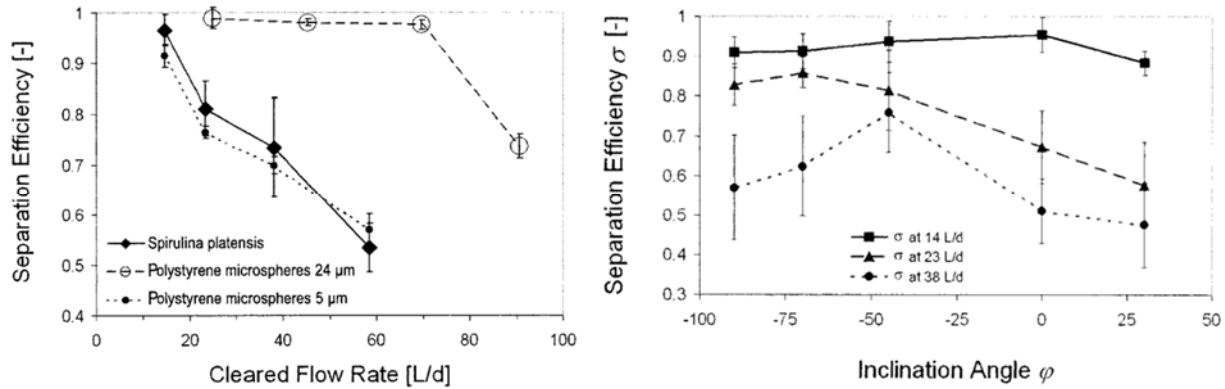
Figure 9. Efficiency results an h –shaped unit. The left figure shows the influence of the flow rate and the right figure shows the influence of the inclination angle. Reprinted with permission from John Wiley and Sons, Inc.

Other concept to separate the cells is to use the phenomena of band formation. However, the use of ultrasonic frequencies of 1 MHz or above represents an engineering challenge for direct separation of the cell bands. The aggregation planes will be separated only by half wavelength, what reduces the plane distance to the order of 0.5 mm or less. Technical obstacles, centered on the small scale of engineering required for a parallel array of narrow outlet separation channels, has limited the approach. One potential solution is the design of an expansion chamber, designed proposed by Hawkes as indicated in Figure 10. The expansion chamber was designed to increase the distance between bands where (A) is the metal reflector, (B) piezoelectric crystal and (C) the expansion chamber. The thickness of each channel is (mm): stabilization (1.1); acoustic field (1.1); expansion and observation area (8). The proposed device was successful in maintaining cell bands while increasing the separation among them. However, such a proposed configuration was only tested at small flow rates less than $0.5 \text{ L} \cdot \text{h}^{-1}$.
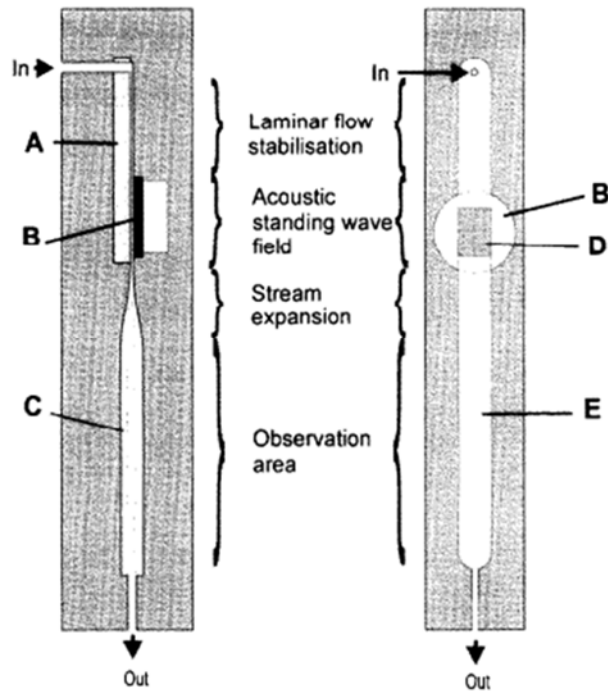
Figure 10. Scheme of expansion chamber. The expansion chamber separates the agglomeration planes to facilitate harvesting. Reprinted with permission from Elsevier

The h – shaped geometry can be also used to perform particle fractionation in the micron scale. Particles with different sizes will have different resulting acoustic radiation and drag forces. This can be used to determine different paths across an acoustic-flow field. Johnson and Feke designed a fractionating device with a flow channel of 3 mm operating at 250 kHz [27]. The authors modified the strength of the acoustic potential, flow rate and thickness what modified the sum of forces over the particles as indicated in Figure 11.
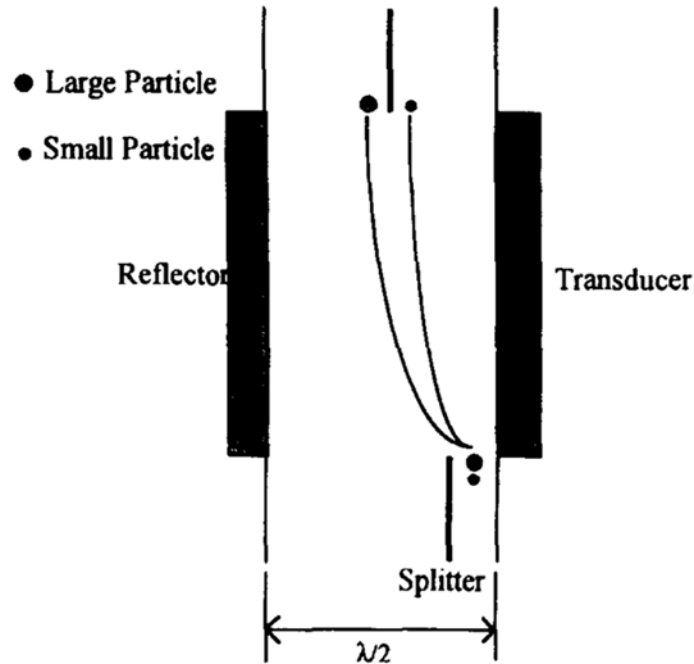
Figure 11. Fractionation unit based on cell size. This principle can be used for small scale units with a width of few wavelengths. Reprinted with permission from Elsevier

2.3 Miniature Filters

Miniature filters are becoming more popular in microfluidics applications [14]. In particular, acoustophoresis is an emerging technique since the small chambers used in this application (1 mm and less) allow for a very controlled particle movement. A predictable laminar flow regime combined with highly parallel reflecting surfaces can be achieved with different construction techniques such as PDMS interface bonding.

Nilsson et al proposed the so called "Y" shaped resonator [28]. This device was built by the use of photolithography and anisotropic wet etching producing a chamber of 750 μm wide and 250 μm deep. The cross geometry indicated in Figure 12 (a) was the first attempt but the presence of dead zones that accumulated bubbles did not provide an efficient separation. Figure 12(a) is a photograph of a 45˚structure with two band formation. Figure 12(b) shows the particles

in different resonant overtones with 2, 3 and 4 bands respectively. The authors improved the design by proposing the "Y" shape achieving a separation efficiency of 90%.

| (a) | (b) | (c) |
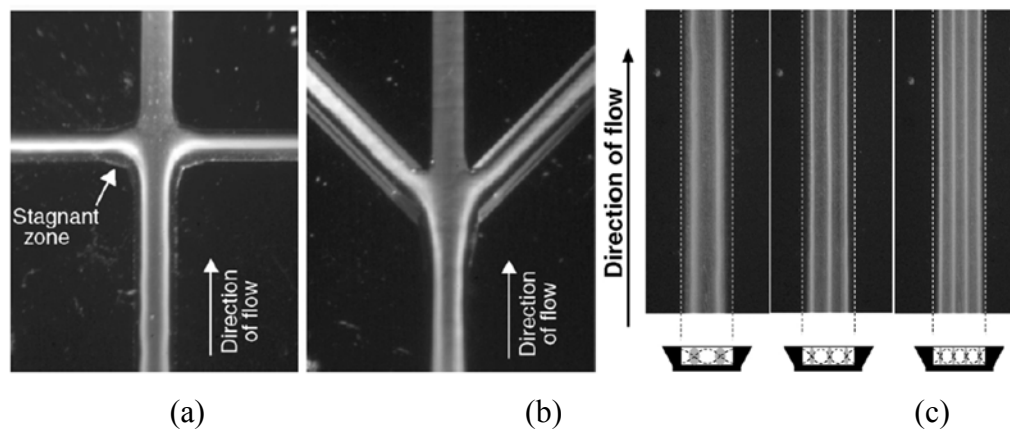
Figure 12. Cross type structure with a two band formation. The cells can be separated by a cross configuration (left) or "y" configuration (center). Different acoustic modes where use to create concentration planes. Reprinted with permission from Royal Society of Chemistry

Harris et al. explored a different geometry where two outlets were located in the same side of a 250 µm chamber [29]. The designed was based in a half wavelength standing wave that placed the band in the center of the chamber while the first outlet recovered the clarified fluid. The further outlet contained the "dirty" particle stream. The authors also established a model to determine the energy frequency product as a variation of cavity depth. The acoustic separator and its acoustic energy for different cavity depths is shown in Figure 13. A previous work has demonstrated that a good indication of actual filtration performance can be predicted by the product of the acoustic energy stored in the fluid and the driving frequency (the "energy frequency product") [30]. The peak of such a product was calculated at 240 µm for fixed thickness of the driving surface and the reflector. The researchers also calculated an energy density of 44 J·m^{-3} if the system was operated at 3 MHz.
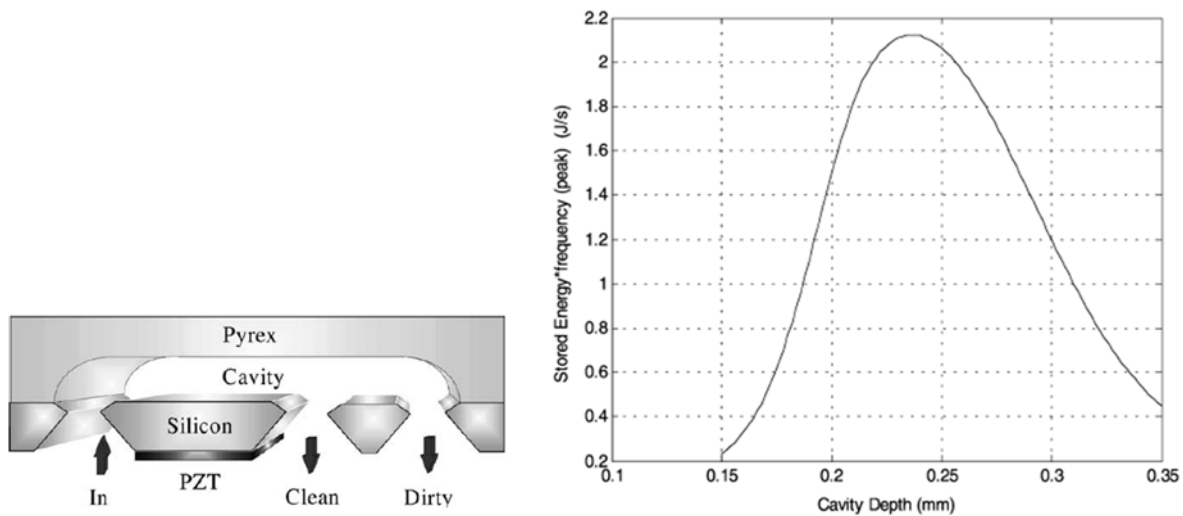
Figure 13. Acoustic separator and its acoustic energy. The depth of the device influences the acoustic energy density and frequency. Reprinted with permission from Elsevier

Hawkes et al proposed a modified "y" shape acoustic resonator for cell separation [31]. The acoustic particle filter has a thickness of half wavelength (ca. 300 µm) and the particles collect in the center of the channel while the clarified media exits through the left branch (Figure 14). Here, the authors demonstrated a correlation between stored energy and clearance of cells. There was a 20 mm long fluid stabilization length and the acoustic chamber was 40 mm. The chamber was made of stainless steel and powered by a PZ26 piezoceramic element.
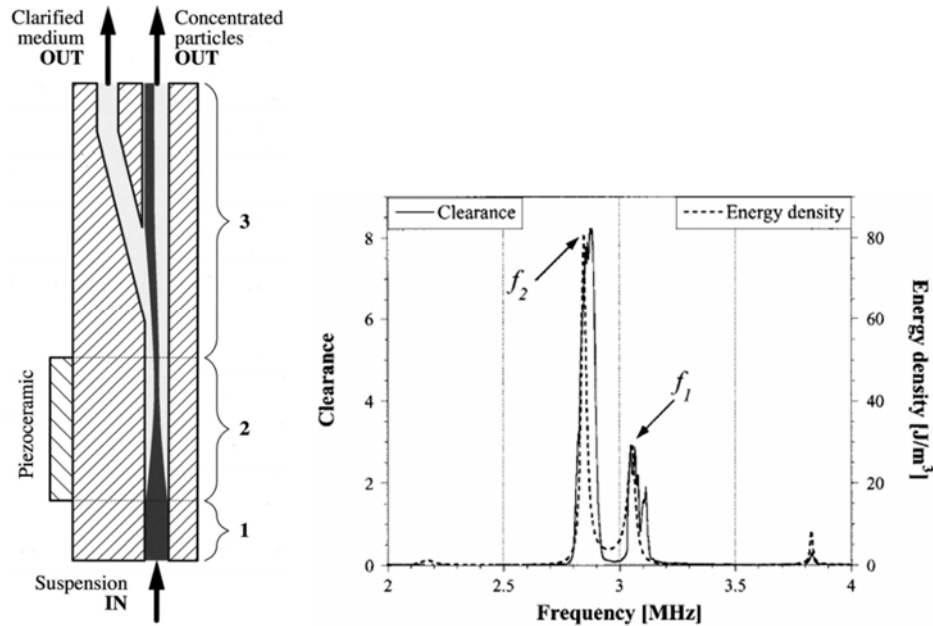
Figure 14. y - shaped acoustic filter. The results indicate the relationship of the acoustic energy density and the performance of the device. Reprinted with permission from AIP Publishing LLC

2.4 Summary of Acoustic Harvesting Designs

A summary of selected acoustic filters reported by the literature is shown in Table 2. All the considered designs have operational volumes bigger than 5 mL since the interest of this research is to scale up and industrial size system. These are the main results of this analysis:

- Inlet Flow Rate: Most of the units reported by the literature operate a relatively small flow rates ranging from 0.3 to 4 $L \cdot h^{-1}$. Gorenflo et al. designed a unit that has four chambers and operates at 10 $L \cdot h^{-1}$ for mammalian cells [32].

- The superficial velocities reported in the literature have a maximum of 2 $mm \cdot s^{-1}$. This low superficial velocity could be a consequence of low Reynolds number required for cell agglomeration.

- The units reported ranged from 7 to 50 mL. Gorenflo et al. published a design which has a chamber of 290 mL.

- Acoustic Length: The only data reported by the literature is 20 mm. The acoustic length is relevant since it impacts the attenuation of the wave and the resonance modes.

- Heat Removal is required by the first six designs. These designs are also the ones relying on enhanced sedimentation what seems to be an indication of high energy consumption.

- The reported designs have been tested with a variety of cells. Different cells have different sizes. A list of cell size from bigger to smaller is: animal cells, chinese hamster ovary, yeast, microalgae and bacteria.

- The energy density is the amount of power divide by the volume. The energy density is directly proportional to the acoustic energy density (E_{ac}) mentioned in Equation (2). The energy density is almost the same across the reported designs, ranging from 0.1 to 1 W·mL^{-1}.

- The energy consumption is highest for the devices relying on sedimentation (listed as Gaida, Bosma and Gorenflo). This might be an indication that a sedimentation approach requires more power. The h – shaped design reports the lowest energy consumption [26].

- The frequency used range from 1 – 3 MHz. This might be a consequence that at lower frequencies the cavitation threshold decreases.

Table 2. Comparison of different acoustic separation designs in the literature

Paper	Concept	Inlet Flow Rate (L/h)	Superficial Velocity (mm/s)	Volume (mL)	Heat Removal	Culture	Cell Type	Energy Density (W/mL)	Energy Consumption (Wh/L)	Efficiency (%)	Frequency (MHz)
Doblhoff et. al DC	ATL	3.25	1		One Chamber, Air Cooled	Animal Cells		0.1			
Doblhoff et. al DC	ATL	3-4	1-4		Double Chamber Water Cooled	Animal Cells		0.5			
Gaida 1996	ATL	1.5	0.25 - 1.50	50	Double Chamber Water Cooled	Animal Cells		0.3 - 1.14	19 - 30	99 - 60	
Hawkes et. al	Sonosep	0.3			Double Chamber Water Cooled	Bacteria Yeast	*E. Coli S. Cerevisae*			99	1, 3
Bosma 2003	Sonosep	0.25		7		Microalgae	*Monodus Subterraneus*	0.57	16	90	2.1
Gorenflo 2002	Sonosep 200L	10		290	VWR Refrigerated Water Bath Circulator	Chinese Hamster Ovary		0.20 - 0.31	9 or 36	95	1.4
Hawkes et al, 1998	Expansion Chamber	0.36	10	0.6		Yeast Cells					
Bohm 2002	h - Shaped	1.16			None	Microalgae	*Spirulina plantesis*		3.44	95 - 54	2.0

2.5 Emulsion Characterization: Compressibility and Speed of Sound

The dependence of the primary radiation force on the density and the speed of sound in the particle requires a better understanding of these properties for biological cells and particularly microalgae. This section describes an approach to characterize the acoustic contrast factor for different algae strains. Furthermore, this characterization could also indicate properties such as culture density and cell composition.

Several methods have been identified to characterize particle suspensions. Properties of multiphase systems are finally a relationship between the properties of each component. Some of the methods currently used to characterize suspensions are static, electrical, optical and acoustics[33]. Static measurements require a significant difference of the densities between the particle and the media while electrical measurements are based on specific properties such as conductivity and capacitance. Optical methods are based in light transmittance. Algae characterization has relied typically in optical methods being optical absorbance the main parameter. Algae suspensions are characterized by absorbance which is an indication of cell density and finally the amount of grams of biomass per liter of water. However algae cultures are not transparent and light transmission is only feasible for dilute solutions ($\varphi < 2$ g/L) [34]. Instead, ultrasound offers the potential to characterize concentrated emulsions that are up to 40% v/v [35]. Ultrasound characterization has the potential to become a rapid, reliable and applicable to real in situ growing conditions for microalgae cultivation and processing.

The concept of acoustic properties as dependent of particle concentration can be better understood in Figure 15. The properties of a compression wave propagating through particles embedded in a continuous phase is going to be an average relationship between the volume of

the particles and volume of the liquid media. When such particles are in liquid state the system is known as an emulsion while if the particles are solid is known as a suspension [36].
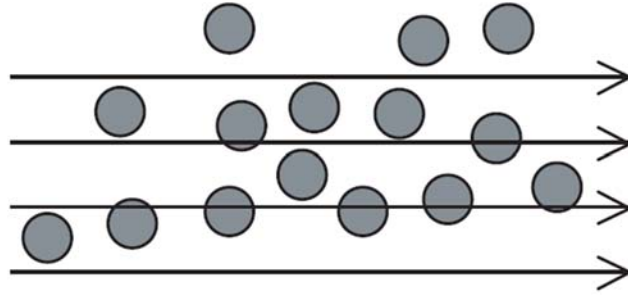
Figure 15. Propagation of a compression acoustic wave through emulsions. The acoustic waves travel through regions of media and cells. Reprinted with permission from Royal Society of Chemistry

Urick presented in 1947 two equations to describe the change of density and compressibility of emulsions and suspensions. The equations 13 and 14 are based on the assumption that the resulting speed of sound would be the ideal case of a solution of two substances or phases. Here, ρ_o and β_0 are the resulting average density and compressibility of the suspension, ρ_s and β_s are the density and compressibility of the particles, ρ_f and β_f are the density and compressibility of the liquid and φ is the volumetric concentration of particles in the emulsion.

This equation have been experimentally confirmed when the particles are smaller than the wavelength of the acoustic wave ($\alpha \ll 1$). The same principle can be also applied to Equation 15, which can be used to estimate the compressibility of cells. Urick estimated the compressibility of oil particles as well as blood cells from horses by measuring the speed of sound and density at different concentrations (Urick, 1947).

28

$$\rho_0 = \rho_S \varphi + \rho_f (1 - \varphi) \tag{13}$$

$$\beta_0 = \beta_S \varphi + \beta_f (1 - \varphi) \tag{14}$$

$$c = \frac{1}{\left(\rho_{eff} \beta_{eff}\right)^{1/2}} \tag{15}$$
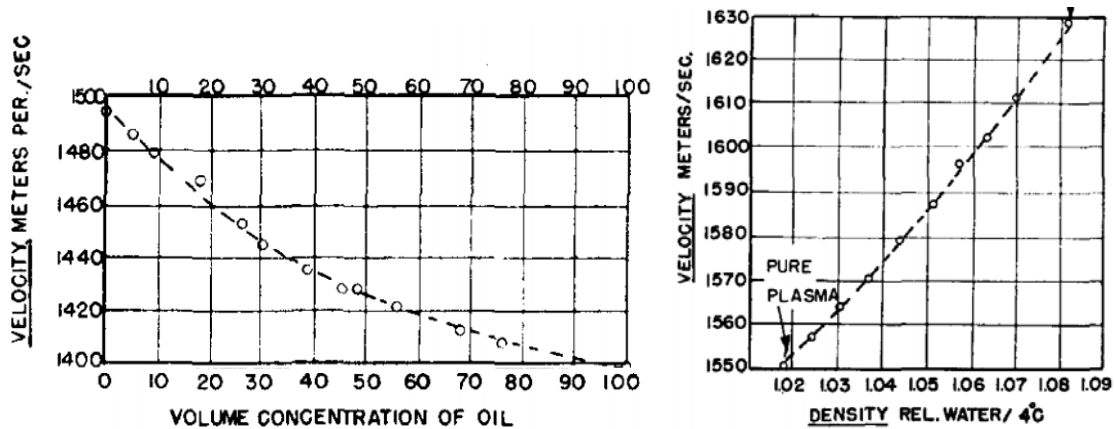
Figure 16. Change in the speed of sound for oil (left) and horse red blood cells (right) in agreement with Urick's equations. Reprinted with Permission from AIP Publishing LLC

The compressibility of a particle in a suspension under acoustic waves is shown in Figure 17. The particle is compressed and expanded by the energy of the wave. The compressional wave will compress the particle and then expand it as the energy moves away as kinetic energy of the wave. The compressibility of the particle (i.e. cell) and the media can be the equal which in case they will compress and expand at the same time. However, if the cell's compressibility is different, there will be a compressibility contrast that will create scattering and wave phase shifts in the cell vicinity [35].
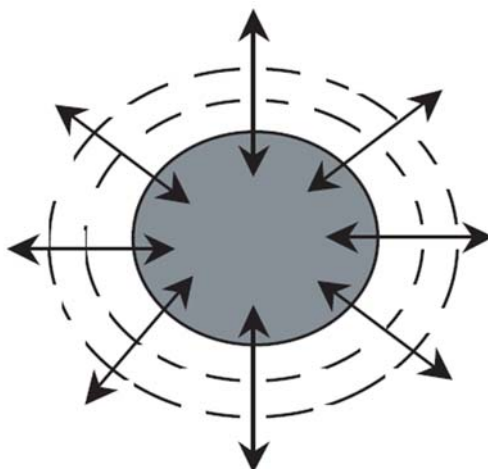
Figure 17. Particle or cell under an acoustic field. The compressibility mismatch is responsible for the acoustophoretic force. Reprinted with permission from AIP Publishing LLC

The density and speed of sound of different materials are properties intrinsically related to the structure of the molecules. Different atomic structures will influence those two parameters. The acoustic contrast factor introduced in Equation 2 will be different as indicated in Table 3. Some values of the velocity ratio and density ratio are calculated from data published in the literature [37]

Table 3. Experimental and theoretical values of velocity and density ratios

Liquid	Velocity Ratio (σ)	Density Ratio (Λ)
Paraldehyde	0.776	0.994
Hexane	0.719	0.719
Benzene	0.861	0.861
Toluene	0.862	0.862
Chlorobenzene	0.848	0.848

A previous study from 1959 did not found any concentration dependence of microalgae and the speed of sound [38]. However, the accuracy of speed of sound measurement has increased in the recent years. Tests by the researcher performed with the algal species *Nannochloropsis salina* and *Nannochloropsis oculata* found a change in the speed of sound in the culture as a function of algae concentration as indicated in Chapter 5. The cell composition influences the cell's speed of sound and density, changing the acoustic contrast factor (*F*).

2.6 Modeling of the Radiation force and resonators

The literature reports attempts in modeling the resonance of different material layers under the concept of acoustic impedance. The impedance in acoustic systems is defined by Equation 19 where p is the instantaneous excess pressure and ζ is the particle velocity. The acoustic impedance emerge as a consequence that p and ζ are not always in phase, resembling the electric impedance, potential difference and current in alternate current circuits [39].

$$z_s = \frac{p}{\xi} \tag{19}$$

Hill et *al* analyzed the peak amplitudes of a layered resonator [40]. Acoustic traps are usually composed of a piezoelectric transducer bonded to a carrier or matching layer which in turns drives a fluid layer as indicated in Figure 18 (a). The impedance of the complete system is a consequence of the thickness, speed of sound and wave number in each layer. Then, the acoustic energy as a function of voltage can be found for each frequency as indicated in Figure 18 (b). The cited work concluded that the model predicted the resonant overtone frequencies of an experimental chamber. These overtone resonances are located in between the

eigenfrequencies of the transducer. It was also found that the resonant patterns were very sensitive to changes in the geometric variables.
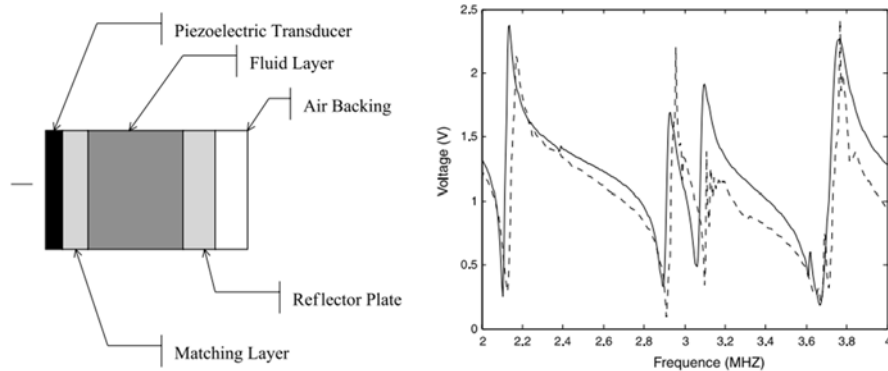
Figure 18. Cross section of a resonator and its vibrational model
Reprinted with permission from Elsevier.

2.7 State of the art in acoustic harvesting and acoustic characterization

This chapter explored previous concepts in acoustic harvesting. The first approach, using enhanced gravity settling, has been used to harvest biological cells. However, the direct opposition of the gravity force and drag force is a challenge. Currently designs are operated semi continuously to avoid the drag force problem. This design has been used successfully for small scale biological separation but could be difficult to use un the continuous flow design required for algae biofuels and bioproducts.

3. DESIGN CONSIDERATIONS FOR THE DEVELOPMENT OF A MICROALGAE ACOUSTIC HARVESTER

3.1 Introduction

Cell acoustophoresis has received increasing interest within the algae industry as an efficient, gentle and label free method to manipulate algae cells. Microalgae separation in an ultrasonic filter offers innate advantages relative to conventional methods such as membrane filtration or centrifugation. Ultrasonic harvesting is a promising and potentially low energy approach to solve the algal dewatering problem.

However the systems built thus far, as indicated in Chapter 2, have not been optimized to minimize energy consumption and have only been demonstrated 11x concentration at small scales on the order of 100 to 200 mL·h⁻¹. New designs and configurations need to be developed to maximize efficiency and enable scale up. Here we present different design iterations that were proposed and evaluated to design a novel acoustic harvester.

3.2 Designs

The h – shaped design reported by Bohm et al. has been found to have the lowest energy consumption of the available designs (Table 2). This design was replicated in order to characterize efficiency (η) and concentration dependence with inlet flow rate. This information was used to compare new designs and the h – shaped approach as explained below.

3.2.1 Characterization of a baseline design

Several translucent experimental chambers were built based in the literature review presented in §2.2. In the experiments, a signal generator was used to generate a sinusoidal wave.

The generator drove an RF wide band amplifier. The signal from the amplifier drove the piezoelectric transducer (PZT) creating the acoustic field. An oscilloscope connected to the amplifier was used to monitor the amplification of the voltage signal. The Optical Density (O.D.) was determined from aliquots at the inlet and concentrated outlet as explained in §6.2. The performance of the harvesting process was measured as a percent and compared to previous designs in the literature [41].
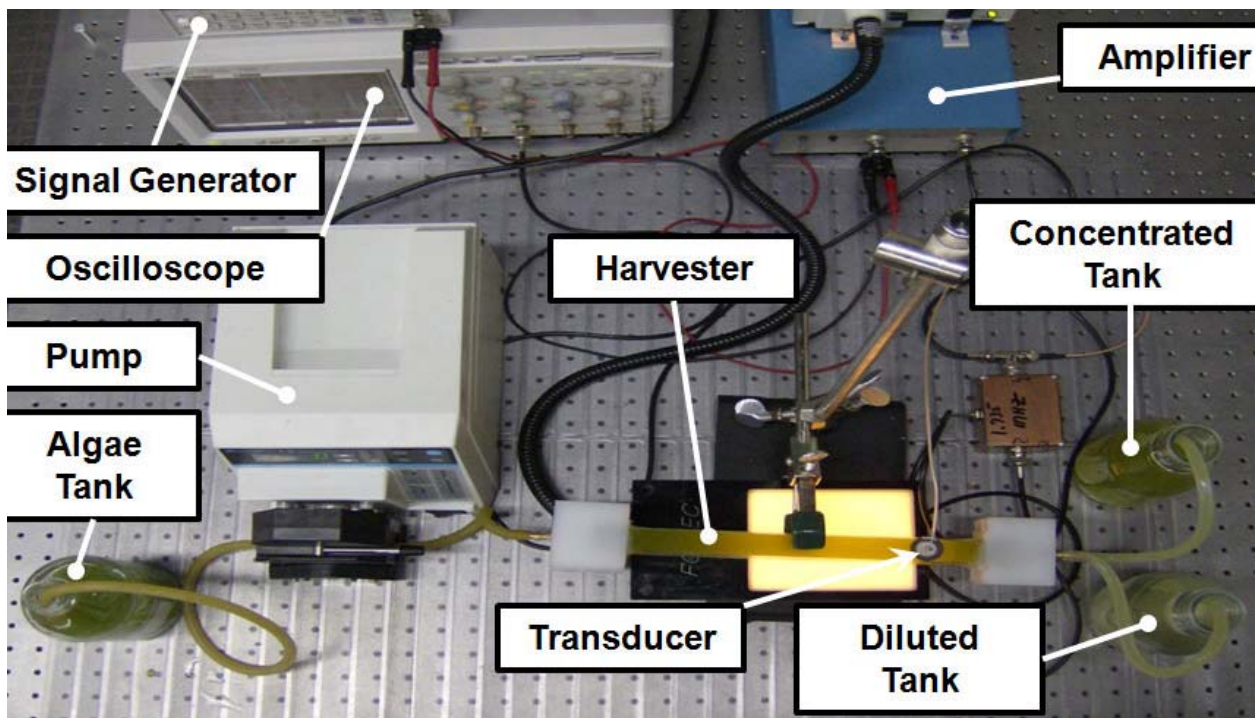
Figure 19. Acoustic set up for harvesting testing

3.2.2 Particle Surrogate

The agglomeration of microalgae cells due to the acoustic pressure is the main variable to measure the performance of the harvester. However, it was difficult to monitor the separation process because the nature of the microalgal cells with self-shading and light absorption. This

research used 5 and 20 µm polyamide seeding particles (Dantec Dynamics Inc, Holtsville, NY, USA) as a surrogate for some of the design experiments instead of using microalgae cells.

The seeding particles had different magnitudes of the acoustophoretic force. The calculated acoustic force for the microalgae (*Nannochloropsis* spp.) and polyamide particles are shown in Figure 25. The magnitude of the force is calculated using Equations 2 and 3. The radiation force acting on the 20 µm polyamide particles was 30 times higher than the radiation force acting on the microalgae cells. The radiation force acting on the 5 µm polyamide particles was doubled compared to the microalgae cells.
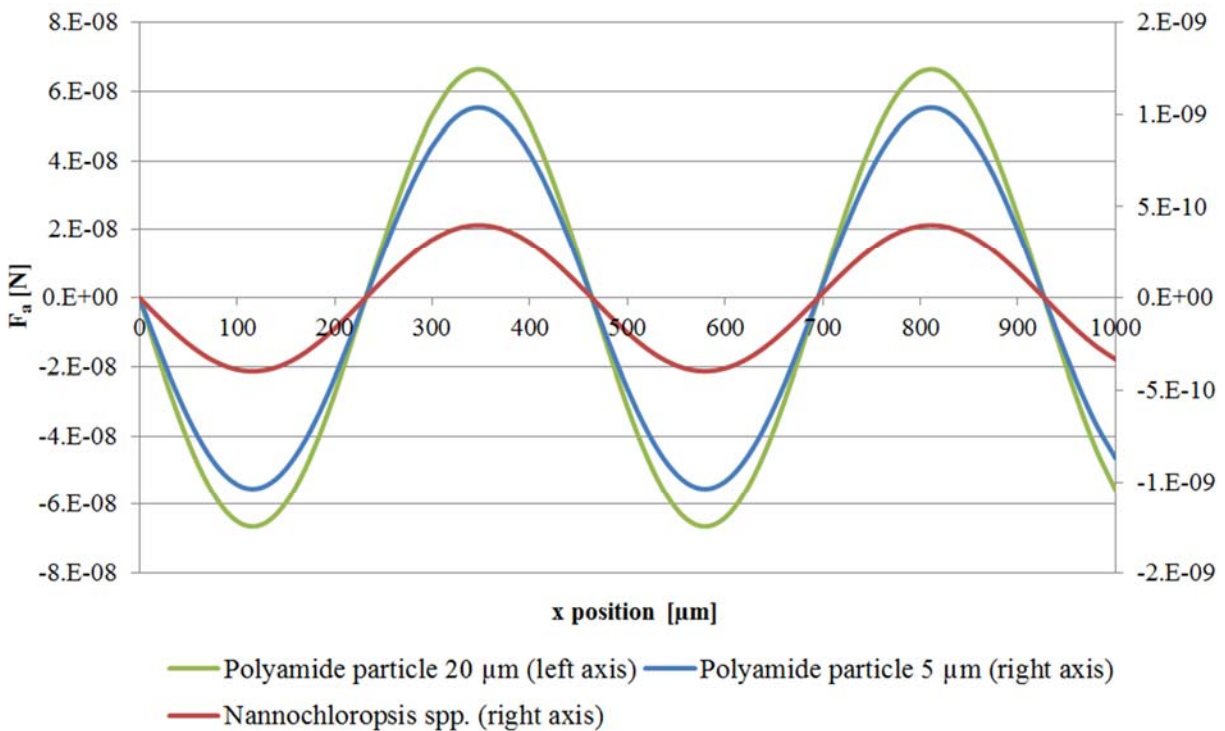
Figure 20. Calculated acoustic radiation pressure for microalgae and polyamide particles

The filtration efficiency was calculated according to the following equation [42]:

$$\eta = \left(1 - \frac{C_0}{C_i}\right) \cdot 100 \qquad\qquad (16)$$

Where C_i was the cell concentration at the entrance of the acoustic separation device and C_0 was the cell concentration of samples taken from the outlet of the resonator. The experimental technique consisted in collecting instantaneous samples of the top and bottom inlets.

3.2.3 Design Generations

- 1st generation

The "h" first generation device had one inlet and two outlets as seen in Figure 21. Algae water entered through an inlet near the bottom and the microalgae cells were trapped in the acoustic field created by the piezoelectric transducer. The geometry was designed to trap the algae in the lower portion of the device and then forced to exit through the bottom outlet. This design was based on the earlier work of Bohm et al. as shown in Figures 7 and 8.

The first generation device had a plastic separation chamber that measured one square inch in area and approximately 18 inches long. The endcaps were made of milled ultra-high molecular weight polyethylene. The chamber was fixed directly to a flat surface on the inlet and outlet endcaps. Two 1.5 MHz PZTs were placed opposite of one other on the chamber. When the first generation device was tested no separation was detected. The device also suffered from significant culture leaking from the endcaps.

It was determined that the primary reason that there was not acoustic separation was the fact that the PZTs were not creating a standing wave within the separation chamber. This was a result of the plastic chamber walls. The plastic was not transmitting the acoustic force efficiently and also the walls were not parallel to achieve the standing wave.

- 2nd generation

The second generation device was designed and manufactured using a three inch length of 10 x 30mm borosilicate glass as the separation chamber with the 30 mm side parallel to the ground. The new endcaps changed from the first generation device and were manufactured using a 3D printer. The endcaps were optimized to reduce physical size while maintaining a laminar input flow. This was done by adding a smooth entry diffuser. Instead of being permanently fixed to a flat surface like the first generation endcaps, the new endcaps were fit around the glass chamber, creating better rigidity when sealed with silicon. The new endcaps had 1/8" inch diameter holes for the inlet and outlets. This generation achieved a separation efficiency of 10% using *Nannochloropsis salina*. However the separation was a minimal and a new generation was designed.

- 3rd generation

The main changes from the second to third generation device were the ability to easily test individual properties. The new end caps had a rectangular slot extruded that fit into the glass separation chamber. A custom rubber gasket was placed between the chamber and the endcaps to prevent leakage. The device was held in place using all threaded rods and wing nuts to ensure adequate force on the gaskets to prevent leaking. This allowed different lengths of glass chambers to be easily removed and tested. However the concentration factor remained lower than 1.5x but we did notice agglomeration of algae cells in front of the acoustic field.

- 4th generation

The fourth generation device had new printed caps utilizing a water-resistant resin manufactured by stereolithography. The key differences for the fourth generation were a 90 degree rotation in orientation, meaning the plane of the PZT's was now perpendicular to the

37

horizontal plane. This change took advantage of the gravitational force of the agglomerated algae to improve the separation forces. The lip on the bottom of the extrusion that fit into the separation chamber was removed (Appendix II), allowing the algae to have a straight, undisturbed, horizontal exit rather than be forced to climb over a lip to reach the outlet which was a problem with the third generation. Multiple end caps were created to test different outlet geometries and fluid flow characteristics throughout the new device. The fourth generations of h – shaped devices are shown from left to right in Figure 21.
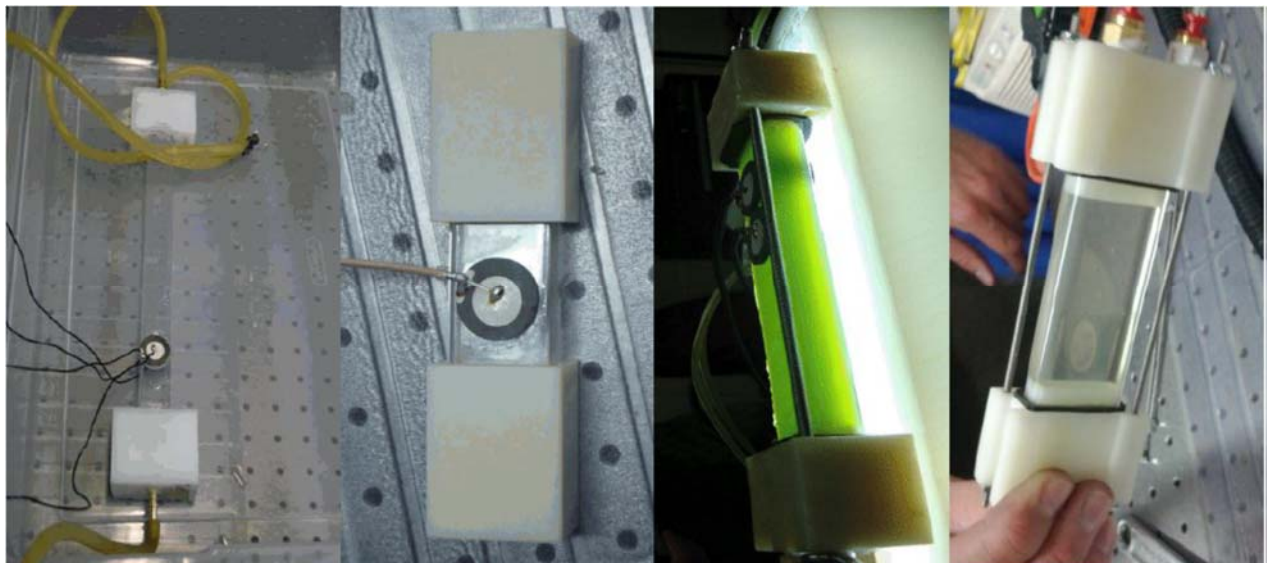
Figure 21. Photographs of different generations one (*left*) through four (*right*) of acoustic harvesters

Two types of devices were fabricated as part of the 4th generation. The generation 4th "horizontal" consisted in a horizontal oriented h – shaped flow through device as indicated in Figure 21. The body of the device connecting the inlet and outlet caps was made of a rectangular 30 x 10 mm Borosilicate tube (Glass Dynamics LLC, Vineland, NJ USA). The length of the tube was 6". The inlet cap was designed to provide a bottom discharge while the outlet cap had two outlets (upper and lower, Figure 22 right side). The aim of this approach was to trap the algae

cells in the bottom wall and force them to leave towards the bottom outlet in a similar concept as

presented in §2.2. In this design the acoustic standing wave planes were horizontal and parallel

to the XZ plane indicated in the figure. The gravity acted in the -Y axis direction.
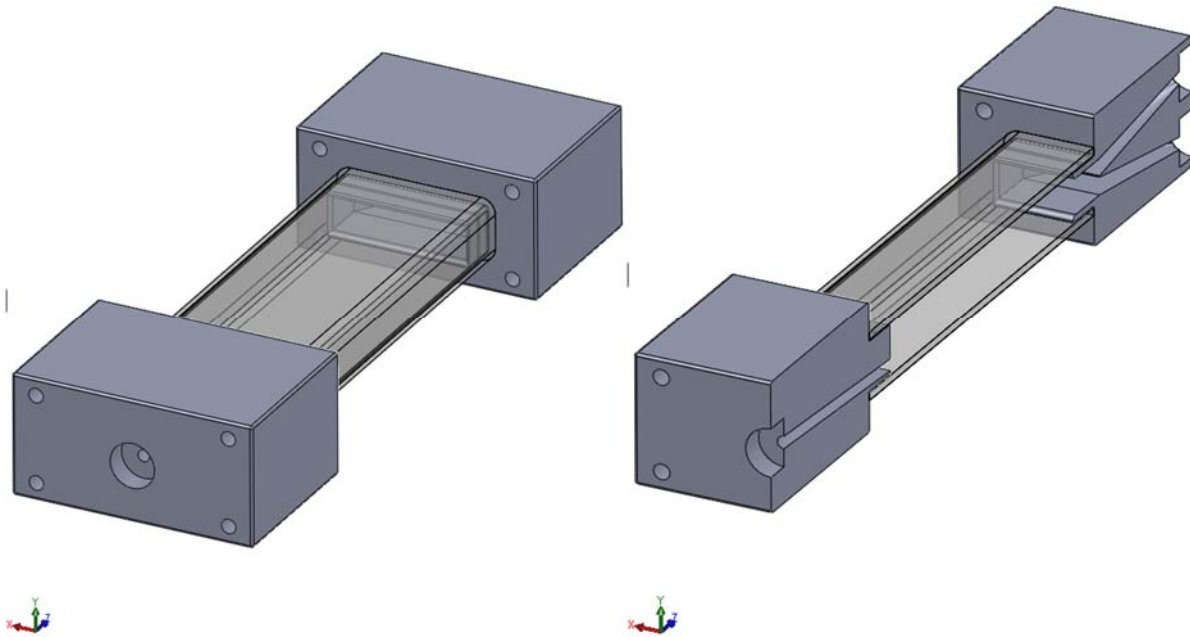
Figure 22. Fourth generation h – shaped horizontal device. The designed had one inlet and two
outlets for cleared and concentrated streams.

This horizontal approach was effective to create microalgae clumps as shown in Figure

23. So far, although bands were seen in these experiments, they were only present in the vicinity

of the piezoelectric as indicated by the Finite Element Model in the right figure. The bands

disappear in the areas far away of the piezoelectric. Because of the localized acoustic effects of

the piezoelectric, the bands were only present in few millimeters of the total length, thereby

leading to a remixing of the cells with the media as the fluid approached the downstream outlet.
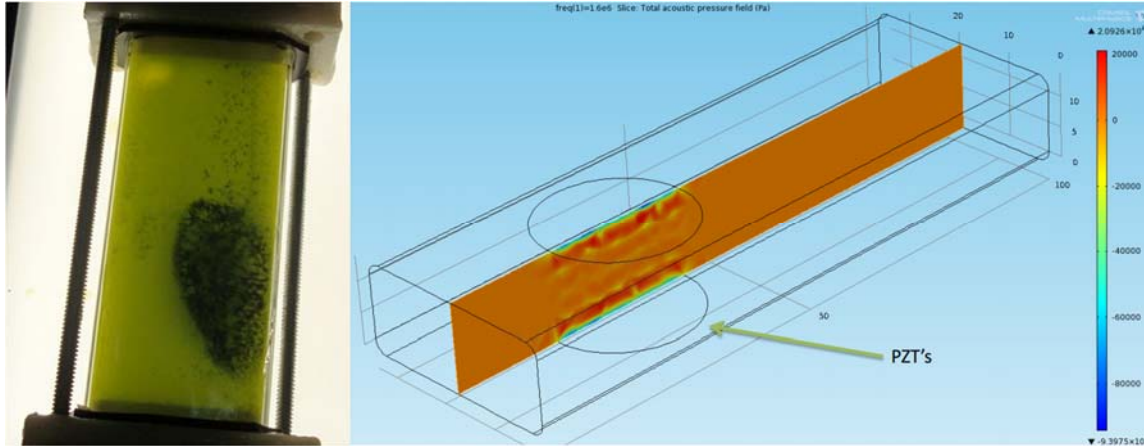
Figure 23. Horizontal h –shaped separator photograph and FEM model. Agglomeration of microalgae biomass (left) in front of the predicted acoustic field (right)

With the absence of an extended acoustic field through the tube, a new design was proposed to increase the separation between the top and bottom outlets. Here, we refer to this configuration as the 4th "vertical" design. The orientation of the device was rotated 90° as indicated in Figure 24 and 25. The acoustic standing wave planes were generated parallel to the XZ plane and the gravity was in the +X direction. Therefore the separation between both outlets was increased from 8 mm to 24 mm for the same dimensions of the borosilicate tubing.
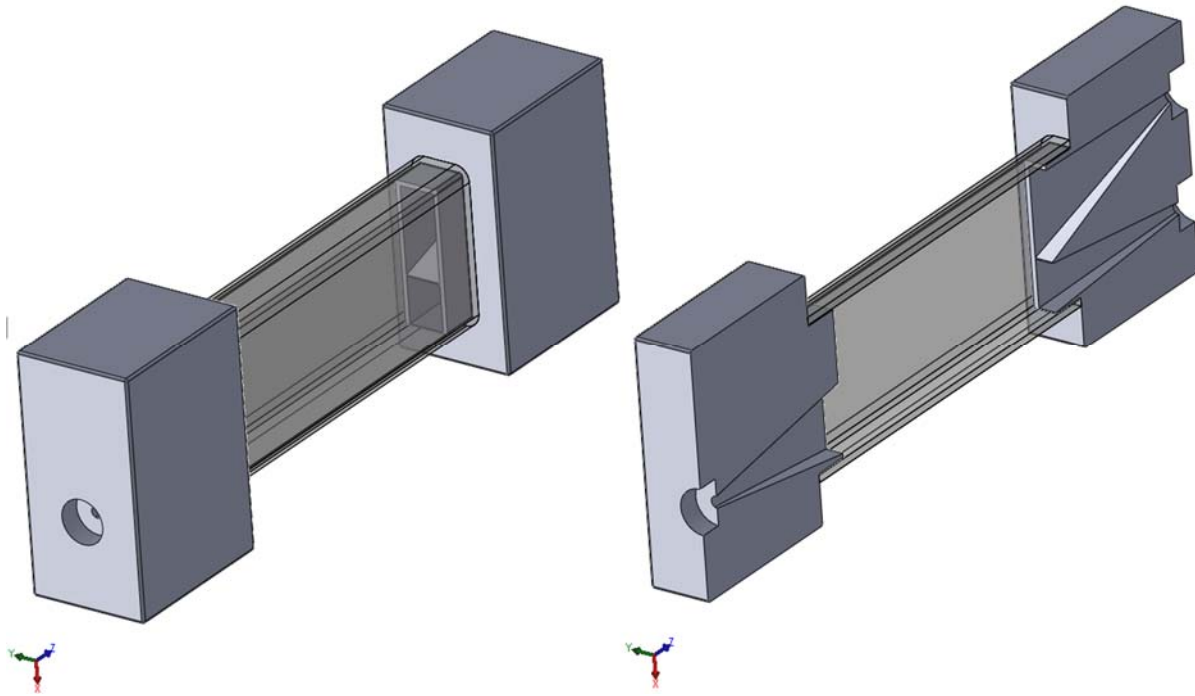
Figure 24. h – shaped vertical device. The design had a larger separation between the cleared and concentrated streams.
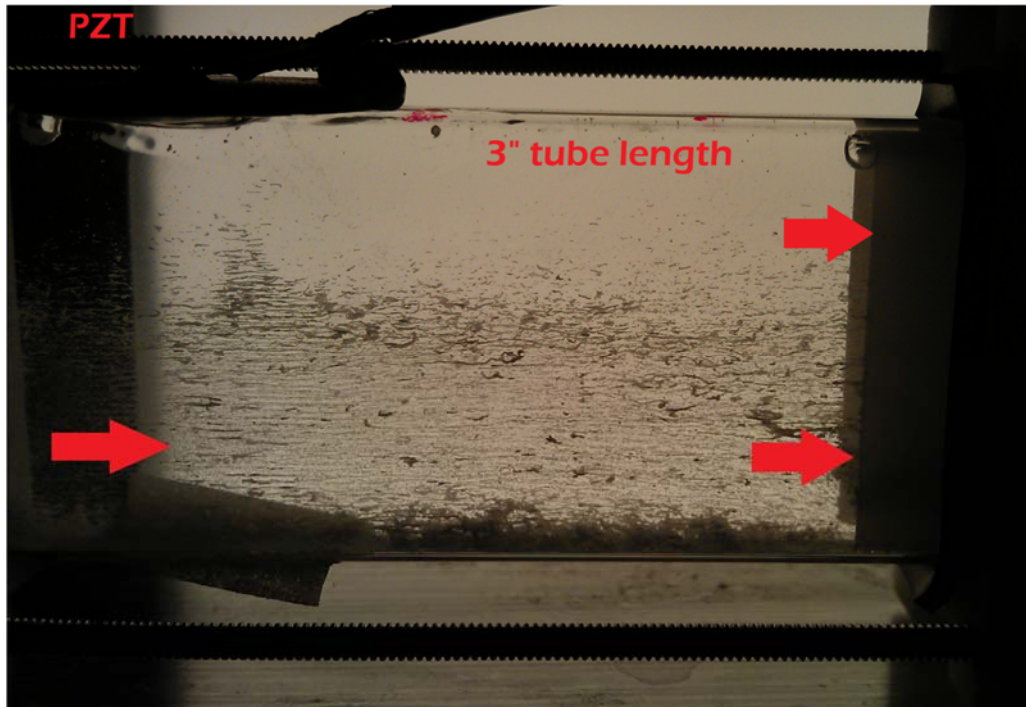
Figure 25. Separation of polyamide particles in an h – shaped vertical resonator

3.2.6 Particle Tracking Velocimetry

The gravity force was detected as critical component to enhance separation. The small magnitude of the acoustophoretic force acting on the microalgae did not create any separation and the separation efficiency was always less than 10%.

We used Particle Tracking Velocimetry (PTV) to measure the influence of the gravity force. Recent developments in PTV provide revolutionary new tools for studying particle trajectories in different applications [43]. PTV facilitates time resolved measurements of particle trajectories. Particles under and acoustic field will agglomerate and create particle clumps. The particle clumps will follow a path according to the flow regime, size and shape. It was important to characterize or predict the trajectory of the clumps.

To investigate the particle trajectories under the acoustic field, repeated recordings were performed and their *x(t)* and *y(t)* path analyzed by employing the free video analysis tool

Tracker 2.6. This software enables tracking of any particle by mouse-clicking on the particle position x and y on each movie frame, for which the time is known. The length scale was calibrated by the scaling the know size of the piezoelectric as indicated in Figure 26.
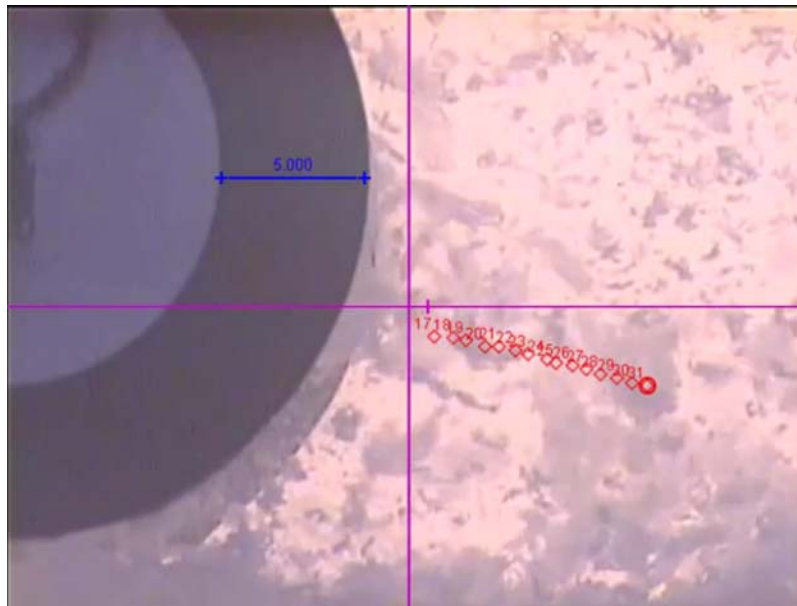
Figure 26. PTV indicating the path of a sedimentation clump

By measuring the trajectory of the agglomerated particles, we discovered that there was a pattern of trajectories as a consequence of flow rate and acoustic field. Measurements in the "h" vertical flow device containing seeding particles of 20 μm showed that three out of five particles (B, C and E) followed a negative slope ranging from -0.34 to -0.22 as indicated in Figure 26 and that settling effects could potentially increase the separation process.
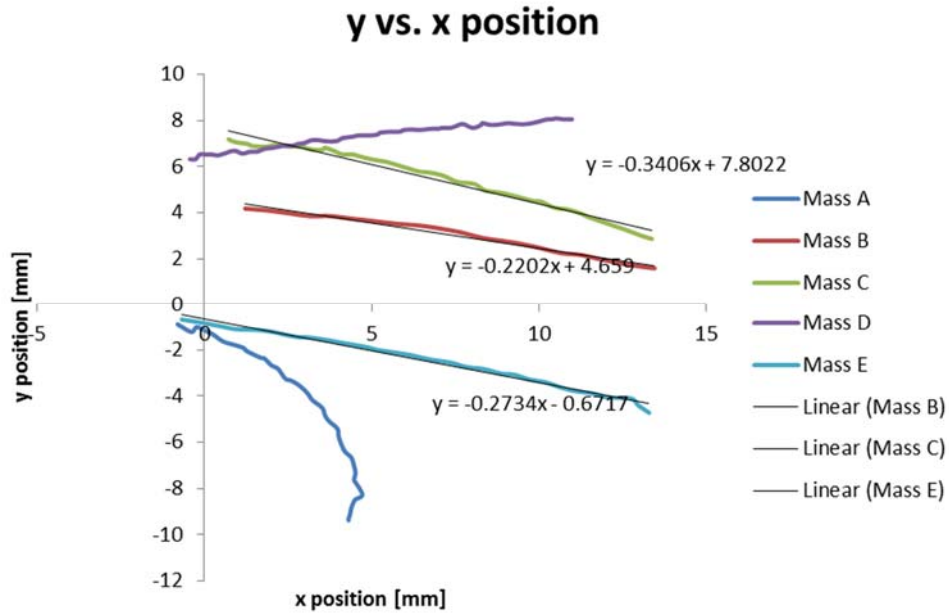
Figure 27. Particle Tracking Velocimetry of agglomerated particles indicating their sedimentation velocity (y) combined with the drag velocity (x).

- 5th generation – h Device

The new generation of the acoustic harvesting separator was a single body printed in SLA as indicated in Figure 28. Here, the advantage was an increase in the acoustic length from 10 mm to 25 mm combined with a complete utilization of the total PZT disc surface. An aluminum end plate was designed to provide the sealing with a rubber gasket between the glass and the chamber body in a sandwich configuration (Figure 29).
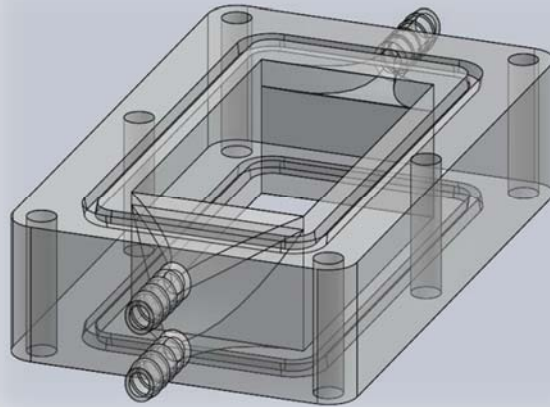
Figure 28. Transparent CAD design of the acoustic chamber

a)

b)

c)
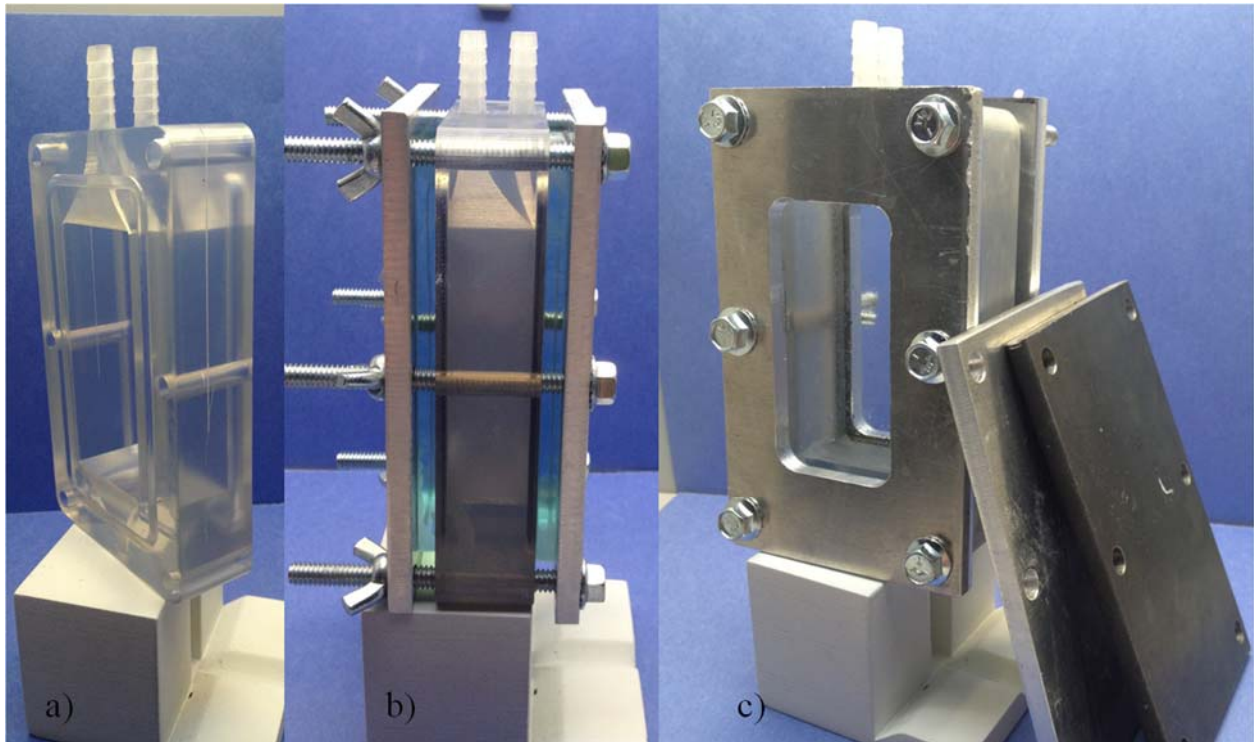
Figure 29: Photographs of the acoustic separation device

- 6th generation – Vertical

The chamber shown in Figure 26 was also designed to operate vertically as indicated in Figure 27. Here, the advantage was the use of the gravity force to create the separation of the microalgae cells from the media.
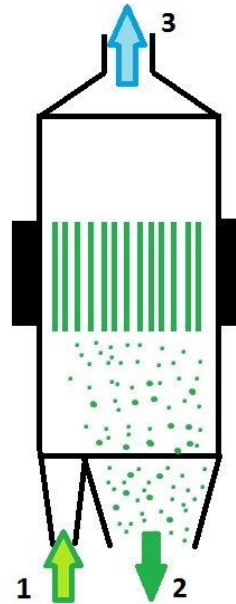
Figure 30: Gravity enhance acoustic separator

3.3 Performance analysis

The filtration efficiency results are shown in Figure 32. The results showed that the h-device did not result in a significant filtration efficiency compared to the vertical oriented design. The h-design relies solely in the acoustophoretic force to overcome the drag force. The drag force could be two to three times higher due to the low acoustic contrast factor of microalgae cells and their small diameter. Therefore, a more efficient separation device should be designed accounting for the positive effect of the gravitational force. This device is currently called an acoustic inclined settler as described in Chapter 6.
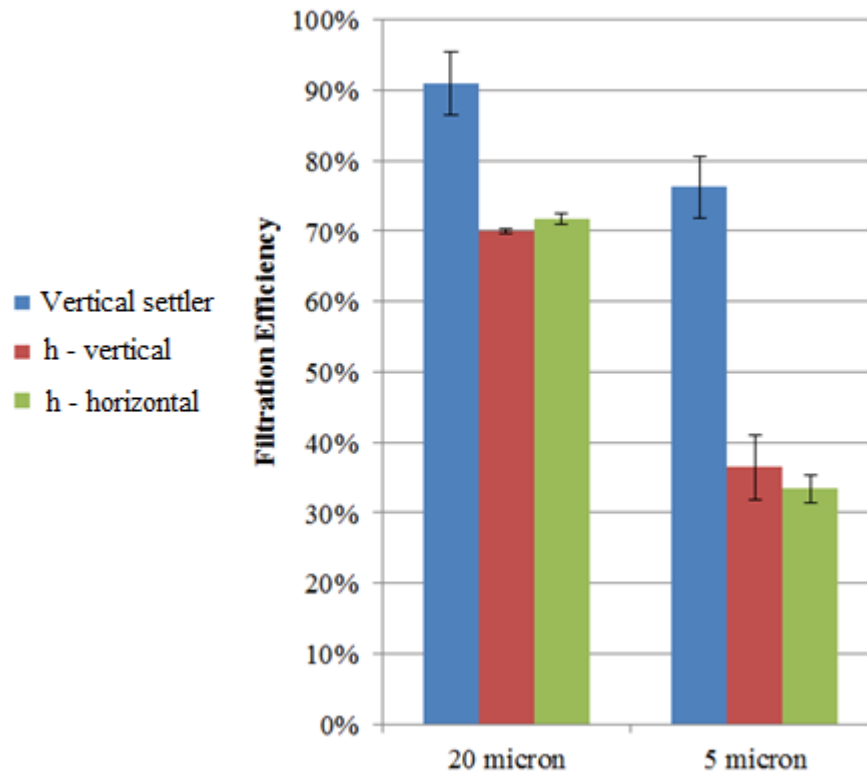
Figure 31. Performance comparison of different design concepts

4. DEVELOPMENT OF A FEEDBACK CONTROL SYSTEM FOR RESONANCE FREQUENCY TRACKING

4.1 Introduction

Particles in water can be suspended and agglomerated by being passed through acoustophoretic fields. The concentration of microalgae cells in growth media could be increased using this method of agglomeration and then harvested through a continuous flow device. In order to maximize the primary acoustic radiation force on the algae cells, acoustic standing waves must be established. The acoustophoretic force is three orders of magnitude less when a traveling wave is used instead of a standing wave. The acoustic force is also proportional to the acoustic energy density which is dependent of the chamber resonance. Therefore, it is critical to monitor and maintain a resonance condition inside the chamber to maximize the separation process. However, the resonance modes of the device change in amplitude and frequency with changes of temperature and microalgae agglomeration. Here, we present the development of a controller algorithm which can detect the optimum resonance frequency of the system and maintain it over time to increase the separation efficiency of a continuous flow acoustic separation device.

4.2 Resonance Frequencies

The magnitude of the acoustophoretic force has a strong dependency with the acoustic resonance of the ultrasonic wave in the water layer. The acoustophoretic force is also dependent on the acoustic energy density which is a function of the voltage applied to the system. Therefore

it is necessary to design and implement a frequency tracking algorithm that will continuously scan the resonance frequencies of the device and maintain the best operating frequency.

4.2.1 Changes of the resonance frequency in the water layer

The resonance frequencies of the water layer are dependent on the thickness and speed of sound inside the layer as expressed in the following equation:

$$f_n = \frac{nc}{2L} \tag{17}$$

Here f_n is the fundamental n^{th} frequency, c is the speed of sound in the media and L the thickness of the water layer or internal thickness of the separation chamber. The electric current passing through the piezoelectric transducer delivers heat to the system and increases the temperature of the water and also the speed of sound (c). This increase in the speed of sound will correlate to an increase in the fundamental frequency of the wave for the same layer thickness (L). The increase in the speed of sound changes the resonance frequency.

4.2.2 Changes in the resonance frequency of the layered resonator

The best resonance condition is achieved when the highest acoustic energy is delivered to the water layer in the device. The acoustophoretic force (F_{ac}) is proportional to the acoustic energy density (E_{ac}) as indicated in Equation 2. It has been shown that the acoustic energy density is proportional to the Voltage peak to peak (V_{pp}) squared that is applied to the piezoelectric transducer [44]:

$$E_{ac} \propto V_{pp}^2 \tag{18}$$

The voltage applied to the transducer for a specific power input is maximized when all the layers are in resonance. The acoustic separator is composed of four layers as indicated in Figure 32.
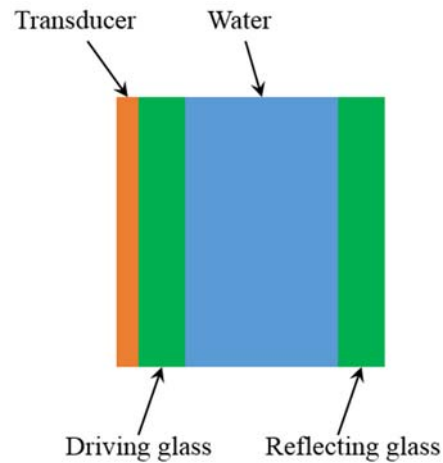
Figure 32. Layers of the acoustic resonator

Changes in the temperature of each layer affect the overall resonance of the system and therefore decrease or increase the voltage peak to peak that can be applied to the transducer for the same power used.

4.2.3 Changes in the propagation medium by microalgae accumulation

Another factor that causes the fundamental frequency to drift is the agglomeration of particles or microalgae in the acoustic field. Particles agglomerate in front of the piezoelectric transducer as shown in Figure 33. The acoustic wave is traveling perpendicular to the page plane in this figure. This is a photograph obtained through the reflecting glass of the UEIS device. This device is described in more detail in Chapter 6. Particles have a different speed of sound than water. This increase in particle density alters the speed of sound in the water layer what shifts the

resonance frequency. The agglomeration of particles also creates scattering and prevents the resonance of the wave.
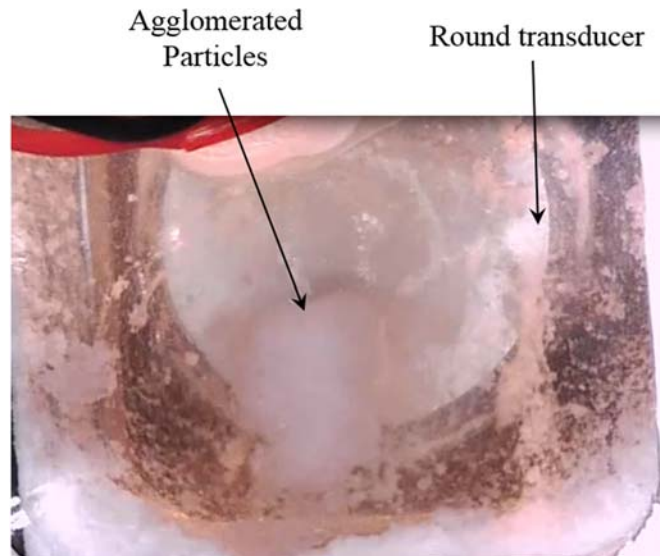
Figure 33. Agglomeration of white particles in front of the piezoelectric transducer

4.2.4 Change of the optimum operating frequency

The impact of the temperature change in the resonance modes is shown in Figure 34. The blue line indicates the voltage vs. frequency of the device at the beginning of the experiment. The voltage peaks correspond to the resonance modes of the system. The red line is the voltage frequency response after 10 minutes when a power of 0.5 W was applied continuously. The difference between the blue and red peaks represent the change in the resonance frequency and their magnitude. The acoustophoretic force is maximum when operating in the maximum voltage peak only and it quickly decreases if the device operates outside that resonance peak.
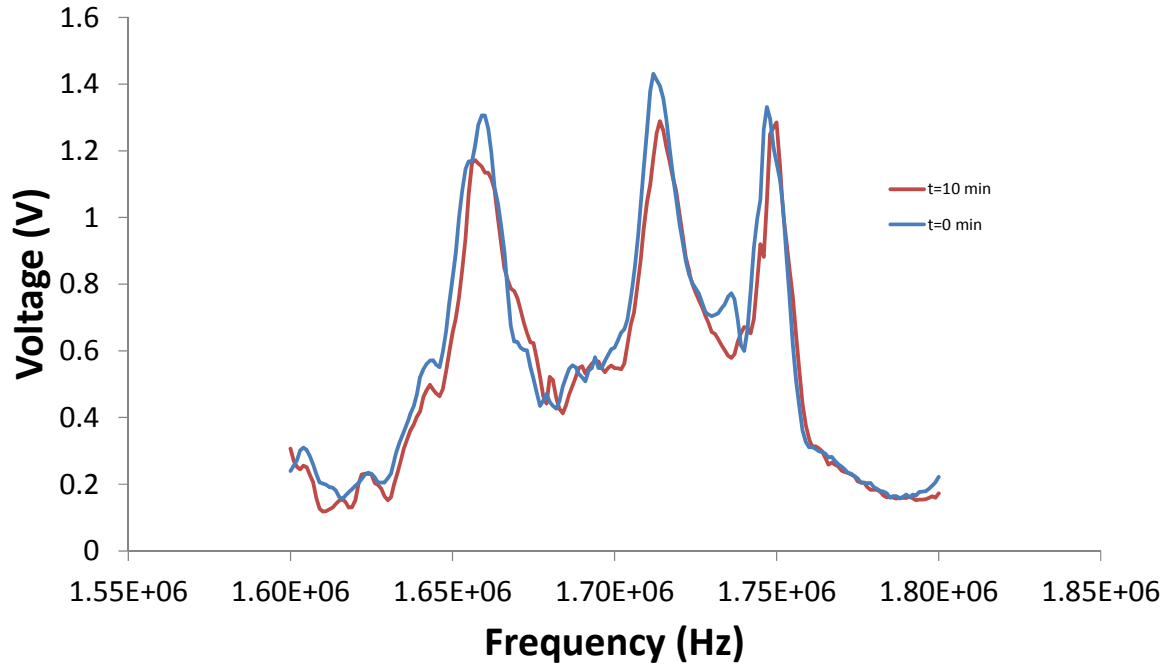
Figure 34. Shift in the resonance modes during the operation of the device

4.3 Transducer and Electronic Control

The optimum frequency for microalgae separation drifts as a consequence of temperature changes and the agglomeration of cells in front of the transducer. Therefore, it is necessary to implement a control system that monitors and maintains the best resonance condition. The proposed system is a closed loop feedback algorithm also known as a *controller*. It is possible to implement a controller by using LabView®, a new sensing transducer and an oscilloscope as indicated in Figure 35. The algorithm has a close loop by reading the voltage of the sampling transducer and using this to make adjustments to the frequency of the driving transducer.
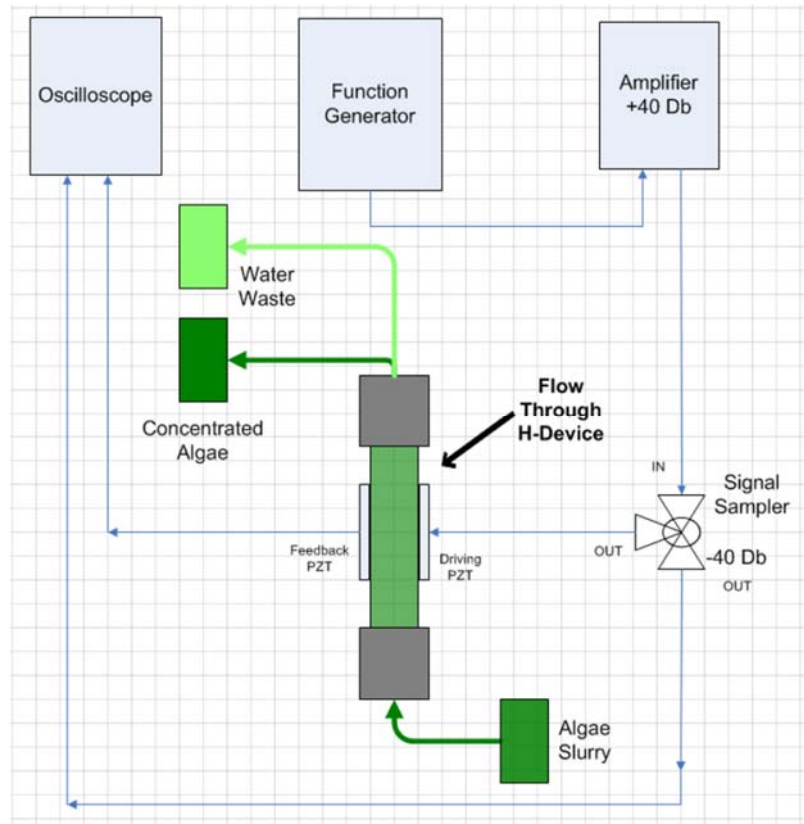
Figure 35. Schematic diagram of the frequency feedback controller

4.3.1 Controller Hardware

The computer, which is running the control algorithm through the software program Labview®, is connected to an Agilent 33120A Function Generator and a Hewlett Packard Infinitum Oscilloscope through a GPIB connection. The operating wave frequency are sent to the function generator through the GPIB from the computer. The waveform is then amplified + 40 dB through a radiofrequency power amplifier. A lead zirconate tintanate piezoceramic disc transducer is connected to the amplifier with a coaxial cable. The transducer is then connected to the acoustic separation device to generate the acoustic standing wave. Opposite to the driving piezoelectric transducer, another sensing transducer is placed, which is connected to the oscilloscope with a coaxial cable. The oscilloscope is connected through a GPIB cable to the

computer and provides frequency and voltage measurements. The main hardware of the

controller is shown in Figure 36.
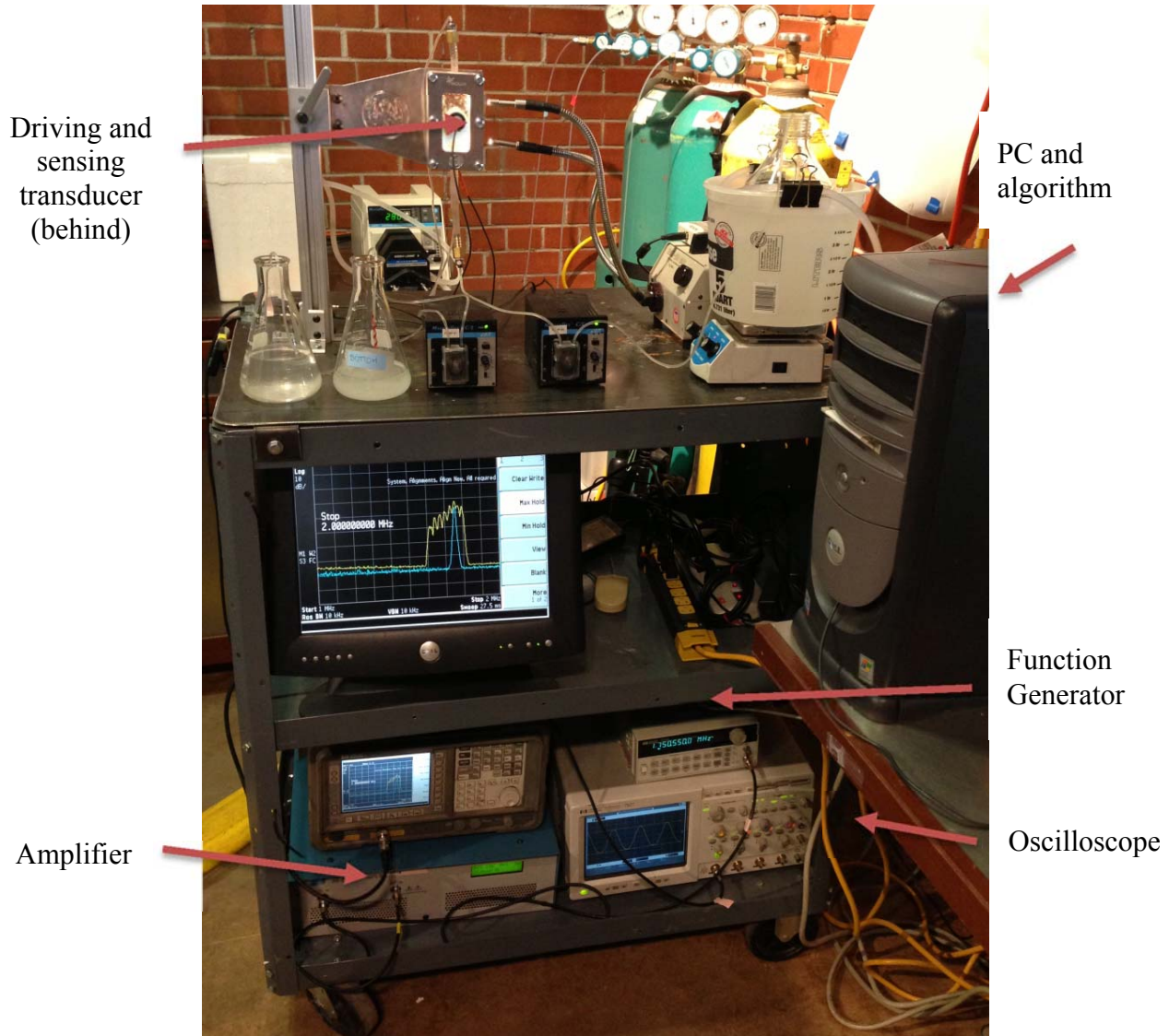
Figure 36 Function generator, radiofrequency amplifier and oscilloscope

4.4. Algorithm

To detect the best operating frequency the control loop performs a series of steps. The

resonance peaks corresponding to the highest voltages in a 1" thick water layer are spaced every

60 kHz. The system starts by performing a first frequency sweep with a frequency step of 6000

Hz. This corresponds to 10 voltage measurements between each resonance peak. The voltage is recorded for each frequency step for a frequency range selected by the user. The suggested frequency range should cover three resonance peaks that in this case is 200 kHz. The range should begin in the first thickness resonance mode of the piezoelectric transducer as explained in §6.2.4.

Each resonance frequency has different voltage magnitudes as shown in Figure 33. The best operating frequency will correspond to the highest voltage detected in the feedback transducer.

The algorithm identifies the highest voltage in the frequency range. The highest voltage will be close to the best resonance peak. However the resonance frequency could be in between the 6,000 Hz frequency step and a secondary scan is required. The second step performs a secondary fine sweep around the peak with a frequency step of 600 Hz. The frequency is finally set to the highest voltage of the system. The control loop then tracks the voltage as it decreases due to local effects of temperature and agglomeration as explained before. The unit restarts the sweeping again to find the best operational frequency if the voltage decreases below a certain threshold.

The structure of the algorithm in the LabView platform is a finite state machine. The finite state machine can only be in one state at a time and is triggered by an event or condition to switch states. A diagram of the different states of this algorithm is shown in Figure 37.
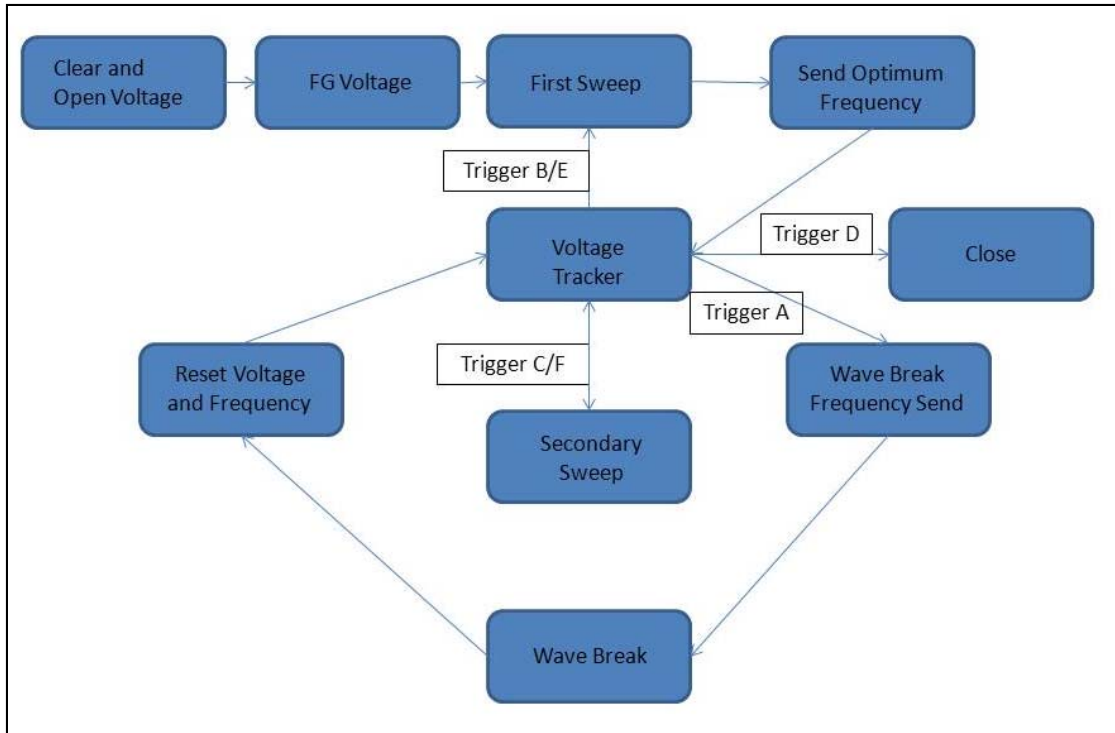
Figure 37. States of the closed control loop software. The system performs two frequency scans and monitors the feedback voltage to determine the best resonance frequency.

4.4.1 Algorithm Structure

This section describes the different states or subroutines of the algorithm. The algorithm has seven states as indicated in the figure above. The Initial state which is only active once, during a single operation of the program, is the "Clear and Open" state. In this state, all the stored information is cleared and set to zero. This state also sends a command to the oscilloscope to be prepared to return the voltage amplitude reading of the feedback amplifier. The second state is the "FG Voltage" state. This is the next step where the user specifies the voltage in millivolts that is sent to the radiofrequency amplifier.

4.4.1.1 First frequency sweep

The third state is the "First Sweep" subroutine. The algorithm performs a frequency sweep using a loop structure where the feedback voltage is captured by the oscilloscope. The

56

frequency step for this loop is defined as described previously. The oscilloscope is then requested to return a voltage reading from the feedback transducer for each frequency step. These frequency and voltage values are stored into arrays by the program. These arrays are graphed in the PC screen as this state is being executed, showing the resonance peaks of the first sweep as indicated in Figure 38.
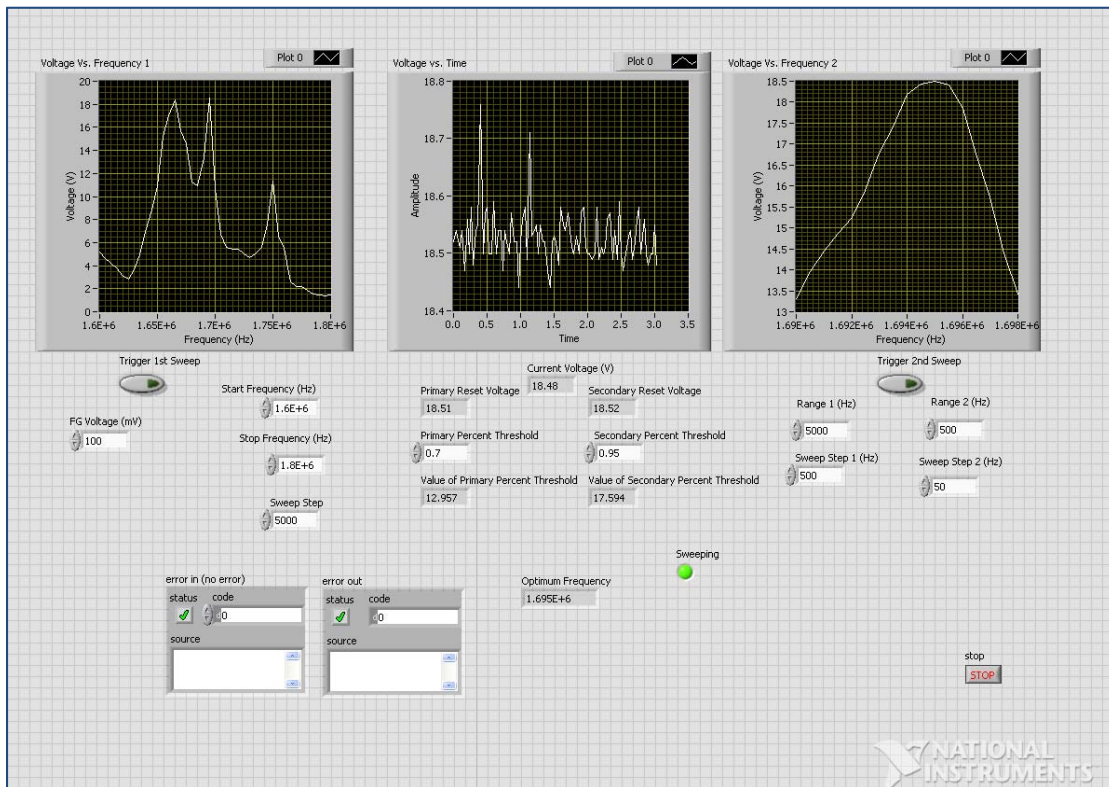
Figure 38. Screen of the frequency tracking algorithm showing the first frequency scan (left), voltage tracking (center) and second frequency scan (right)

4.4.1.2 Second Sweep

"Second Sweep" is the fine frequency sweep where the algorithm performs a fine frequency sweep with a smaller range and frequency step around the resonance peak.

4.4.1.1 Voltage tracking

The voltage tracking subroutine measures the voltage in the feedback amplifier 12 times per second. This data is graphed against the running time of the program as shown in Figure 38. This subroutine also has a threshold value defined as a percentage of the original voltage detected. The first frequency sweep stage is restarted when the voltage drops below 90%

4.5 Results

4.5.1 Effectiveness of the frequency algorithm

The benefit of the resonance tracking algorithm is shown in Figure 39. The acoustic chamber was set to one of the resonance frequencies and the feedback voltage was monitored over time. The results of the case without frequency control (beta) are plotted in blue in comparison to the case when the frequency control algorithm was used (red). The feedback voltage decreased overtime when the tracking algorithm was not used as consequence of heating and algae agglomeration in front of the PZT discs and therefore a resonance drift. The use of the algorithm maintained the resonance of the system by performing frequency sweeps that are the small steps in the graph.
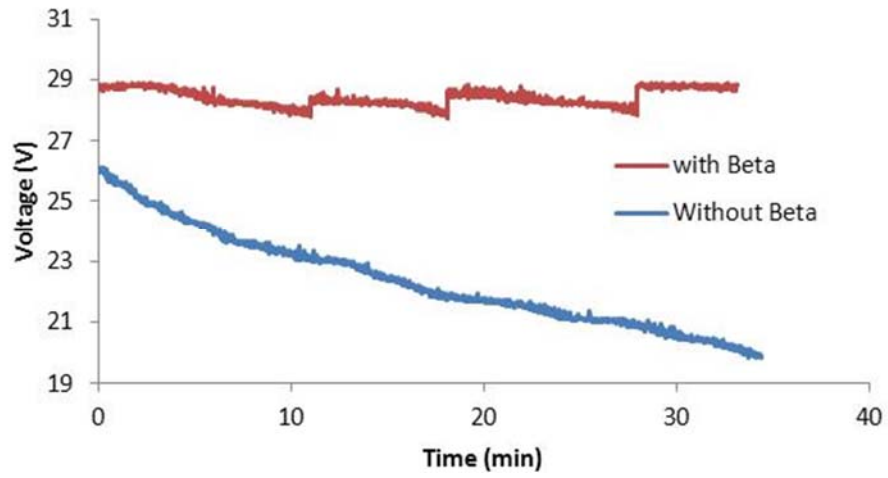
Figure 39. Feedback voltage with and without frequency control indicating the effectiveness of the resonance tracking

5. MEASUREMENT OF THE ACOUSTIC CONTRAST FACTOR OF MICROALGAL CELLS

5.1 Introduction

Acoustic harvesting could potentially be an ultralow cost technology to harvest microalgae for biofuels and bioproducts. However, the physics of acoustophoresis indicate that the acoustic force is proportional to the acoustic contrast factor of the biological cell. This acoustic contrast factor has not been studied previously for microalgae cells and, as explained below, this factor could theoretically achieve a null value canceling the acoustic force. Here we present a novel strategy to measure the acoustic factor and its measured value for some microalgae strains.

5.2 Acoustic Harvesting by USW

Ultrasonic Standing Waves (USW) can be used as a method to manipulate cells in suspension within a liquid media and this technology has already been used for concentrating various biological cells at relatively small batch volumes and/or low throughput. Baker concluded in 1972 that the USW where responsible for the agglomeration and settling of red blood cells using 1 MHz and 3 W·cm^{-2} power [45]. For example, there are numerous designs reported in the literature for concentration of cells using USW at volumes in the range of 5 to 500 mL and flow rates between 15 to 60 L · d^{-1} with different microorganisms such as *Spirulina platensis* [46]. The literature reports even more designs for Lab on a Chip applications where physical dimensions are on the order of 300 microns [47]. The use of acoustic waves for cell harvesting has the following advantages:

•   Acoustic cell harvesting systems do not rely on centrifugal forces or filtration membranes, which suggests the potential for lower operating costs.

•   Acoustic cell harvesting systems have virtually no moving parts, which suggests that maintenance cost may be lower than rotating equipment such as centrifuge or belt presses.

•   Acoustic cell harvesting does not affect the viability of the cell since the acoustic waves produce a gentle movement of the cells preserving them viable [48].

•   Acoustic cell harvesting systems do not require high kinetic energy or pressure, which suggests the potential for lower energy consumption per unit of volume of media processed.

A disadvantage of acoustic harvesting systems (particularly for continuous flow systems) is the lower superficial velocities required to maintain laminar flow required for cell agglomeration. However, this issue might be offset by improved characterization of the different forces imparted on the cells by the acoustic and flow fields. New designs and configurations need to be developed to maximize efficiency and facilitate scale up. A more complete understanding of the fundamental physics remains a core issue in the further development of acoustic separation devices in general. To achieve this fundamental objective, quantitative, high resolution, stable and reproducible measurements of acoustophoretic motion for microalgae are necessary.

5.3 Acoustophoresis

Acoustic waves can be mathematically described by the so called wave equation in terms of the acoustic pressure. There is a special case when an acoustic wave ends in a rigid boundary condition such as a reflecting surface. In this case, no power leaves the fluid and the wave is fully reflected with a 180° phase difference. This case is called a standing wave and it will double the amplitude when the interference is constructive [49]. A perfect spherical particle in suspension in this fluid becomes a scattering point for the acoustic wave as indicated in §1.3.1. This scattering,

or compressibility mismatch, is responsible for the creation of an acoustic force on the sphere [18].

The USW's exert this acoustic radiation force (F_{ac}) that collects the particles in acoustic nodes (or anti-nodes) according to the following equation:

$$\mathbf{F}_{ac} = 4\pi R^3 k E_{ac} F_{con} \sin\langle 2kx \rangle \tag{19}$$

where R is the radius of the spherical particle (μm), k the wavenumber (m^{-1}), E_{ac} the acoustic energy density in the fluid (J·m^{-3}), x the distance from a pressure node (μm) and F_{con} the acoustic contrast factor. The acoustic contrast factor is defined as follows:

$$F_{con} = \frac{1}{3}\left[\frac{5\Lambda - 2}{1 + 2\Lambda} - \frac{1}{\sigma^2\Lambda}\right] \tag{20}$$

where Λ is the ratio of density of particle and the media ($\Lambda = \rho_p/\rho_m$) and σ the ratio of the speed of sound in the particle and in the media ($\sigma = c_p/c_m$). The ratio of $1/\sigma^2\lambda$ could be replaced for the ratio of particle and media compressibility (κ_p/κ_m) since $\kappa = 1/\rho c^2$. This phenomenon of particle migration with the sound pressure is known as acoustophoresis. Possible approaches to maximize the acoustophoretic force acting on the cells according to Equation 19 are:

- *Increase of the acoustic energy density*. The energy density can be increased by improving the resonance of the geometry or increasing the power input into the separation unit as described in Chapter 4. However, there is a an upper limit of the acoustic energy where cavitation and acoustic streaming could occur, negatively affecting the separation process[50]

- *Increasing the cell size*. The diameter of the cell plays the highest impact on the acoustic force since it is cubed according to Equation 19. Therefore bigger cells will have a higher acoustophoretic force. However, cell size is small for some of the microalgae strains such as *Nannochloropsis* species (less than 3 µm), *Chlorella* spp. and *Scenedesmus* spp. (ca. 10 µm). An interesting case occurs with cells that have a cylindrical shape such as *Phaeodactylum tricornutum*. They align perpendicular to the acoustic propagation direction and their characteristic length becomes the diameter of the cylinder that is the smaller dimension of the cell.

- *Understanding and optimizing the acoustic contrast factor of the cell*. The contrast factor is a function of the cell density and speed of sound. Utilizing the acoustic separation with cells that have a high contrast factor or are in a stage that maximizes the contrast factor will increase the separation efficiency and reduce the energy consumption.

A time sequence of a proof-of-concept test performed by our research group using the microalgae strain *Nannochloropsis salina* is shown in Figure 40. The photograph shows the band formation for the microalgae cells at 0, 4 and 10 seconds after the acoustic field is applied. The *N. salina* culture was subjected to an ultrasonic standing wave applied to a quartz cuvette via a piezoelectric disc transducer vibrating at a frequency of 1.7 MHz and amplitude of 10 Volts (V_{pp}). The photographs are at **(a)** t = 0 s prior to energizing the piezoelectric, **(b)** at time = 4 s the cells are beginning to migrate toward the wave node as a result of the acoustic field and **(c)** at t = 10 s, the majority of the cells have agglomerated in the nodal plane.
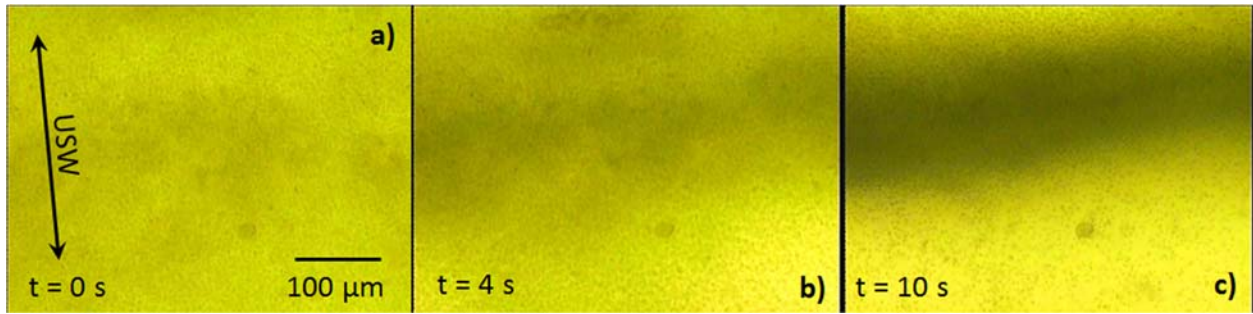
Figure 40. Acoustophoretic movement of microalgal cells. Initial distribution of cells (left) and distribution of cells 4 s after the USW is applied. Final agglomeration of cells in the acoustic node at t = 10 s.

The acoustic radiation force, F_{ac}, depends heavily on the density and the speed of sound in the particle as indicated by Equations 19 and 20. Accordingly, a major objective of this study is to accurately characterize these acoustic parameters for a variety of microalgae strains currently under consideration for large scale cultivation of biofuels and bioproducts.

5.4 The Acoustic Contrast Factor and Acoustic Property Characterization

Our results strongly suggest that the physical properties of the microalgae cells (e.g. acoustic properties, mean diameter and shape) have a profound impact on the ability to maximize the acoustic radiation force imparted on the cells by the USW. As defined by Equations 19 and 20, the acoustic radiation force, F_{ac}, is proportional to the mean cell radius cubed and directly proportional to the acoustic contrast factor, F_{con}. The acoustic contrast factor, as defined by Equation 20, depends on the speed of sound (c) within the cell and the cell density (ρ). These properties are dependent on the microalgae strain and cell composition since lipids, carbohydrates and proteins have different values for ρ, c and compressibility (κ).

The calculated acoustic contrast factor, F_{con}, for particles in water suspension is also listed in Table 4. The table shows the values obtained by experiments in our laboratory for two cultures of *N. Salina*, pure water, artificial sea water (ASW) and soybean oil. The values reported

in the literature for protein and carbohydrates are also shown. The acoustic contrast factor is

calculated for particles in a water suspension. The results for *N. salina* strongly suggest the need

to quantify these properties for various strains under various growth conditions to determine the

conditions under which the acoustic radiation force would be enhanced or degraded. Indeed,

assuming that the accumulated storage triglycerides of "harvest ready" microalgae cells have

similar acoustic properties to that of soybean oil, there may be some conditions under a particular

combination of lipid, proteins and carbohydrates inside the cell could result in an acoustic

contrast factor that approaches zero. Therefore, the acoustic contrast factor could be responsible

for two very different scenarios in acoustic separation: success or failure.

Table 4. Density, speed of sound and compressibility

	Density (kg·m^{-3})	Speed of Sound (m · s^{-1})	Compressibility (m^2 · N^{-1} x 10^{-10})	Acoustic Contrast Factor in water
N. salina from culture 1	1042.74	1545.91	4.01	0.06
N. salina from culture 2	1068.72	1503.37	4.14	0.06
Demineralized Water	988.29	1482.99	4.60	0.00
Artificial Sea Water	1016.28	1509.37	4.31	0.03
Protein[51]	1350	2721	1.00	0.36
Soy Bean Oil	905.40	1470.59	5.10	-0.07
Carbohydrate[52]	1590	1714	2.14	0.32

To date, despite the potential of acoustic harvesting, very little work has been done to understand the sensitivity of the acoustic contrast factor to different microalgae strains and growth conditions. As with any potential new technology, the best scenarios for its deployment must be identified. For example, the microalgae strains with higher inherent F_{con} would be preferred for acoustic dewatering. Also, the change of F_{con} with the growth stage could also impact the best harvesting time to maximize dewatering efficiency while minimizing energy consumption. Moreover, the benefits of acoustic dewatering could depend on the downstream fuel conversion technology, since technologies such as hydrothermal liquefaction (HTL) convert the entire algal biomass into crude oil and therefore do not require high percentages of lipid accumulation to yield high conversion efficiencies.

5.4.1 Objectives of the Acoustic Contrast Factor Characterization

To achieve the overall goals of the study, the following specific objectives of the study are listed below:

Objective 1. Determine the acoustic response of algal cells in the presence of the ultrasonic standing wave and quantify the acoustic radiation force acting on the microalgae cells.

Objective 2. Quantify the speed of sound and density of different microalgae strains.

Objective 3. Determine the magnitude of the acoustic contrast factor.

5.4.2 Determination of the Principal Forces

The first step in this research study was to characterize the different forces acting on the microalgae cells and determine their dependence on variables such as the acoustic contrast factor as well as the applied acoustic energy density. A key goal of this project was to demonstrate that the acoustic radiation force can achieve the required magnitudes required to overcome the particle

drag force and, via purely fluid mechanical means, to direct the cells toward a harvesting outlet while the media is directed toward a dilute outlet. To quantify F_{ac}, we used microscopic video recording of the acoustophoretic motion combined with particle tracking velocimetry (PTV) as explained further in §5.6.3.

5.4.2 Effect of Microalgae Strain and Growth Stage on Acoustic Contrast Factor

This section describes the approach that was employed to characterize the acoustic contrast factor for different strains of microalgae, as well as examining the effects of culture density and cell composition. Algae suspensions are presently characterized by absorbance which is an indication of cell density and culture density. However, algae cultures are not transparent and light transmission is only effective for dilute solutions ($\varphi < 2$ g/L) [53]. Instead, ultrasound offers the potential to characterize concentrated emulsions that are up to 40% v/v [54]. Indeed, although not the focus of the proposed study, ultrasonic techniques have great potential for development of instrumentation to characterize microalgae culture density and lipid content in situ. The proposed work in ultrasonic characterization had three objectives: 1) characterization of the acoustic contrast factor as a function of strain and growth conditions, 2) improvement of estimates of the ultrasonic behavior of algal suspensions and 3) determination if noninvasive ultrasonic tests are indicative of culture density.

A previous study from 1959 did not find any dependence of microalgae concentration on the measured speed of sound [55]. However, the accuracy of speed of sound measurements has increased dramatically in the recent years.

The density (ρ) and speed of sound (c) were determined with an Anton Paar DSA-5000 vibrating tube densitometer. This technique is broadly used to characterize the composition dependence of ultrasound properties for suspensions [51]. The ρ and c of the media (without

microalgae) was also determined and combined with the results for various culture density to compute the acoustic contrast factor (F_{con}) for each microalgae species. The contrast factor was then evaluated for *Chlamydomonas reinhardtii* sta6 mutant at different stages of growth as will be discussed in §5.7.3.

5.6 Materials and Methods

5.6.1 Cell Cultures

5.6.1.1 *N. gaditana*, *N. oculata* and *P. tricornutum*

Nannochloropsis gaditana (CCMP 1654), *Nannochloropsis oculata* (CCMP 525) and *Phaeodactylum tricornutum* (CCMP 630) were obtained by Solix Biosystems from the national center for marine algae and microbiota. The microalgae was cultivated in Artificial Sea Water (Instant Ocean) with a salinity of 27 g·L^{-1}. The nutrient solution f/2 supplemented with 5 mM NO$^-_3$ and 0.368 mM PO$^-_4$ was used to cultivate the salt water microalgae strains in a 13 L AGS 4 industrial scale photobioreactor under artificial light conditions ca. to 400 μmol m^{-2} s^{-1}.

5.6.1.2 Chlamydomonas reinharditii with nitrogen depravation

Chlamydomonas reinhardtii CC4349 (wild-type), CC4334 (starchless-Sta-7 mutant) were obtained from Chlamydomonas Resource Center and cultivated mixotrophically in TAP media in an Multitron II at 18 °C and 400 μE m^{-2} s^{-1} for 8 days until they reach stationary phase. CC4334 (starchless-Sta-7 mutant) was also grown under different nitrogen stressed conditions with different NH$_4$ concentrations as explained elsewhere in the literature [56].

5.6.1.3 Chlamydomonas reinharditii *sta6* (obese)

Chlamydomonas reinhardtii sta6 (starch null) CC-4348 mutant strain was kindly provided by Carrie Goodson and Dr. Taylor Weiss from Department of Biology at Washington

University in St. Louis, MO, USA. The *C. reinharditii* sta6 cells under nitrogen deprivation and a 20 mM acetate boost after 8 to 10 days are known to become obese due to the presence of large lipid bodies in their cytoplasm and chloroplasts. Here, we performed PTV on the sta6 cells to analyze the change of acoustic contrast factor due to lipid accumulation. The *C. reinharditii* cells were grown in phosphate buffered high salt medium (HSM) with a nitrogen and acetate source as indicated elsewhere. The media was replaced by nitrogen deprived HSM with 20 mM acetate. Two days later the cells were boosted with 20mM acetate. PTV measurements were performed at days 3, 5 and 9.

5.6.2 Speed of Sound, Density, Cell Count and Biovolume

A 140 mL of sample was obtained at day 6 of cultivation in the Solix AGS photo bioreactor. The algae samples were centrifuged at 1048 g for 20 minutes to separate the cells from the media. The media and the algae cells were separated. Then, the microalgae cells were re-suspended to obtain a 13 mL concentrated emulsion of microalgae cells and media. The solution was diluted with media to create aliquots of different cell concentration.

Speed of Sound and Density were determined by a DSA – 5000 m bench top instrument (Anton-Parr, Graz, Austria). This technique is broadly used to characterize the composition dependence of ultrasound properties for suspensions. This instrument is equipped with a "time of flight" ultrasound sensor capable to obtain the speed of sound with an accuracy of $0.01 \text{ m} \cdot \text{s}^{-1}$. The instrument determines the density by a vibrating tube densitometer (VTD) that is based in the matching frequency principle. The apparatus is able to determine the density with an accuracy of $0.000005 \text{ g} \cdot \text{cm}^{-3}$. We calibrated the instrument each day with an air/water check as suggested by the manufacturer. The instrument was flushed with DI water and non-denatured alcohol before each test and then dried and air flushed. A 3 mL algae sample aliquot was added

and the speed of sound and density determined. Then media was used to flush the sample and the new sample tested. Lugol solution was used to immobilize the cells for the cell count. The cell count of the highest density sample was obtained with a Hemocytometer. Ten cell counts were performed, five in each side, following and X pattern. Cell biovolume was obtained with a Hitachi KP-D50 (Japan) camera coupled to a TMZ Nikon (Japan) microscope and a photocapturing computer. The algae sample was placed in a calibrated scale with 10 μm divisions. The pictures were scaled using the computer Software Autocad (California, USA) and random cells were selected for biovolume determination as indicated in Figure 41. The biovolume for each strain was determined according to the procedure described elsewhere [57]. The strains *N. oculata* and *N. gaditana* where assumed to have a prolate spheroid volume, the *P. tricornutum* as a double cone and *C. reinharditii* as a sphere. Random cells were measured and their biovolume averaged for $n = 25$ cells. The cell concentration and the average biovolume were multiplied to obtain the microalgae volumetric fraction of each sample.
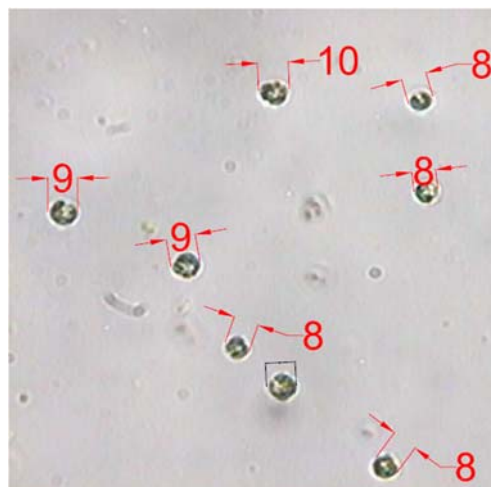
Figure 41. Micrograph of *C. reinhardtii* cells and biovolume determination by measuring the cell diameter

The averaged bulk cell density and cell speed of sound were calculated using the Urick's equations presented in §2.5. These values were obtained by solving Urick's equations in each sample. The supernatant c and ρ were measured and considered to be the terms c_m and ρ_m of Equation 3.

5.6.3 Particle Tracing Velocimetry

A quartz 4 mL cuvette was used to expose the cells to acoustophoresis. The acoustic field was generated with a 25 mm diameter SM111 Piezo Electric Ceramic Disc Transducer (Steminc, Miami, USA). The ultrasonic wave was generated by an Agilent Function Waveform Generator (33120A, Agilent, CA) at 10 V_{pp}. The forced frequency response of the system was obtained by a PZT Disc located in the opposite wall and connected to an ESA Spectrum Analyzer (E4405B, Agilent Technologies, CA). The resonance modes of the cuvette and water were identified and the maximum resonant peak, ca. 1.650 MHz was chosen as the operating frequency. The Olympus inverted microscope was placed in vertical position and a 40X magnification lens was used to record the acoustophoretic movement. Seeding particles of known size and composition where used to determine the acoustic energy intensity in a similar method previously described in the literature. Here we used the Particle Tracking Velocimetry software Tracker® 2.6 (Douglas Brown, CA, USA) to measure the movement of the cells vs. time.
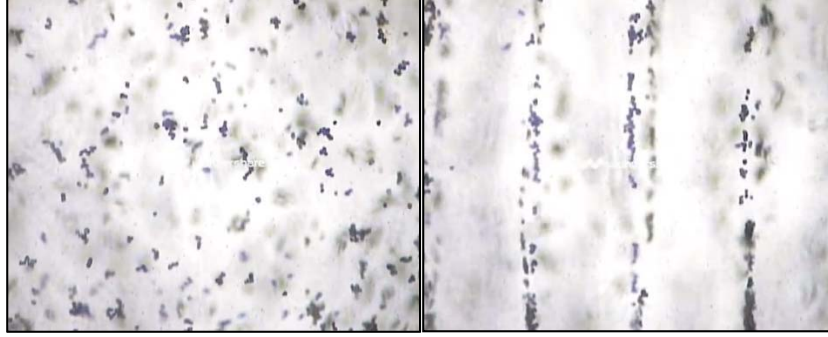
Figure 42. 20 µm polyamide in suspension (*left*) and under acoustophoresis (*right*)

We used the Finite Element Software COMSOL Multiphysics Particle Tracing Module to compare the PTV results. The software provided the coordinate, velocity and acceleration of particles under and arbitrary force. The force was selected as F = A*sin(kx) to simulate the acoustophoretic force predicted by Equation 1. The software COMSOL also compensated the acceleration of the particles by computing the drag force.

In this section, we will explain in detail how this quantification process works based on our results for *N. Salina* shown in Figure 43. Polyamide particles of known density (ρ = 1.05 kg·m^{-3}), compressibility (κ) and diameter (θ = 20 µm) are exposed to a standing wave and their position is recorded over time via PTV. The acoustic wave is created by a disc PZT vibrating at approximately 1.7 MHz with amplitude of 10 V$_{pp}$. The particle velocity and acceleration are computed as a function of time as shown in the Figure 43. A COMSOL Multiphysics model is then used to calculate different acoustic forces with the known polyamide particle properties (ρ, κ, θ). The model also calculates $\mathbf{F}_D$ as the particle accelerates and decelerates during its transition from an acoustic antinode to a node. The model is exercised with different values of $\mathbf{F}_{ac}$ until good agreement with experimental velocity profiles are obtained, which for the case shown in Figure 43 was $\mathbf{F}_{ac}$ = 0.1 nN. Since the acoustic contrast factor and diameter is well characterized

for the polyamide particles, this approach enables the determination of an acoustic energy density of 4.2 J·m^{-3} from Equation 1.

Having calculated the acoustic energy density, the same physical setup is then used to determine the F$_{ac}$ acting of *N. salina* algal cells. The cell trajectories are again measured using PTV in the same conditions described above. The COMSOL model is then used to compute trajectories under different magnitudes of the acoustic radiation force. As shown in Figure 43, the results indicate that the acoustic radiation force acting on the *N. salina* cells in this configuration is bounded by 0.1 pN $< F_{ac} <$ 1 pN.   After the magnitude of the acoustic radiation force is determined, the acoustic contrast factor can be then computed from Equation 1. These preliminary results indicate an *N. salina* contrast factor of 0.06, which is in reasonable agreement with the measured results by using a density meter and direct speed of sound presented in Table 4.
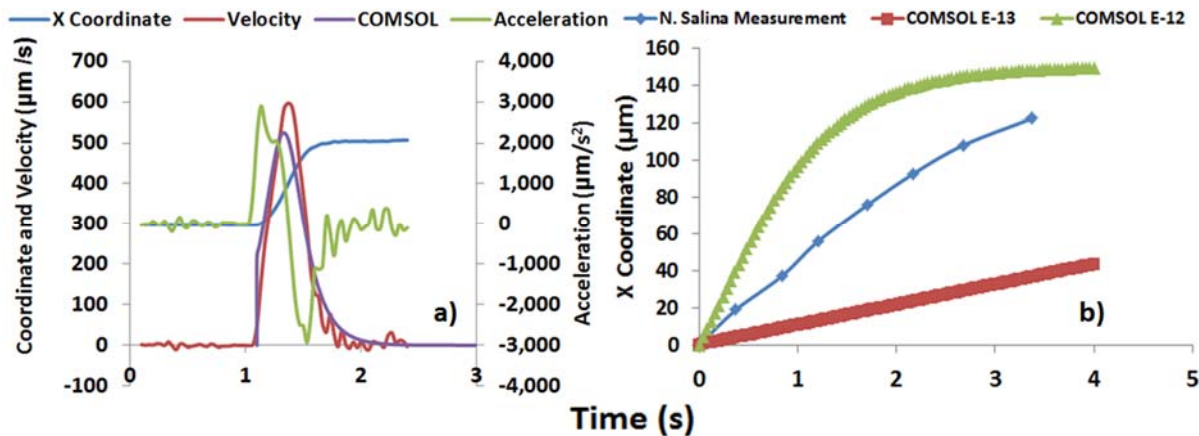
Figure 43. Displacement, velocity and acceleration measured by Particle Tracking Velocimetry on a 20 μm polyamide particle in an acoustic field. A COMSOL® model of the particle (purple) shows good agreement with the experimental velocity with $\boldsymbol{F_{ac}} = 1 \times 10^{-10}$ N, which yields an effective acoustic energy density of 4.2 J m^{-3}. (b) The trajectory of a *N. salina* algal cell as determined by PTV along with COMSOL results.

5.7. Results and Discussion

5.7.1 Speed of Sound and Density

Speed of sound and density of the algae samples varied with the volumetric fraction as shown in Figure 38 and 39 for *N. gaditana*, Figures 40 and 41 for *N. oculata* and Figures 42 and 43 for *P. tricornutum*. Most notably, there is a linear relationship between c and ρ with volumetric ratio and this is an indication that the proposed Urick's equations are valid for microalgae cultures. For example, the R^2 linear coefficient for the *N. gaditana* for ρ vs. volumetric ratio tests are 0.99, 0.99 and 0.99 while for c vs. volumetric ratio are 0.98, 0.99 and 0.98. The same highly linear behavior was observed for all the microalgae samples in this study as indicated in the subsequent figures. Thus, the Urick's equations provide a good estimate for the speed of sound and density of known algae concentration or vice versa when dense algae samples are used. Therefore, these relationships could be used to estimate the speed of sound and density of known algae concentration.
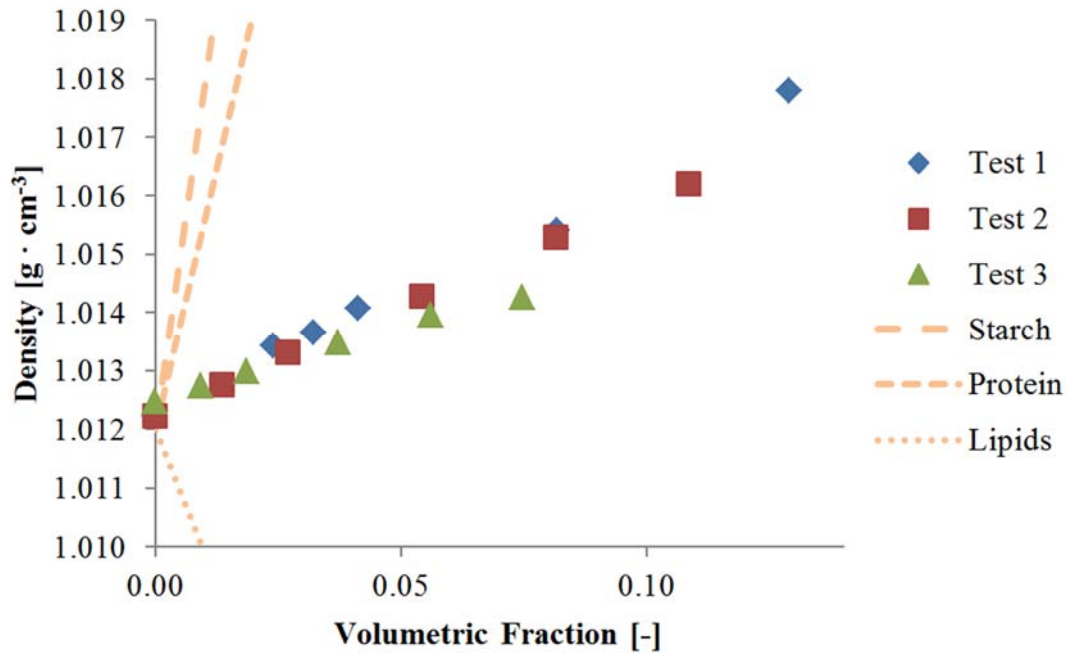
Figure 44. Volumetric Fraction calculated by multiplying cell concentration and cell biovolume vs. emulsion density measured in a vibrating tube densitometer for three cultures of *N. gaditana*
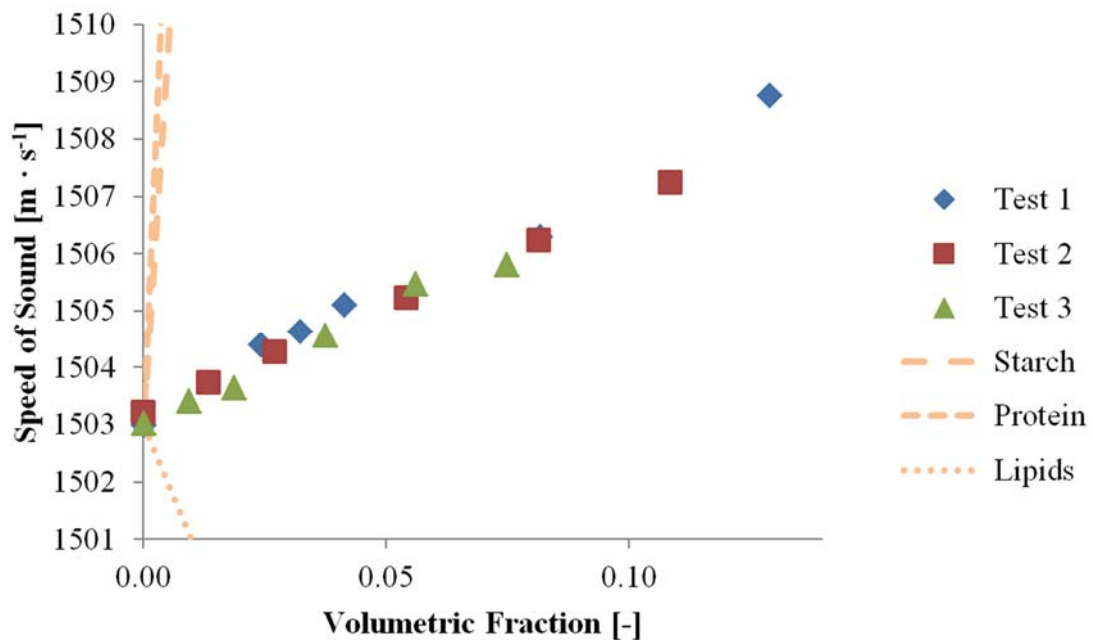
Figure 45. Volumetric Fraction calculated by multiplying cell concentration and cell biovolume vs. speed of sound measured in a vibrating tube densitometer using a "time of flight" technique for three cultures of *N. gaditana*
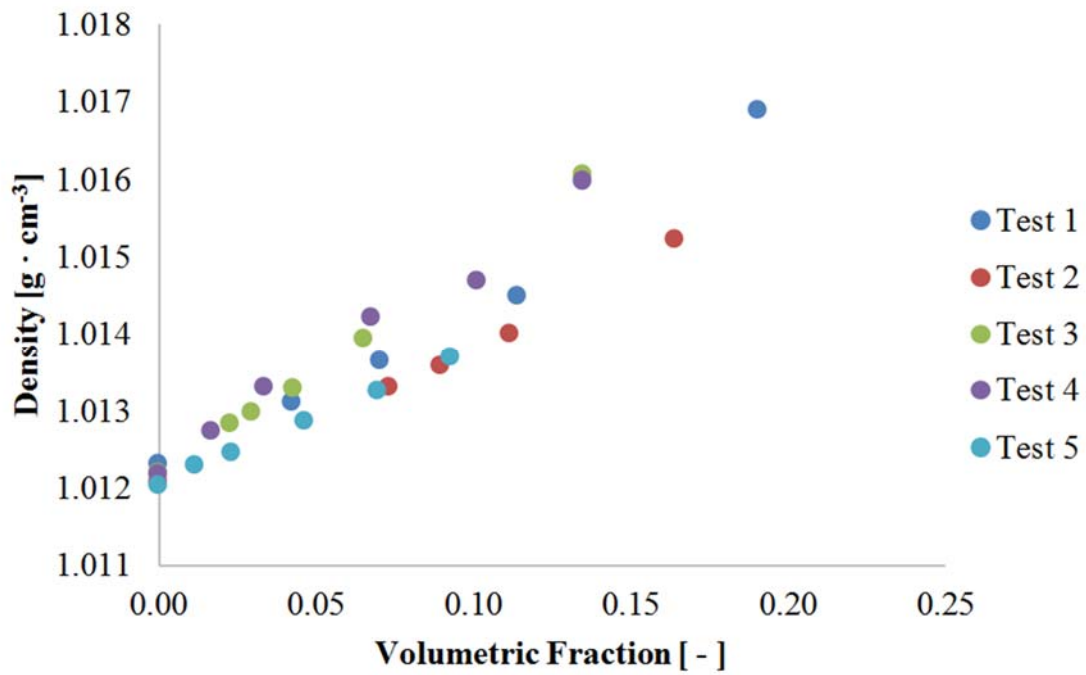
Figure 46. Volumetric Fraction vs. emulsion density for five cultures of *N. oculata*
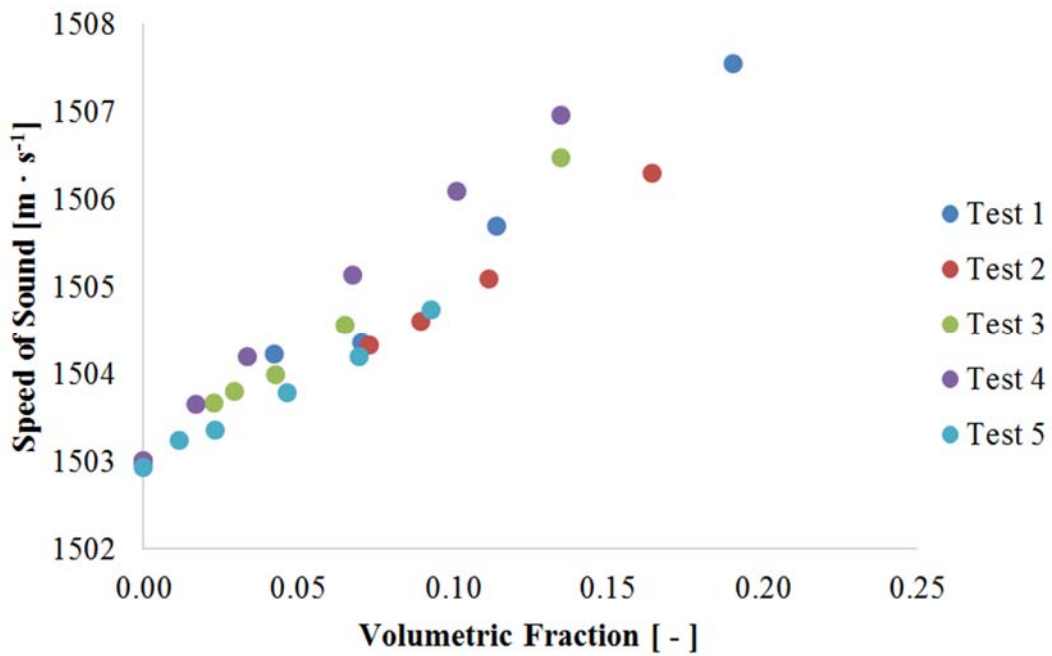
Figure 47. Volumetric Fraction vs. emulsion speed of sound for five cultures of *N. oculata*
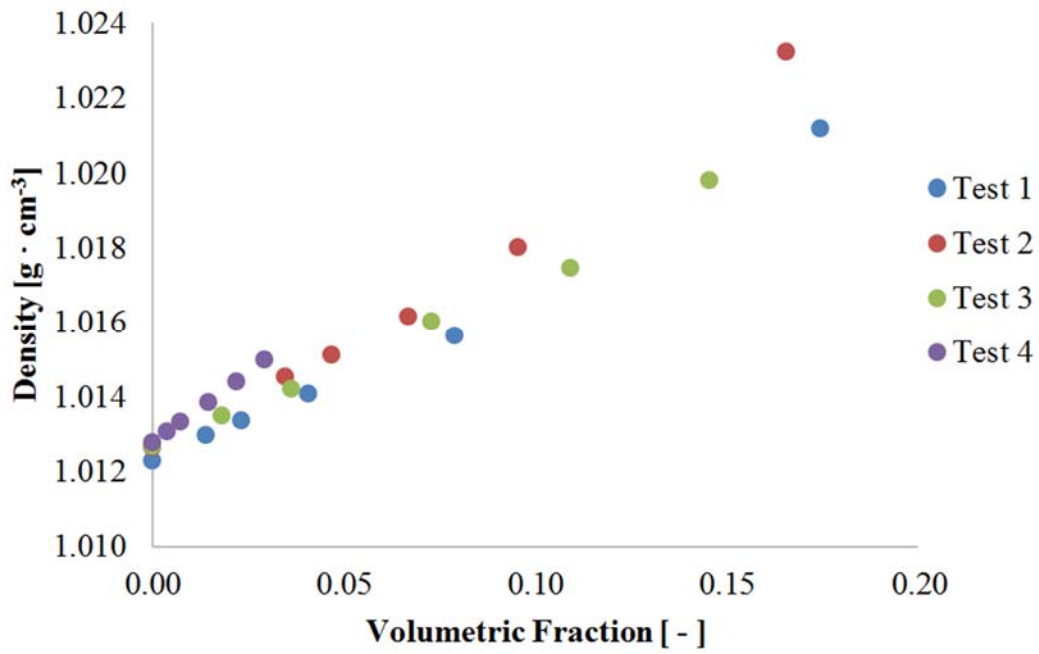
Figure 48. Volumetric Fraction vs. emulsion density for four cultures of *P. tricornutum*
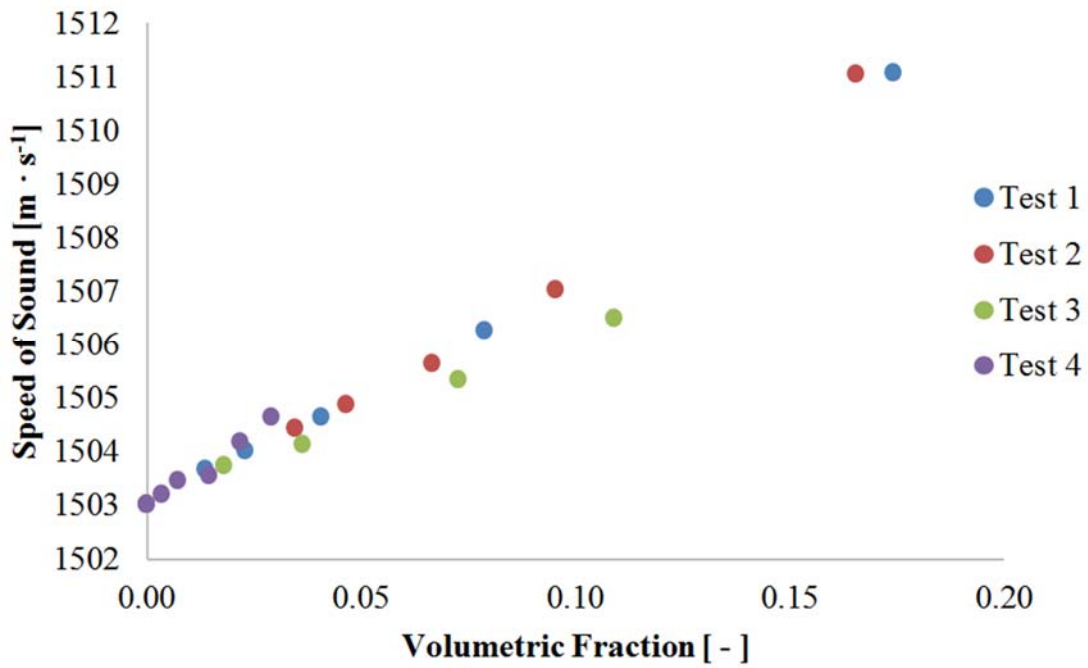
Figure 49. Volumetric Fraction vs. emulsion speed of sound for four cultures of *P. tricornutum*

The values reported by the literature for cornstarch [52] (ρ=1.6 g·cm^{-3} and c=2810 m·s^{-1}),

protein[58] (ρ=1.37 g·cm^{-3} and c=3473 m·s^{-1}), and triacylglyceride[58] (TAG, ρ=0.8 g·cm^{-3} and

c=1300 m·s^{-1}) where used to calculate the hypothetical case of an algae cell composed solely of

those constituents. The lines for each case are pictured in Figures 38 and 39. The starch and

protein present a positive slope as an indication of higher values of density and speed of sound

while the lipid line has a negative slope due to lower values of ρ and c. Each calculated case of

carbohydrate, protein and lipid represents the theoretical boundaries of a cell composition.

However, the cell is a mixture of all those three constituents and therefore the speed of sound and

density lines are in somewhere in between the carbohydrate, protein and lipid lines as indicated

by the results shown in Figures 38 and 39.

5.7.2 Acoustic Contrast Factor

The calculated density and speed of sound for the microalgae cell of each test are given in

Table 5. These values were calculated by solving the Urick's equations in each data point of

Figures 38 to 43 combined with the estimated cell count and cell biovolume. The fact that

microalgae samples had a strong linear behavior as explained before yielded a low standard

deviation when the calculated ρ and c where averaged. *N. gaditana* cells had a density with a

range from 1.039694 to 1.055641 g·cm^{-3}, *N. oculata* from 1.022502 to 1.047939 and *P.

tricornutum* from 1.057795 to 1.090233. The cell c and ρ were similar for this three microalgae

strains and one possible explanation is that they were cultivated under the same conditions of

growth media, light exposure and temperature. In addition, the reported density values are

similar to other microorganisms reported in the literature such as *Saccharomyces cerevisiae*

density determined by VTD (1.1029 ± 0.0026 g·cm^{-3}) and *Dunaliella salina* determined by

density gradient (1.104 – 1.128 g·cm^{-3}). To confirm whether this low value for density makes

sense, it was assumed that the cell was composed of 50% osmotic water and 50% of dry weight as suggested elsewhere[59], where the later can be assumed as 30% protein, 30% carbohydrates and 40% lipid as one the potential growth conditions for *Nannochloropsis*. The results for this calculation yield an algae cell density of 1.060 g·cm^{-3}.

Table 5. Measured density and speed of sound of microalgae and S. cerevisiae cells

Strain	Sample	Cell Density (g·cm^{-3})	Cell Speed of Sound (m·s^{-1})
N. gaditana	Test 1	1.055 ± 0.004	1550 ± 6
	Test 2	1.050 ± 0.001	1540 ± 1
	Test 3	1.039 ± 0.002	1543 ± 4
N. oculata	Test 1	1.028 ± 0.001	1519 ± 2
	Test 2	1.022 ± 0.001	1541 ± 1
	Test 3	1.023 ± 0.002	1516 ± 2
	Test 4	1.047 ± 0.004	1543 ± 3
	Test 5	1.034 ± 0.002	1526 ± 4
P. tricornutum	Test 1	1.059 ± 0.003	1547 ± 3
	Test 2	1.068 ± 0.004	1546 ± 3
	Test 3	1.057 ± 0.001	1539 ± 4
	Test 4	1.090 ± 0.002	1556 ± 8
S. cerevisiae		1.162 ± 0.008	1596 ± 37

S. cerevisiae presented the highest density and speed of sound of all the samples what could be a consequence of its composition mainly as protein and carbohydrates.

The acoustic contrast factor of the cell and the media was calculated according to Equation 1. The results are shown in Figure 50. *N. oculata*, *N. gaditana* and *P. tricornutum*

presented a similar acoustic contrast factor in the range of $F_{ac}= 0.03 – 0.07$. These strains presented a low acoustic contrast factor compared with a theoretically cell composed solely of carbohydrates ($F_{ac} \approx 0.3$), protein ($F_{ac} \approx 0.2$) and lipids ($F_{ac} \approx -0.2$). The acoustophoretic force is proportional to the acoustic contrast factor and the radius of the cell cubed (R^3). These two factors combined are shown in the right axis of Figure 50. It can be seen that most of the samples of *N. oculata*, *N. gaditana* and *P. tricornutum* had a $F_{ac} \times R^3$ factor of less than 5×10^{-18} m^3. This corresponds to an acoustophoretic force of less than 5×10^{-14} N assuming an acoustic energy density of 5 J·m^{-3}. *S. cerevisiae* had a calculated contrast factor of $F_{ac} = 0.13$ what could be a consequence of the high composition of carbohydrates and proteins of yeast. The $F_{ac} \times R^3$ factor was close to 30×10^{-18} m^3 or 6 times the factor obtained for the microalgae strains. Therefore *S. cerevisiae* could potentially be a biological cell easier to separate by acoustophoresis when compared with *N. oculata*, *N. gaditana* and *P. tricornutum*.
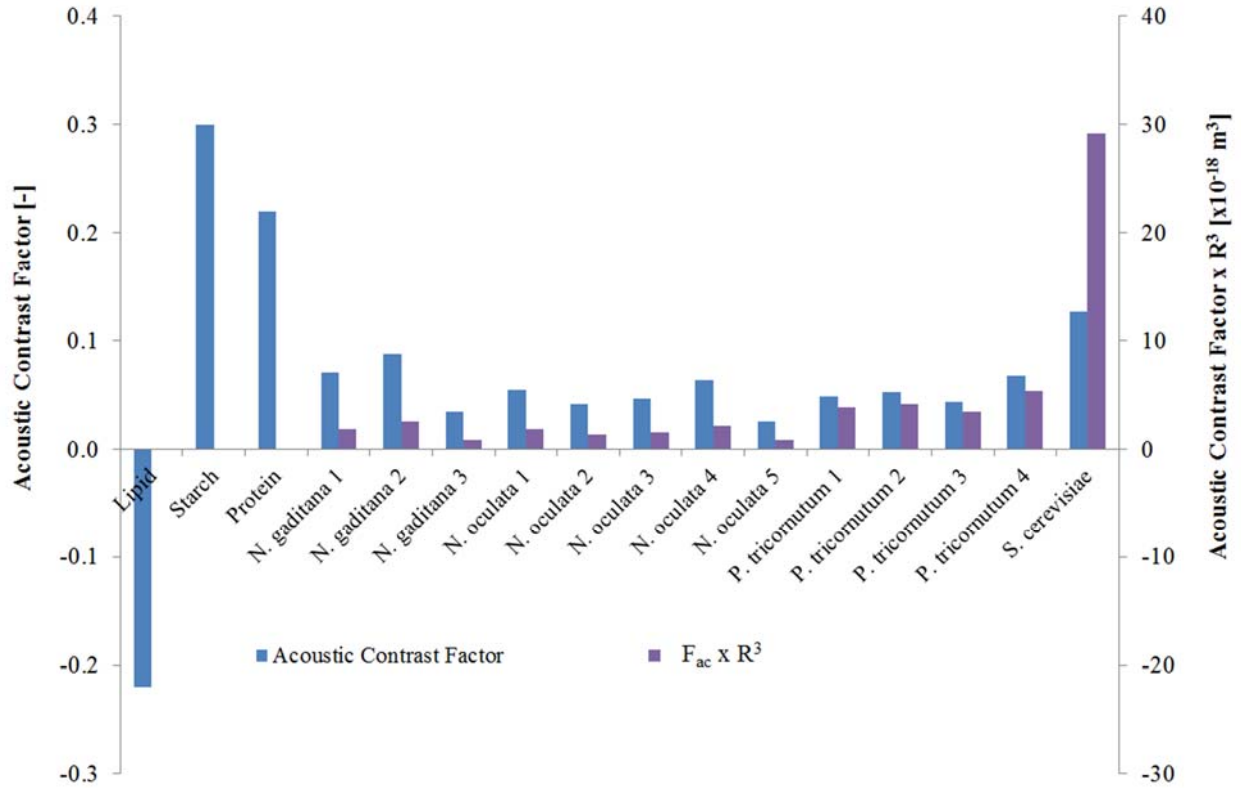
Figure 50. Acoustic contrast factor and F x V for different microalgae strains and yeast

5.7.3 Particle Tracking Velocimetry

PTV was used to compare the measured acoustic contrast factor by the vibrating tube densitometer and "time of flight" speed of sound measurement with the predicted acoustic response using Finite Element Analysis. *C. reinharditii* cells cultivated in nitrogen abundant and nitrogen depletion conditions were used for this test. The measurements in the vibrating tube densitometer resulted in $F_{ac} = 0.37$ for the nitrogen abundant cells and $F_{ac} = -0.02$ for the nitrogen depleted media. The results of the PTV analysis are indicated in Figures 53 and 54. First, we measured the position (acoustophoretic coordinate) of a polyamide particle of 20 μm diameter and $F_{ac} = 0.05$ calculated with the density and speed of sound of the polyamide. The COMSOL® Particle Tracing Finite Element Analysis module was used to compute the acoustophoretic coordinate vs. different force magnitudes. In this case, there was a good

agreement between the COMSOL predicted response for the 100 pN case and the particle

response as indicate in Fig. 53. Therefore, it was possible to estimate an acoustic energy density

of 5 J·m^{-3}. Then we measured the acoustophoretic movement of the *C. reinharditii* cells as

indicated on the figure. We found a good agreement of the cell movement with the COMSOL

model when using and acoustic contrast factor of 0.05 corresponding to a force of 5 pN. We

repeated the procedure with a solution of polyamide particles an *C. reinharditii* from the nitrogen

deprived culture. The acoustophoretic motion of the control particles was similar to the response

of the particles from Figure 53. However, the movement of the cells was slower than the

measured response of the N+ treatment. The COMSOL model was used to calculate a contrast

factor of 0.02 as opposed to the contrast factor of 0.05 for the nitrogen abundant treatment. This

change of the contrast factor is in agreement with the change measured using the VTD technique.
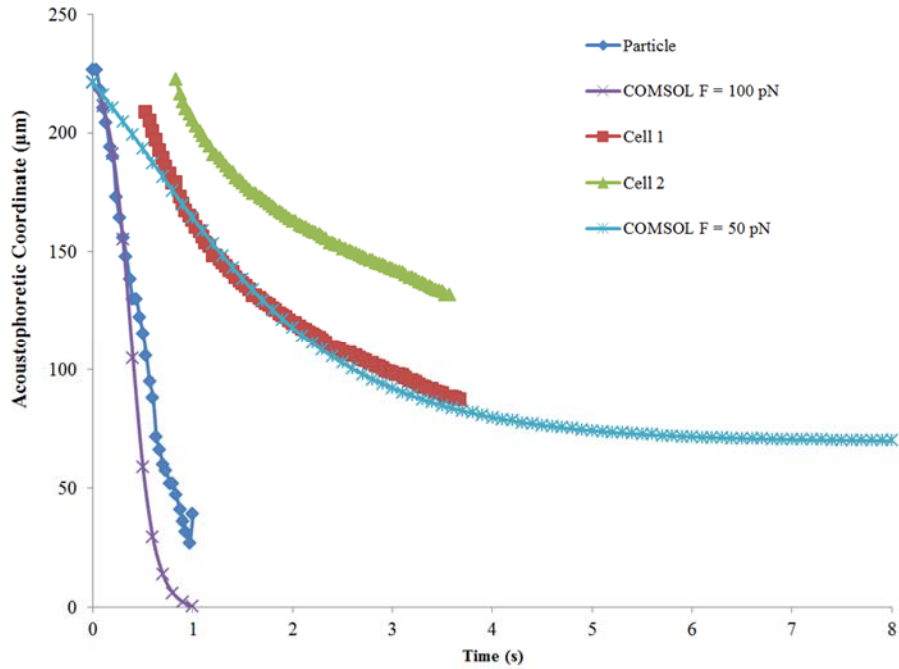
Figure 51. Particle Tracking Velocimetry combined with FEA to estimate the acoustic contrast factor of *C. reinhardtii* cells with nitrogen abundant media
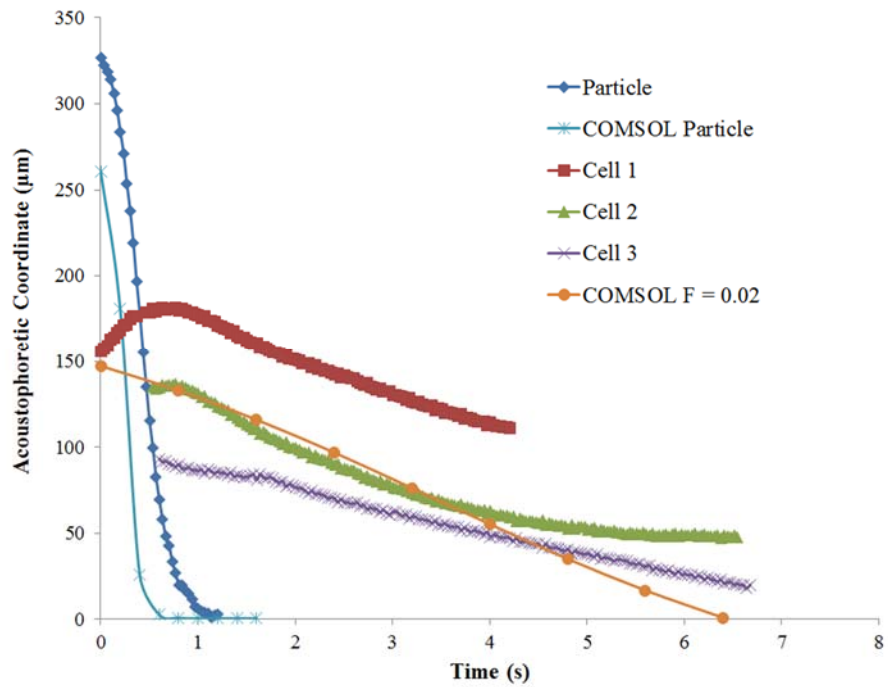
Figure 52. Particle Tracking Velocimetry combined with FEA to estimate the acoustic contrast factor of *C. reinhardtii* cells under nitrogen depletion

5.7.3 Change in the Acoustic Contrast Factor

We used the STA6 *C. reinhardtii* cells to determine if an increase in the lipid content will be responsible of a change in the acoustic contrast factor. Figure 55 is a micrograph of the culture under acoustophoresis at day 9 after the acetate boost and nitrogen depravation. We detected the agglomeration of cells in the wave antinode as an indication of the negative contrast factor. Here, we used the polyamide particles with a known acoustic contrast factor of positive 0.05. The polyamide particles agglomerated in the nodes of the wave while the lipid obese cells agglomerated in between corresponding to a negative contrast factor.

In fact, our experimental data indicate that the acoustic contrast factor changed from a positive to a negative value for STA6 *Chlamydomonas reinhardtii* cells as they accumulate lipids (Figure 56). Specifically, cells at day 1 after an acetic acid boost registered a positive contrast factor. At day 3 the cells presented a $F_{con} = 0$ as they did not respond to the acoustic field. At day 9 the cells registered a negative contrast factor migrating to the antinodes of the acoustic field as indicated in the bottom figure. One potential explanation for this phenomenon might be variation in lipid content among the algae cells in the culture, resulting in a variation in acoustic contrast factor. Our results indicate that the cells suffered a change from a positive to a negative contrast factor as indicated in Figure 56. A negative contrast factor indicates a high lipid concentration in this "obese" state.
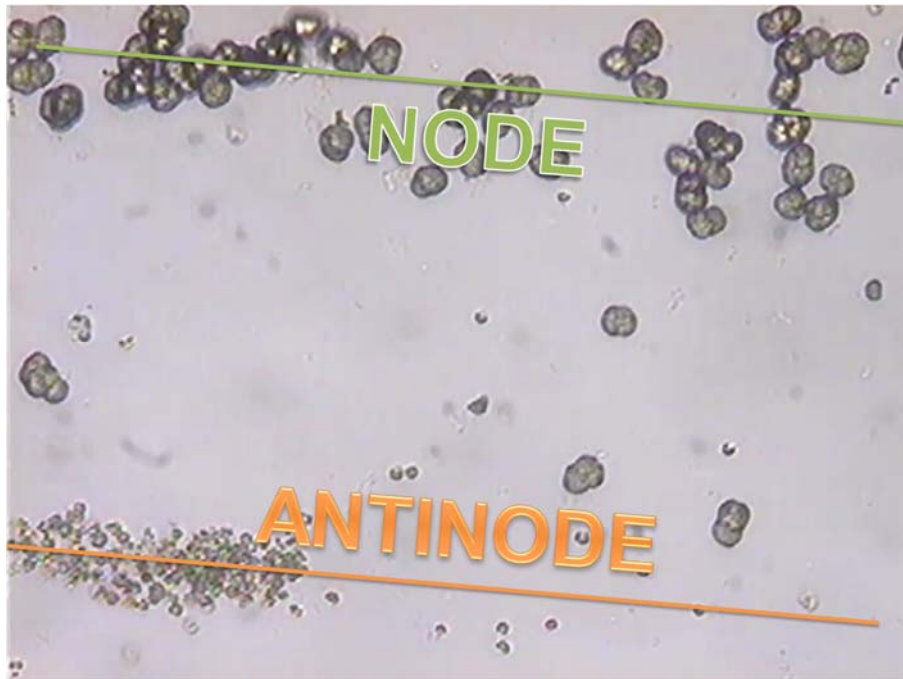
Figure 53. PTV results indicating a change in the contrast factor for Chlamydomonas reinhardtii cells.
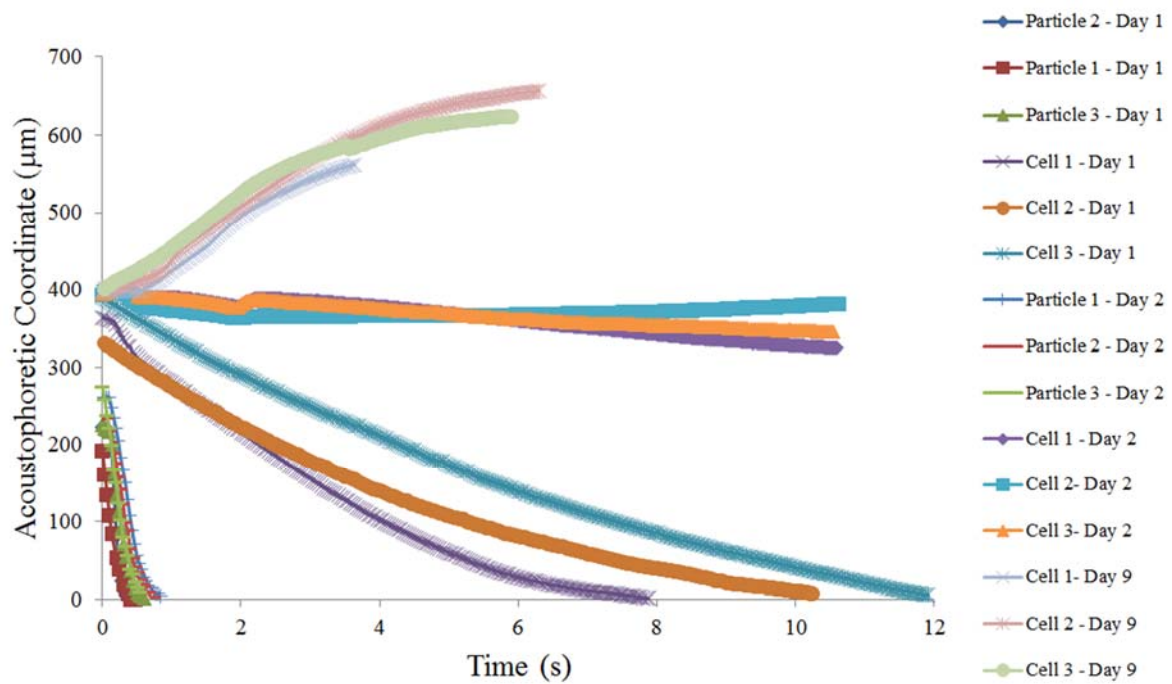
Figure 54. PTV results indicating a change in the contrast factor for Chlamydomonas reinhardtii cells.

5.7.4 Implications of the acoustic contrast factor

This chapter presented a novel approach to measure the density and speed of sound of microalgae by using a vibrating tube densitometer, speed of sound cell and the Urick's equations. The acoustic contrast factor found for the microalgae species tested was small, in a range from 0.03 – 0.08. It was also found that the factor of FxR^3 was 10 to 20 times smaller compared to yeast, indicating that microalgae is a challenging feedstock for acoustic separation. It was also found that under a certain conditions, microalgal cells can change from a positive to a negative acoustic contrast factor. Therefore caution should be exercised when attempting to separate microalgal cells with an acoustic contrast factor of zero.

6. AN ULTRASONICALLY ENHANCED INCLINED SETTLER FOR MICROALGAE HARVESTING

Microalgae have vast potential as a sustainable and scalable source of biofuels and bioproducts. However, algae dewatering is a critical challenge that must be addressed. Ultrasonic settling has already been exploited for concentrating various biological cells at relatively small batch volumes and/or low throughput. Typically, these designs are operated in batch or semicontinuous mode, wherein the flow is interrupted and the cells are subsequently harvested. These batch techniques are not well-suited for scale up to the throughput levels required for harvesting microalgae from the large scale cultivation operations necessary for a viable algal biofuels industry. Here we present a novel device for the acoustic harvesting of microalgae

6.1 Introduction

6.1.1 Ultrasonically Enhanced Sedimentation (UES)

The use of ultrasonic standing waves has been reported in the literature as an approach to manipulate particles in a fluid. The standing wave is the condition when $f_n = nc/2L$, which is also known as the resonance mode where f_n are the resonance frequencies, n the resonance number, c the speed of sound in the acoustic layer and L thickness of the layer. The standing waves exert an acoustic radiation force that collects the particles in acoustic nodes or antinodes according to the following equation [44]:

$$F_{ac} = 4\pi R^3 k E_{ac} F \sin\langle 2kx \rangle \tag{21}$$

where R is the particle radius, [μm^{-1}], k is wave number [m^{-1}], E_{ac} the acoustic energy density [$J \cdot m^{-3}$], F the acoustic contrast factor. Equation 21 shows that the wavelength of the acoustophoretic force is half that of the acoustic wavelength. Therefore, the acoustophoretic force has alternating bands of zero and its maximum magnitude every $\lambda/4$ where λ is the acoustic wavelenght. Also, the acoustic contrast factor, F, is an important physical property that has a direct influence on the magnitude of the acoustic force imparted on the particle. The acoustic contrast factor, F, can be expressed as follows [44]:

$$F = \frac{1}{3}\left[\frac{5\Lambda - 2}{1 + 2\Lambda} - \frac{1}{\sigma^2 \Lambda}\right] \tag{22}$$

where Λ is the ratio of density of particle and the media ($\Lambda = \rho_p/\rho_m$) and σ the ratio of the speed of sound in the particle and in the media ($\sigma = c_p/c_m$). Th acoustic contrast factor will be different than zero if there is a relative difference in speed of sound and density between the cell and the surrounding fluid medium. A laboratory scale test performed by our research group is shown in Figure 55 in which the acoustophoretic effect is demonstrated in batch mode using polyamide particles and *N. oculata* cells, respectively. There is, however, a decrease in the acoustophoretic force when $f_n \neq nc/2L$, a condition also known as a progressive wave. For a progressive wave, the acoustophoretic force is much smaller since it is proportional to the R^6 rather than R^3 [60].
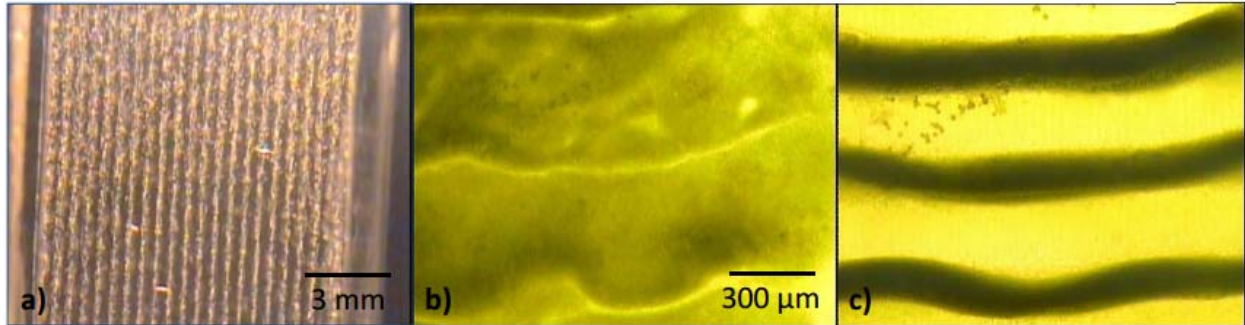
Figure 55. (a) Laboratory scale experiment indicating the formation of acoustic agglomeration lines with a 1.7 MHz standing wave in a quartz cuvette using polyamide particles (b) at time = 0 s for the algae strain *N. salina* (c) at *t* = 3 s after applying the acoustic field

The dewatering process of cells by acoustophoresis in an upward flow chamber is a competing effect between different forces. The acoustic and gravity forces act as main drivers for the separation while the drag force associated with the upward fluid velocity has an opposing effect. In previous work, the use of "pulsed" or "on/off" acoustic cycles, also known as semi-continuous devices, have been suggested as a solution to the drag force problem [61]. Another option suggested in the literature is the use of the displacement of individual cells in the acoustic field, also known as sub-wavelength design [61]. Although the movement of cells is the primary effect of the acoustophoretic force, this movement is on the order of microns because the frequencies used for this behavior are typically between 1 - 10 MHz [62] and therefore $\lambda/4 = 374$ to 37 μm. Therefore, while this principle has been successfully applied for *Lab-on-chip* applications, it has not been demonstrated for the large bulk separation required in the bioenergy industry.

Another approach is the use of a continuous flow enhanced gravity settling as presented below. Assuming the Stokes derived drag equation for low Reynolds number (Re <1), and the gravity force equation of a particle *suspended* in a fluid, the following equation for critical particle radius can be derived [63]:

$$r_c = \left[\frac{9}{2} \frac{\eta v_f \sin(\gamma)}{(\rho_p - \rho_m)g} \right]^{0.5} \tag{23}$$

Here, the critical particle radius (r_c) is the radius at which drag force balances the gravity force [μm], η the viscosity of the media [Pa · s⁻¹], v_f the fluid velocity [m · s⁻¹], γ the inclination angle from horizontal axis [°] which is 0° for horizontal flow and 90° for upward flow, g the acceleration due to gravity [m · s⁻²], ρ_p the density of the particle [kg · m⁻³] and ρ_m the density of the media [kg · m⁻³]. For example, assuming a liquid velocity of 1 mm · s⁻¹, the viscosity of water, a vertical orientation with $\gamma = 90°$, a density difference of $\rho_p - \rho_m \approx 50$ kg · m⁻³, the critical radius is 100 μm, which is roughly equivalent to an agglomerated radius of 3×10^5 cells. The maximum achievable radius is limited by the frequency of the acoustic wave. The acoustophoretic force will agglomerate the cells in the vicinity of λ/4 or a maximum agglomerated radius of λ/8 as has been explained previously in the literature [63]. Therefore, lower frequencies are better to enhance settling since they create larger clumps. However, it is also important to note that the acoustophoretic force is proportional to the frequency and it is desired to operate at the highest frequency without decreasing the agglomerated radius. Here, the highest frequency to achieve an agglomerated radius of λ/8 = 100 μm was found to be 1.86 MHz.

A major challenge in utilizing acoustophoretic force for microalgae harvesting is that microalgae cells typically have a density and speed of sound close to the media, which results in very small acoustic contrast factors and thereby very low magnitudes of acoustophoretic force ($F_{ac} \approx 1 \times 10^{-14}$ N). In addition to the problem of low acoustic contrast factor for microalgae cells in water, the small radii of microalgae cells also results in low acoustophoretic force since the force is proportional to particle radius to the third power. At the same time, the small

difference between ρ_p and ρ_m results in a larger critical settling radius, r_c, for microalgae

($r_c = 59$ μm and $\rho_p = 1.05$ g · cm^{-3}) at a fluid velocity of 0.4 mm · s^{-1} in comparison to other cells

such as insect cells ($r_c = 35$ μm and $\rho_p = 1.15$), yeast ($r_c = 41$ μm and $\rho_p = 1.11$) or bacteria

($r_c = 45$ μm and $\rho_p = 1.09$) [64]. These factors make microalgae a particularly challenging cell

culture to separate by acoustophoresis.

6.1.2 Inclined plate settling

Inclined plate settlers have been widely employed as a separation principle in the

wastewater, minerals and biotechnology industries. In these applications, the media inside the

settling chamber precipitates on the inclined plane creating a sludge layer that slides to the

bottom of the container. This principle of settling stratification is also known as the Boycott

effect and was originally discovered in an experiment with red blood cells [65]. Inclined settlers

have a higher settling area in a smaller footprint when compared with traditional settling devices,

which is the reason why they are often called supersettlers. The literature reports successful

applications of inclined plate settlers for hybridoma [66] and chinese hamster ovary cells [67].

However, these applications have been shown to perform well for cells with a mean diameter of

between 10 to 20 μm, whereas some algae cells of interest such as *Nannochloropsis* have mean

cell diameters less than 5 μm.

In this research, the authors suggest a new approach to this challenge, which is the use of

an inclined plate in conjunction with ultrasonic standing waves. The Ultrasonically Enhanced

Inclined Settler (UEIS) device produces acoustic flocculation combined with the compacted area

maximization provided by the inclined settler (Figure 56). The main characteristics of the UEIS

device are the acoustic chamber with an internal Acoustic Transparent Layer (ATL). The

inclined ATL and reflector plate increase the settling area creating a layered separation of the

material as indicated by regions corresponding to a different average mass density. An acoustic

wave is generated through the chamber and the ATL to enhance settling and the flocculated

product is recovered in a concentrated fluid that exits from the bottom of the unit while the dilute

fluid exits from the top.
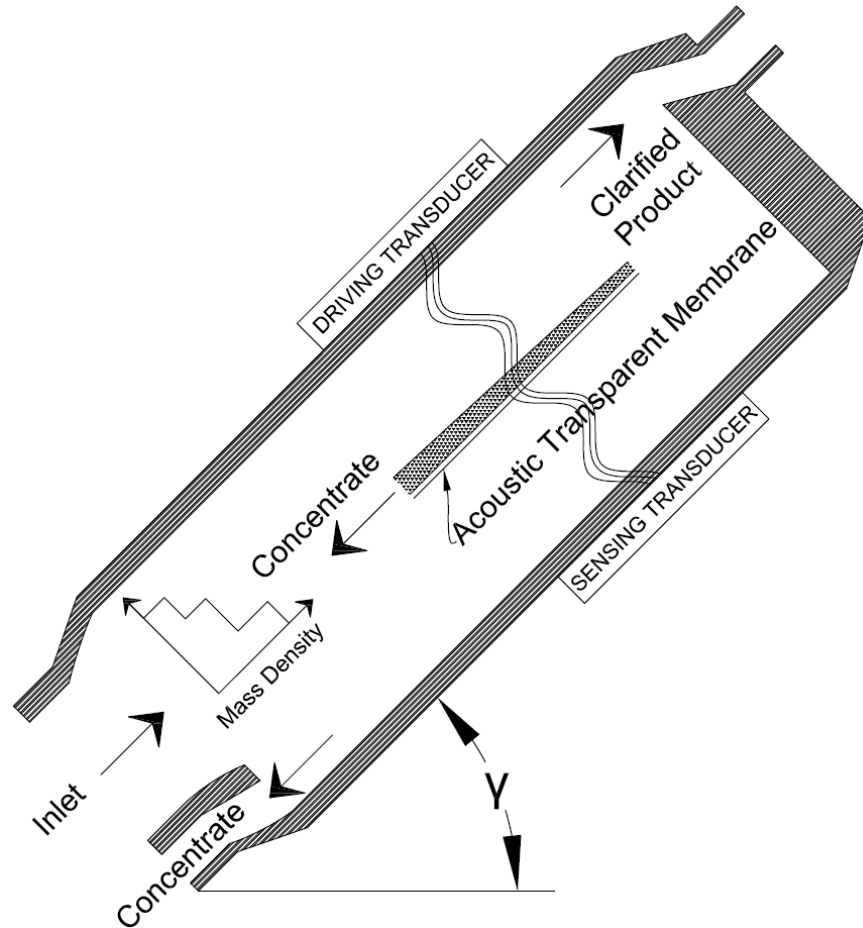
Figure 56. Schematic diagram of the UEIS device indicating the Inclined Chamber and Acoustic
Transparent Layer

ATL membranes have been used in the past to provide the necessary cooling layer for

ultrasonic separation units [63,68]. In acoustics, the transmission of a normal acoustic wave through

an interface is a function of the impedance between the materials:

$$u_t = \frac{2Z_A}{Z_A + Z_B} u_i \tag{24}$$

The acoustic impedance of Kapton® has been estimated at 2 MRayls [69]. The acoustic impedance of water 1.6 MRayls and therefore $u_t \approx 0.88u_i$. Therefore, the majority of the acoustic wave passes through the ATL while, for the fluid, the ATL represents a no-slip barrier such as a plate used in inclined settlers.

Here, we present the performance results of laboratory scale UEIS device used to harvest *N. oculata* and *Saccharomyces cerevisiae* cells. Polyamide particles were also used to assess the performance of the unit.

6.2 Materials and Methods

6.2.3 The acoustic harvester

The components of the laboratory scale UEIS unit are shown in Figure 57. The acoustic harvester consists of a set of aluminum holding plates , driving transducer disc, driving glass plate, chamber body, acoustic transparent membrane, sensing transducer disc and reflector glass. The PZT transducer discs were obtained from Steiner & Martins, Inc (Miami, FL, USA) made from a modified PZT-4 material. The driving disc was chosen with a resonance frequency of 1.5 MHz ± 5% The sensing piezoelectric had a different resonance frequency of 2.5 MHz ± 100 KHz to offset the natural frequencies of the chamber and to obtain an accurate measurement of the resonance modes of the system. Both the driving and reflector plates were made of glass to enable visual observation of the acoustic flocculation inside the chamber. The glass driving plate had 3/16" thickness and the reflector plate was ¼" thick to match the acoustic resonance of the

water layer in the range of 1.6 – 1.8 MHz as explained in §6.1.1. Both the driving and sensing piezoelectric discs were attached to the glass with an epoxy bonding (liquid nails®, PPG Industries, USA). The ATL was fabricated from Kapton® polyamide film of 125 μm and a length of 2". The chamber body was built by stereolithography using a water resistant resin and consisted of one inlet and two outlets. The internal dimensions of the chamber were 1" thick by 1.5" wide by 3" long with an internal volume of 76 mL.
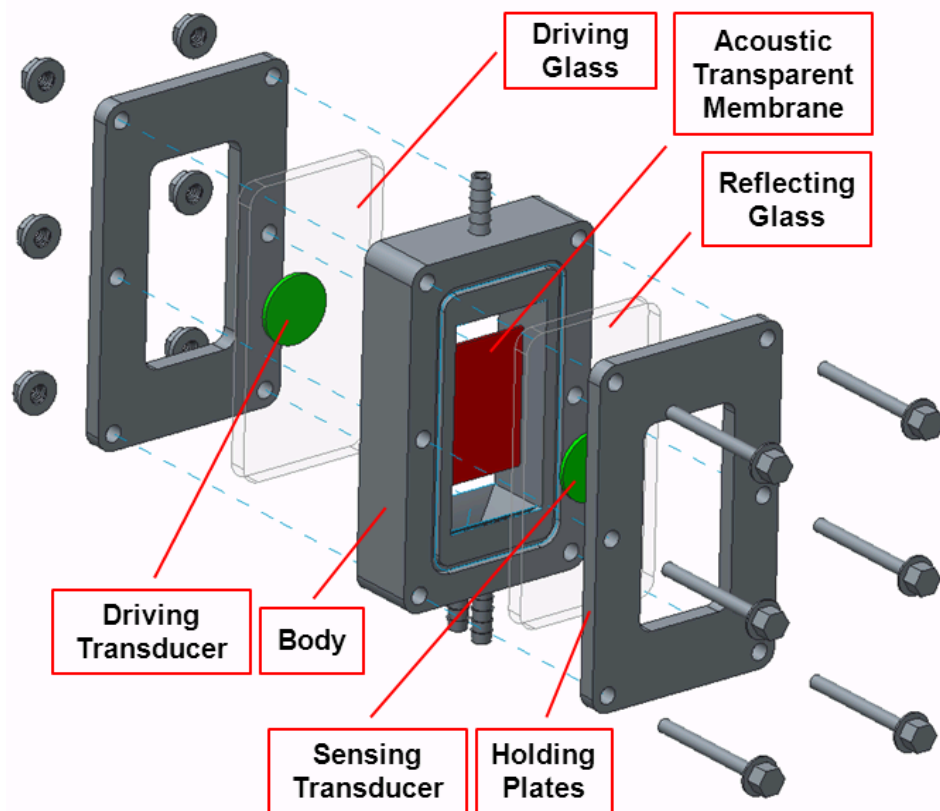
Figure 57. Design of the UEIS device indicating the driving and sensing PZT and reflecting plates

6.2.4 The resonance modes

The resonance modes of the acoustic chamber were characterized by measuring the amplitude in the frequency domain of the chamber using a driving transducer connected to a

sinusoidal waveform generator (33220A, Agilent, USA), which performed a frequency sweep

with a V_{pp} = 5 V. An opposite sensing transducer was connected to an oscilloscope (54855,

Agilent Technologies, USA) that recorded amplitude and frequency. Figure 58 indicates the

amplitude of the transmitted acoustic signal versus frequency. The peaks correspond to the

standing waves of the chamber in which the acoustophoretic force is maximized as explained in

§6.2.1. The largest acoustic response peak was ca. 1742 kHz with adjacent modes every 29 kHz

as a consequence of the water layer thickness (L = 1"). This peak corresponds to a superposition

of the glass reflector resonance (f_n = 1294 kHz, 1741 kHz, etc.) and the driving piezoelectric

resonance (f_n = 1738 kHz).
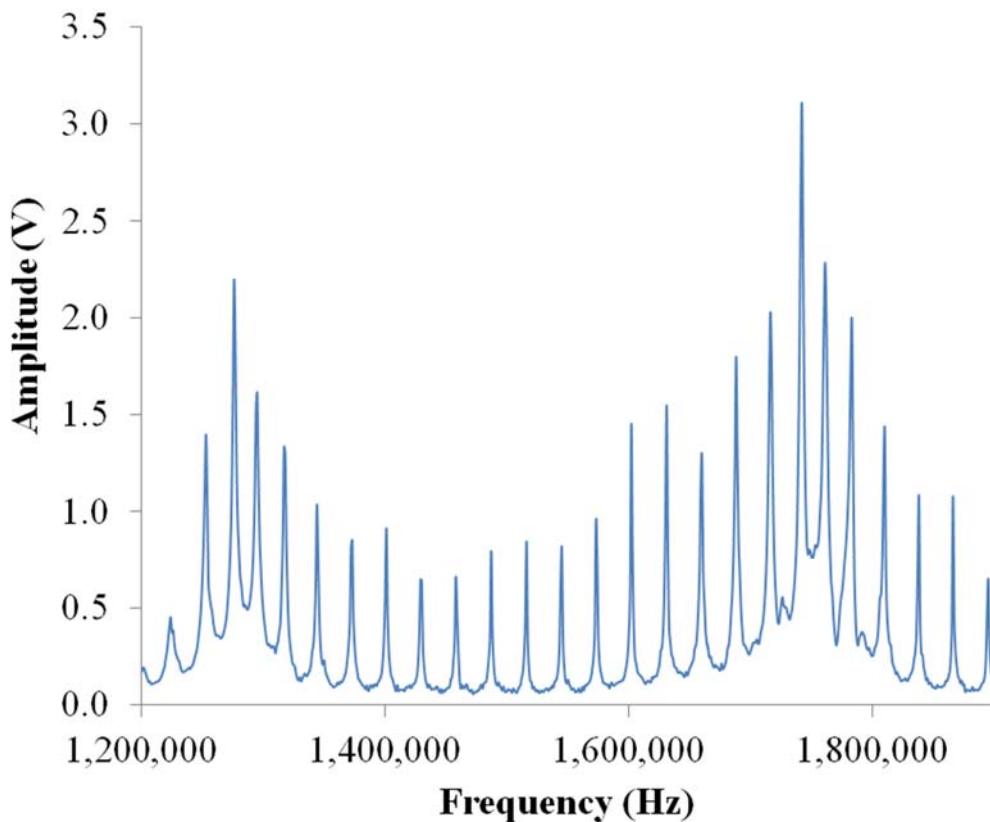
Figure 58. Acoustic frequency response of the UEIS using a sinusoidal excitation signal of 5 V_{pp} and a frequency sweep of 1 Hz. The water resonance modes are spaced every 29 kHz and the best resonance condition is close to 1,742 kHz.

One difficulty of acoustic separation is that the resonance modes shift with the change of the temperature of the liquid layer. This phenomenon is a consequence of the variation of the speed of sound (c) with the temperature and has a critical impact in the acoustophoretic force and therefore the separation performance. To maintain high performance, accurate temperature control is required combined with a frequency tracking algorithm as explained in the following section.

6.2.5 Experimental set up

The acoustic system and experimental setup is depicted in Figure 59. For each set of experiments, samples of *N. oculata*, *S. cerevisiae* or polyamide particles were placed in a graduated glass beaker and constantly mixed by a magnetic stir plate. The container was also immersed in a water bath kept at 15 °C ± 2 °C to preserve the samples for each series of tests. This procedure also maintained the culture temperature constant and therefore the speed of sound constant to reduce the shift in the resonance frequency. The pump #1 (peristaltic pump, Masterflex L/S Digital Drive with Easy-Load II pump head, Cole-Parmer, IL, USA) delivered the sample to the acoustic separator at the specified flow rate (f_i) with platinum-cured silicone tubing (Masterflex, IL, USA). A continuous flow rate (f_c) was drawn from the acoustic chamber with the concentrated cell slurry by pump #2 (Masterflex C/L Variable-Speed Tubing Pump; 50 to 300 rpm, Cole-Parmer, IL, USA) and returned to the sample container for its re-use after stirring. The difference between f_i and f_c provided the diluted flow rate (f_d), which returned to the sampling container for continuous agitation. The concentrated flow rate (f_c) was maintained constant at 1.24 mL · min^{-1}. All of the flow rates presented below are the inlet flow rates obtained by pump #1 (f_i). A separate recirculating loop was used to collect the inlet sample. The

sampling tubing was located next to the inlet tubing as shown in Fig. 59. We obtained the

samples from each returning line by collecting 3 mL aliquots into plastic vials.
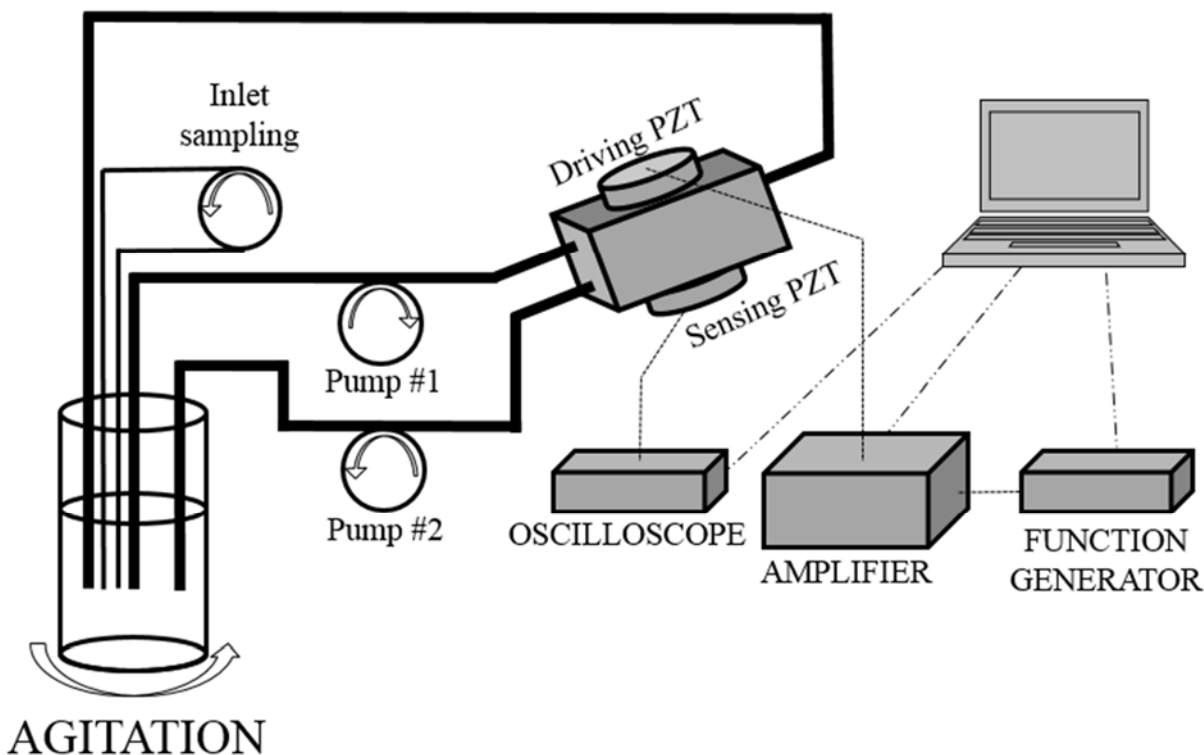
Figure 59. Acoustic testing setup indicating the feedback recirculating loop and the PC control system

An arbitrary waveform generator was used to generate a sinusoidal wave with a peak-to-peak voltage (V_{pp}) of 150 mVpp that was amplified by a broadband linear RF power amplifier (350L, Electronics & Innovation, Ltd. Rochester, NY, USA) to generate the acoustic standing wave. The sensing piezoelectric transducer disc was connected to the digital oscilloscope that measured the frequency and amplitude of the acoustic wave. The oscilloscope and the function generator were connected to a PC workstation. We designed a control algorithm in the graphical programming platform LabView® (National Instruments Corporation, USA) that performed a frequency sweep to detect the resonant modes of the chamber. A similar feedback loop has been

suggested in the literature [70]. The amplifier was also connected to the workstation by an RS - 232 cable and provided readings of the net amplified power supplied to the system ($P_N = P_f - P_r$).

6.2.6 Sampling statistics

The chamber residence time was calculated for each flow rate. The sample rate was defined every two consecutive residence times. For example, for $f_i = 25$ mL $\cdot$ min^{-1} the residence time was 175 s. We collected three samples, one at 175 s, one at 350 s and one at 525 s, or at each two residence times, and this was considered one test ($n = 1$). The unit was then fully drained and rinsed. Next, the test was repeated two additional times ($n = 3$) and the mean and standard deviation was calculated for all of the dependent variables measured. The error bars presented in the figures below represent the calculated standard deviations for all measurements. The inlet concentration was sampled every time to ensure a proper evaluation of the performance of the system since the sample was recirculated in each test. If the variation within the test was higher than 10% the test was discarded.

6.2.7 Cell cultivation, sample preparation and acoustic contrast factor

N. oculata cultures were provided by Solix Biosystems (Fort Collins, CO). The strain used was 525 from the NCMA Bigelow Laboratory for Ocean Sciences and was cultivated in a Solix AGS photobioreactor under outdoor conditions until the cell concentration reached ca. 3 x 10^8 cells $\cdot$ mL^{-1} (dry weight of ca. 3.2 g/L). The media used was a modified f/2 recipe with a salinity of 16 g $\cdot$ L^{-1}, 10 mM NO$_3^-$ L^{-1}, 7.9 mM PO$_4^-$ L^{-1} and 1 mL $\cdot$ L^{-1} of Guillard trace metals.

S. cerevisiae (Brewer's yeast) and Yeast Extract Peptone Dextrose (YPD) powder were obtained from Fisher Scientific (USA). The yeast (1 g) was cultivated in 500 mL of demineralized water with 50 g $\cdot$ L^{-1} of YPD at 27 °C for 48 h until the cell concentration was 3.0 x 10^7 ± 9% cells $\cdot$ mL^{-1}. Spherical polyamide particles (Dantec Dynamics A/S, Skovlunde,

Denmark) with a mean diameter of 5 µm were diluted in demineralized water with surfactant Tween^{TM} 20 at a concentration of 0.01% v/v. The concentration of particles used was 2 g · L^{-1}.

The cell diameter was estimated for n = 25 cells using a microscope and a measuring grid. (Nikon TM-50, Japan). The mean diameter of the *N. oculata* was 3.72 µm ± 23% and for *S. cerevisiae* was 7.8 µm ± 16%. The cell density and speed of sound were measured by concentrating the cells, measuring the biovolume and determining the speed of sound and density using an Anton Paar DSM5000 vibrating tube densitometer. The volumetric factor was computed for each sample and the cell speed of sound and density were determined using Urick's equations [71]. The results for *N. oculata* were ρ = 1.042 g · cm^{-3} ± 2%, c = 1533 m · s^{-1} ± 3% and F = 0.03 and for *S. cerevisiae* were ρ = 1.162 ± 1%, c = 1596 ± 2% and F = 0.12.

6.2.8 Cell density and separation performance

The cell density in terms of number of cells · mL^{-1} was measured using a hemocytometer counting chamber (Bright-Line, Sigma Aldrich). Ten cell counts were performed and the standard deviation reported. The optical density was measured with a spectrophotometer at 750 nm for *N. oculata* (GENESYS™ 20, Thermo Fisher Scientific Inc. USA) using disposable polystyrene cuvettes with a 10 mm light path (Fisherbrand™, Thermo Fisher Scientific Inc. USA). The valid absorbance was defined between 0.1-1 absorbance units [Au] and all the samples were serially diluted until the absorbance was in the mentioned range and the dilution factor was recorded. A calibration curve relating absorbance to cell count was derived for each sample of interest with *N. oculata* (y = 3.7 x 10^{7}OD$_{750}$, R^2 = 0.97) *S. cerevisiae* (y = 6.0 x 10^{6}OD$_{600}$, R^2 = 0.99) and polyamide particles (y = 6.4 x 10^6 OD$_{600}$, R^2 = 0.99).

The filtration efficiency (φ) and concentration factor (ε) were calculated from the following equations as previously suggested in the literature [46,72]:

$$\varphi = \frac{x_i - x_d}{x_i} \qquad \varepsilon = {x_{ctr}}/{x_i} \qquad\qquad (25 \text{ and } 26))$$

where x_i is the inlet cell concentration, x_d the diluted outlet cell concentration and x_{ctr} the concentrated outlet cell concentration.

6.2.9 Effects of concentration, power, flow rate and inclination angle

The applied Voltage (V_{pp}) to the RF amplifier was varied from 50 mV$_{pp}$ to 300 mV$_{pp}$, which corresponded to 1 to 13 W of net acoustic power. The forward power (P_f) into the PZT and reflected power (P_r) from the PZT were measured every 20 s. The net acoustic power was determined by $P_N = P_f - P_r$ over the duration of the test. The standard deviation for P_N was calculated for $n = 3$ and is represented in the error bars.

The effect of flow rate on the filtration efficiency was determined by increasing the inlet flow rate (f_i) from 20 to 80 mL $\cdot$ min^{-1}. The other variables such as γ, c_i and P_N were kept constant for these tests. The influence of cell concentration on the separation performance was also evaluated. For these experiments, the highest culture concentration was used to determine the maximum filtration efficiency. Then culture was serially diluted in original media to determine the change in the performance of the unit. Lastly, the effect of the inclination angle (γ) on the separation efficiency was determined. Specifically, the inclination of the unit was varied from 0 to 90° by using a steel protractor with a precision of ±5°.

6.2.10 Comparison with other designs reported in the literature

The filtration efficiency of the UEIS device was compared with other approaches reported in the literature for cell harvesting. Kilburn *et al.* proposed several designs and one of them is the foundation for the semi-continuous acoustic separator BioSep® [73]. This design is

characterized by a vertical orientation ($\gamma = 0$) and does not use an internal ATL. One challenge of the vertical design is that the flow will create a direct opposition between the drag force and the gravity force. In the present study, we tested a vertical chamber with no ATL as indicated in Table I (a). Another design proposed by Kilburn *et al.* does have an internal ATL. In this design, the ATL is used to create a "U" shaped flow in an attempt to create a settling area at the bottom of the chamber. However, a problem with this design is that the liquid bulk velocity (v_f) is doubled since the cross sectional area is reduced by half. This increases the critical radius required for settling. In the present study, we tested a vertical chamber with an internal ATL in a "U" configuration as indicated in Table 6 (b). Another design reported in the literature uses an inclined chamber with UES [74]. Here, we tested an inclined separation chamber without intermediate ATL as indicated in Table I (c) with $\gamma = 50°$. Another design reported in the literature uses an inclined plate settler without the use of UES [75]. Here, we tested the inclined chamber without UES and $\gamma = 50°$ as indicated in Table 6 (d). To initially compare the performance of the UEIS in comparison with a similar device without UES, the UEIS device was tested as indicated in Table 6 (e) with $\gamma = 50°$.

In this study we tested all the previously mentioned designs of Table 6 with a culture of *N. oculata* and the same conditions of cell inlet concentration ($c_i = 3.08$ x 10^8 mL^{-1}), inlet flow rate ($f_i = 25$ mL $\cdot$ min^{-1}), concentrated flow rate ($f_c = 1.24$ mL $\cdot$ min^{-1}), and applied wave voltage ($V = 200$ mV$_{pp}$).

6.3 Results and Discussion

6.3.1 Effects of Net Input Power and System Throughput

Figure 60 is a plot of filtration efficiency as a function of net power input for *N. oculata*, *S. cerevisiae* and spherical polyamide particles, respectively. These experiments were conducted

at a fixed inclination angle of 50°. As shown in Fig. 60, the filtration efficiency increased with increasing net power applied to the piezoelectric disc by the amplifier for all cells and particles tested. The filtration efficiency (φ) increased sharply for the polyamide particles from 12% ± 4% at 1.9 ± 0.7 W to 83% ± 6% when the power was increased to 7.4 ± 0.9W (equivalent to 99 W · L^{-1}). Similar behavior was observed for the *S. cerevisiae* culture in which an increase in filtration efficiency (φ) from 49% ± 3% to 79% ± 4% was observed. The efficiency also increased when the *N. oculata* cells were used. For the *N. oculata* cells, the filtration efficiency doubled when the power input was doubled. The device achieved a filtration efficiency of 70% with a net power input of 5.5 W for *N. oculata*. This corresponds to an energy consumption of 3.6 kWh · m^{-3}. Collectively, these results suggest a strong dependence of the filtration efficiency with $\boldsymbol{P_N}$. This result is a consequence of higher acoustic power resulting in increased acoustic energy density ($\boldsymbol{E_{ac}}$) and increased acoustophoretic force acting on the particles (See Equation 22). The increased acoustophoretic force results in increased particle velocity towards the acoustic nodes, which promotes agglomeration for enhanced settling. Nii et al. and Leong et al. also found an increasing separation efficiency with power for oil droplets and milk fat creaming [76,77].
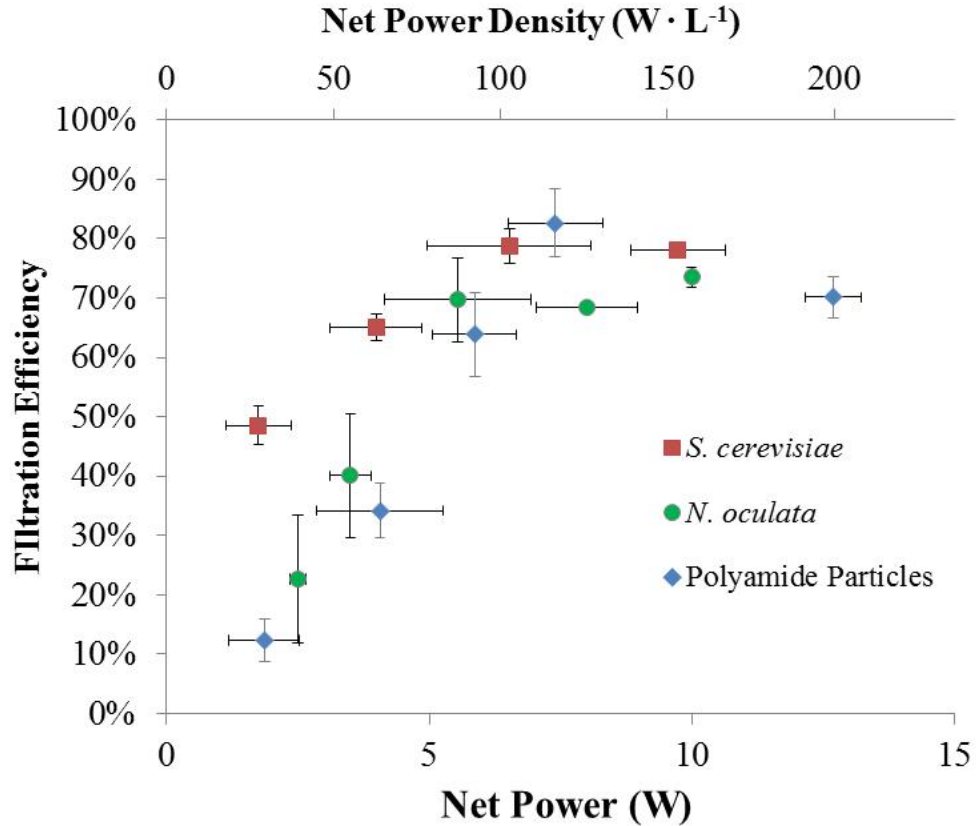
Figure 60. Effect of the power input on the filtration efficiency with a flow rate of 25 mL · mL-1 and γ = 50°for the UEIS. The filtration efficiency and the power input increase proportionally in the UEIS. The error bars indicate the standard deviation.

However, the increase in efficiency with net power was only observed for net power less than P_N = 7.5 W or 100 W · L^{-1}. At higher levels of power input, the filtration efficiency of the *S. cerevisiae* and *N. oculata* were roughly constant and the filtration efficiency for the polyamide particles decreased. We observed the presence of circulation zones in front of the driving PZT, which resulted in flow reversal that limited the performance of the unit for higher power inputs. Previous publications have suggested the formation of convective currents inside the device when the applied power is increased above a certain value [78,79]. For example, it has been shown that temperature gradients inside the chamber produce circulation patterns that inhibit particle flocculation. For this reason, some acoustic separation designs are air cooled [80]. Acoustic

streaming created by the dissipation of acoustic energy has also been suggested as responsible for decreasing the separation efficiency [81]. Acoustic Transparent Layers have been used to decrease the streaming path length and enhance particle flocculation [82].

Figure 61 is a plot of measured filtration efficiency as a function of the total system throughput (i.e. volume flow rate) and associated average bulk velocity for the *S. cerevisiae* and *N. oculata* cultures. The two samples exhibited a decrease in the filtration efficiency with increasing flow rate and liquid velocity. This result is in agreement with Equation 23 since a higher bulk velocity results in a squared increase in the critical radii for settling. Furthermore, increasing the flow rate also decreases the residence time of the cells in the vicinity of the acoustic field, which reduces the time available for flocculation. Similar results of reduced performance with increasing flow rates are characteristic of UES and Inclined Plate devices. Therefore, scaling up the technology will potentially require multiple units to process large flow rates with low superficial velocities. As shown in Fig. 61, the reduction in filtration efficiency with increased flow rate was more dramatic for *N. oculata* in comparison to *S. cerevisiae,* which can be attributed to higher cell volume, higher density and higher acoustic contrast factor of the yeast in comparison to the microalgae. Cells with a lower acoustic contrast factor will require more time to agglomerate in the nodes or antinodes of the acoustic field and this decreases their probability of settling for the same residence time.
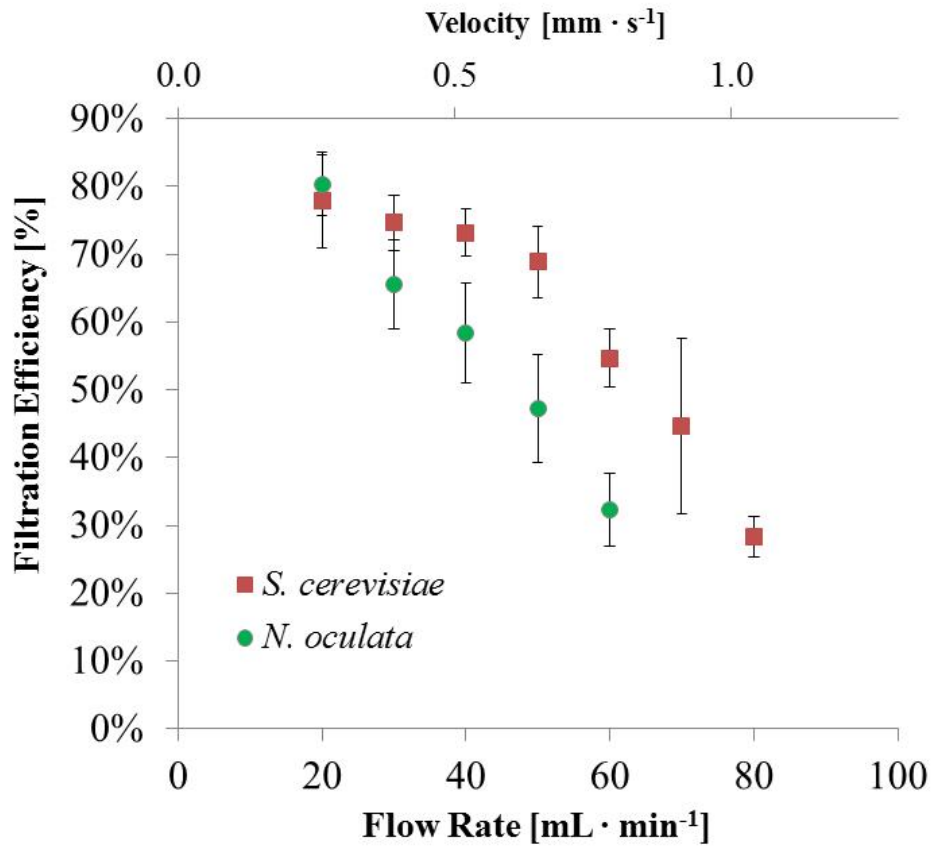
Figure 61. Effect of cell concentration on the filtration efficiency with a flow rate of 25 mL · mL^{-1}, $\gamma = 50°$, and a net power input P_N = 5 W for the UEIS. Lower inlet cell concentration reduces the filtration efficiency of the UEIS.

6.3.2 Effects of Culture Concentration and Inclination Angle

As shown in Fig. 62, the effect of the sample concentration on filtration efficiency was also assessed. When the sample of *S. cerevisiae* had a high cell concentration of 3.1 x 10^7 cells · mL^{-1} the filtration efficiency was the highest at 82% ± 4% and the efficiency decreased logarithmically to 52% ± 6% when the sample was diluted to 9.25 x 10^5 cells · mL^{-1}. A similar effect was observed for the *N. oculata* cells where the highest efficiency of 75% ± 4% was achieved with a cell concentration of 3.1 x 10^8 cells · mL^{-1} (dry weigh of ca. 3.2 g/L) followed by an exponential decrease to 11% ± 9% at 3.1 x 10^7 cells · mL^{-1}. This decrease in the filtration efficiency can be explained by Equation 23. Here, the acoustophoretic force is used to create a

cell agglomeration of 3 x 10^5 cells, which is equivalent to an agglomerated radius of 100 μm. The agglomerated volume will settle only when the critical radius is exceeded. However, the cells can only travel λ/4 and they must do it while passing through the acoustic field. Therefore, decreasing the cell concentration will decrease the number of cells available in the λ/4 vicinity to achieve r_c. Also, farther cells will have to travel a longer distance to achieve r_c, and the probability of the agglomerated volume exiting the acoustic field before the critical radius is achieved will be higher. This logarithmic dependence with the concentration has also been reported in previous publications [79]. The cell concentration required to exceed a filtration efficiency of 50% in our experiments was 5 x 10^5 cells · mL^{-1} for the *S. cerevisiae* and 7 x 10^7 cells ·mL^{-1} for *N. oculata* cells. *N. oculata* cells require a higher cell concentration due to their lower density, smaller cell diameter and lower acoustic contrast factor in comparison to *S. cerevisiae*. However, since *Nannochloropsis* sp. bioreactors usually operate in cell concentrations of 10^8 cells ·mL^{-1} [83], the UEIS described herein is a viable technology for this application. More work will need to be done to achieve reasonable filtration efficiencies for more dilute cultures such as those more typical in open ponds since the efficiency of the UEIS device achieved filtration efficiencies of 30% or lower under these dilute conditions of 6 x 10^7 cells · mL^{-1}.
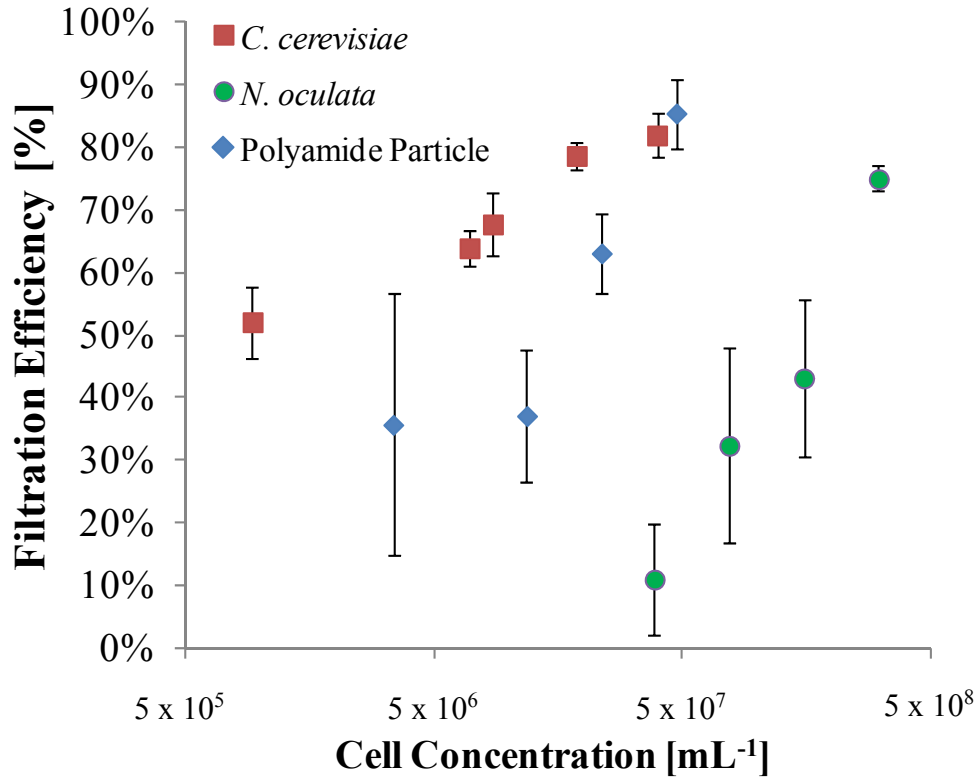
Figure 62. Effect of cell concentration on the filtration efficiency with a flow rate of 25 mL · mL^{-1}, $\gamma = 50°$, and a net power input $P_N = 5$ W for the UEIS. Lower inlet cell concentration reduces the filtration efficiency of the UEIS.

Finally, as shown in Fig. 63, the influence of the inclination angle on the concentration factor (ε) was assessed. The concentration factor is defined as the ratio of the outlet concentration to the inlet concentration. The results of this study suggest a very strong dependence of inclination angle (γ) on the measured concentration factor. The concentration factor increased from 1.2 ± 0.1 when the UEIS was operated horizontally ($\gamma = 0°$) to 8.5 ± 1.9 when the unit was inclined to $\gamma = 50°$. The concentration factor decreased to 2.4 ± 0.1 when the unit was vertically oriented ($\gamma = 90°$). The separation performance is inversely proportional to the angle. Under vertical operation, the critical radius is the largest. However, under horizontal operation, the critical radius is zero but it is difficult to recover the biomass while avoiding clogging of the unit without greatly increasing the fluid velocities due to the constraint in cross

sectional area. The increase in the angle produces a self-cleaning effect on the inclined plates wherein the biomass slides along the inclined plates and settles at the bottom of the unit for its recovery [84]. Here, the optimum angle that results in maximum self-cleaning effect while minimizing critical settling radii was found to occur at $\gamma = 50°$. Other applications for inclined settling have reported optimum inclination angles of 50 - 60° [85].
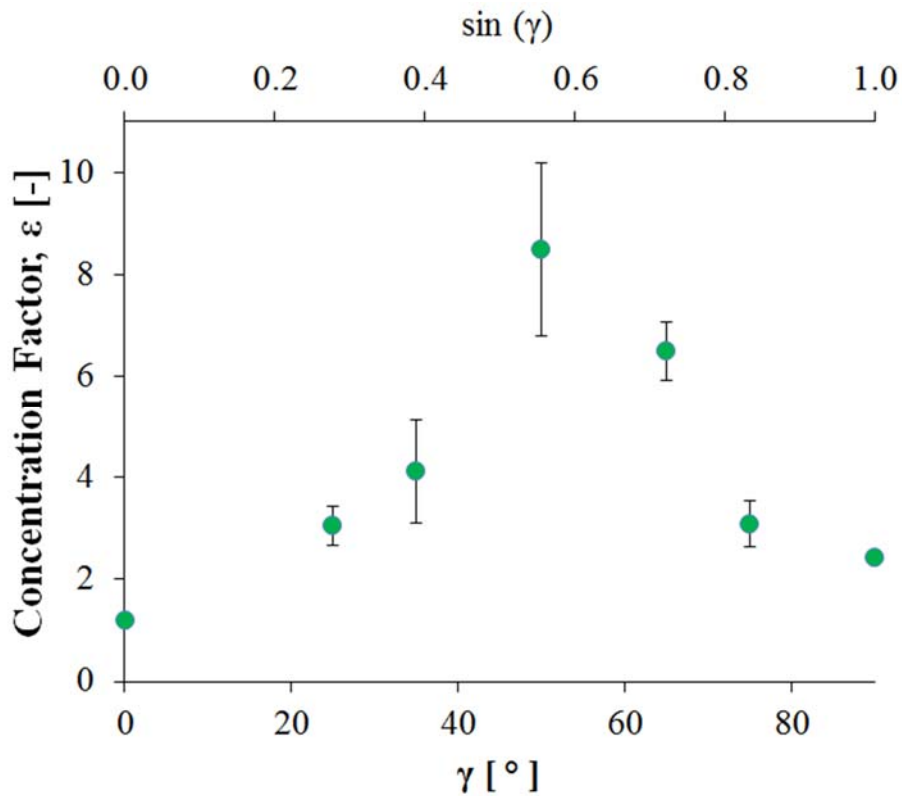
Figure 63. Effect of the inclination angle with a flow rate of 25 mL · mL^{-1}, constant inlet cell concentration and input voltage of 200 mVpp for the UEIS. There is an optimal angle of operation close to 50°.

6.3.3 Comparison of the UEIS with other designs

The results of Table 6 show that the UEIS achieved the highest filtration efficiency of $70\% \pm 5\%$ and a concentration factor of 11.6 ± 2.2. The control inclined plate settler, which was configured as described by Thompson and Wilson (1998) without UES, achieved a filtration

efficiency of 10% ± 1% and a concentration factor of 1.2 ± 0.1. A similar configuration has been successfully used for animal cells [66]. However, as explained in §2.1, the *N. oculata* cells are smaller than those reported by Choo et al (2007) and have a density closer to that of water. This indicates that the increased gravity effect alone did not separate the microalgae cells from the continuous flow. Therefore, the use of the acoustophoretic settling resulted in a factor of 7 increase in filtration efficiency under the same conditions of velocity, angle and cell concentration. The chamber was also oriented vertically ($\gamma = 0°$) with and without a "U" flow divider as previously suggested by Kilburn *et al.* (1997). The results are shown in Table 6 a) and b). The efficiency of the vertical chamber without ATL divider was 30% ± 7% which was lower than the same configuration with the divider (43% ± 7%). This result indicates that the divider enhanced the performance of the chamber by forcing a change in the fluid direction.

Inclined plate settlers increase the effective settling area that results from the projection of the extended area in the horizontal plane. The extended settling surface area equation is defined elsewhere [86]. The calculated surface area for each configuration is shown in Table 6. The effective area for cases a) and b) was considered as the area of the bottom outlet. Both options had similar performance with the "U" shape design slightly superior in terms of filtration efficiency. However, the small settling area combined the direct with opposition of the gravity and drag force in both cases results in a lower filtration efficiency compared to the UEIS. The UEIS reported herein resulted in a twofold increase in filtration efficiency and concentration factor. A benefit of the "U" design is faster biomass recovery, which could be an important criterion for sensitive cells that require low residence times inside the chamber.
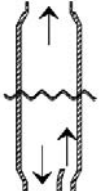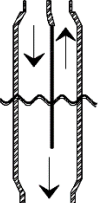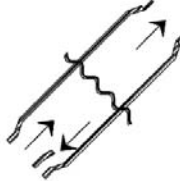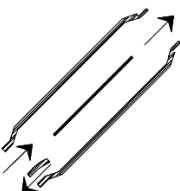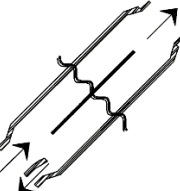
The UEIS was also compared with an inclined chamber proposed elsewhere where the acoustic propagation axis has an acute angle with the flow [74]. The difference between the UEIS

and this design is the presence of an inner ATL for inclined settling, so the effective area can be

increased as shown in Table 6 c) and e). The UEIS had a factor of 1.5 higher filtration efficiency

than the inclined chamber without ATL. This increase in the filtration efficiency was

proportional to the increase in the projected area as a consequence of the ATL.

In conclusion, the UEIS design produced 1.5 to 7.5 fold higher filtration efficiencies than

other designs suggested in the literature when compared under the same conditions of flow rate,

cell concentration and power.

Table 6. Comparison with different designs suggested in the literature

Brief Description	Design Tested	Filtration Efficiency	Concentration Factor	Settling Area
a) Vertical UES harvesting chamber without internal ATL [68,87,88].		30% ± 7%	3.0 ± 0.2	7.7 cm^2
b) "U" shape UES harvesting with an ATL division (Kilburn *et al.* 1997)		43% ± 7%	3.6 ± 0.2	9.6 cm^2
c) Inclined UES harvesting chamber without an intermediate ATL		48% ± 6%	2.0 ± 0.5	20.5 cm^2
d) Inclined cell settler (Thompson and Wilson 1998)		10% ± 1%	1.2 ± 0.1	34.2 cm^2
e) Our design		70% ± 5%	11.6 ± 2.2	34.2 cm^2

7. CONCLUSIONS AND RECOMMENDATIONS

Microalgae harvesting is a critical challenge for the scale up of microalgae derived biofuels and bioproducts. Ultrasonically Enhanced Sedimentation offers an alternative to existing methods for harvesting microalgae cells with no moving parts, suggesting lower operational and maintenance costs.

First, this research proposed the Urick's equations as a valid approach to estimate the speed of sound and density of microalgae cells. The acoustic contrast factor is a critical parameter in acoustic separation and is solely dependent in the differences of speed of sound and density between the media and the cell. We applied this new approach to quantify the acoustic contrast factor of microalgae cells by measuring the density and speed of sound using an Anton Paar vibrating tube densitometer. *P. tricornutum*, *N. oculata* and *N. gaditana* samples exhibited a highly linear relationship between volumetric factor and density and speed of sound. The calculated the density of the cell was *N. gaditana* 1.047 g·cm^{-3}, *N. oculata* was 1.034 g·cm^{-3}, *P. tricornutum* was 1.073 g·cm^{-3}. The calculated speed of sound of the *N. gaditana* cell was 1544 m·s^{-1}, *N. oculata* was 1529 m·s^{-1}, *P. tricornutum* was 1547 m·s^{-1}. The estimated average contrast factor for *N. gaditana* was 0.06, *N. oculata* was 0.05 and *P. tricornutum* was 0.05. The measured *S. cerevisiae* contrast factor was 0.1 indicating that these cells have a stronger acoustic response and therefore are better suited for acoustic separation. The *S. cerevisiae* had a 6 fold higher *RxF$_{ac}$* factor compared to the microalgae strains.

We performed PTV on the acoustophoretic motion of *C. reinhardtii* cells. The nitrogen abundant cells presented a higher contrast factor than the nitrogen deprived cells what was in agreement with the speed of sound and density measurements. The acoustophoretic force was

calculated as 5 pN indicating the small magnitude of this force. Also, the acoustic contrast factor of *C. reinhardtii* sta6 was found to change from positive to negative as consequence of lipid accumulation. This is something that has not been reported previously in the literature.

Here, we also presented a novel design that was developed by a combination of UES and inclined settling. A lab scale UEIS was built with an internal Acoustic Transparent Layer and with an effective settling area higher than other designs.

The results of this study showed that the filtration efficiency of the UEIS device decreased with increasing flow rate. The filtration efficiency increased proportionally with the input power for lower net input power but decreased after a net power input of $100 \text{ W} \cdot \text{L}^{-1}$, which could be attributed to convective currents inside the device. It was found that an optimal operational inclination angle existed at 50°. Higher inlet cell concentrations increased logarithmically the performance of the unit. The UEIS design was compared with previous designs suggested in the literature under the same conditions of flow rate, power and inclination, and it was found that the performance is 1.5 to 7.5 times higher in terms of the filtration efficiency. Overall, the use of UEIS design was successfully demonstrated for *N. oculata* and *S. cerevisiae.*

8. FUTURE WORK

There different areas of suggested future work for this technology. First, a purely experimental approach would require numerous iterations to identify the best combination of forces making the process time consuming and capital intensive. It is possible to develop a Finite Element Model (FEM) that will determine the cell trajectories according to the flow rate and pressure wave intensity. Previous papers have found a good agreement between the predicted radiation potential and the experimental results [89]. Future research could use Finite Element packages such as COMSOL® to determine the best configuration to separate algae. Second, future research could also focus in developing a better understanding of acoustic transparent membranes and a comparison of the best materials for these membranes considering factors such as acoustic impedance and durability. This an important component in the process of scaling up the device.

Third, it should also be noted that the theoretical treatment for the derivation of the acoustic radiation force, $\mathbf{F_{ac}}$, assumes spherical particles of homogeneous composition. While some species of microalgae such as *N. salina* are relatively spherical, many species deviate highly from the spherical assumption. Therefore a future area of research could focus in understating the acoustophoretic behavior of different shapes of cells with strains such as *Scenedesmus sp.* or *Phaeodactylum tricornutum*.

Fourth, although the acoustic contrast factor of the *N. gaditana*, *N. oculata* and *P. tricornutum* was always positive, additional studies are now necessary to find a potential change to negative contrast factor as consequence of stressing and lipid accumulation.

REFERENCES

1. Hirsch RL, Bezdek R, Wendling R. Peaking of world oil production and its mitigation. *Aiche Journal.* 2006;52(1):2-8.

2. Hirsch R, Bezdek R, Wendling R. Peaking of world oil production. 2005.

3. Demirbas MF. Biofuels from algae for sustainable development. *Applied Energy.* 2011;88(10):3473-3480.

4. Chisti Y. Biodiesel from microalgae beats bioethanol. *Trends in Biotechnology.* 2008;26(3):126-131.

5. Mata TM, Martins AA, Caetano NS. Microalgae for biodiesel production and other applications: A review. *Renewable & Sustainable Energy Reviews.* 2010;14(1):217-232.

6. Wang B, Li YQ, Wu N, Lan CQ. CO(2) bio-mitigation using microalgae. *Applied Microbiology and Biotechnology.* 2008;79(5):707-718.

7. Fabregas J, Herrero C. Marine microalgae as a potential source of single cell protein (SCP). *Applied microbiology and biotechnology.* 1985;23(2):110-113.

8. O'Connell D, Savelski M, Slater CS. Life cycle assessment of dewatering routes for algae derived biodiesel processes. *Clean Technologies and Environmental Policy.* 2013;15(4):567-577.

9. Davis R, Aden A, Pienkos PT. Techno-economic analysis of autotrophic microalgae for fuel production. *Applied Energy.* 2011;88(10):3524-3531.

10. Uduman N, Qi Y, Danquah MK, Forde GM, Hoadley A. Dewatering of microalgal cultures: A major bottleneck to algae-based fuels. *Journal of Renewable and Sustainable Energy.* 2010;2(1):15.

11.   Grima EM, Belarbi EH, Fernandez FGA, Medina AR, Chisti Y. Recovery of microalgal biomass and metabolites: process options and economics. *Biotechnology Advances.* 2003;20(7-8):491-515.

12.   *Fundamentals of acoustics.* 4th ed. ed. New York: Wiley; 2000.

13.   Blauert J, Xiang N. *Acoustics for Engineers: Troy Lectures.* Springer; 2009.

14.   Yang L, Kian-Meng L. Particle Separation in Microfluidics using switching ultrasonic field. *Lab on a Chip.* 2011:3167 - 3173.

15.   Gupta S, Donald F, Zloczower M. Fractionation of Mixed Particle Solids According to Compressibility Using Ultrasonic Standing Wave Fields. *Chemical Engineering Science.* 1995:3275 - 3284.

16.   Petersson F, Nilsson A, Holm C, Jonsson H, Laurell T. Continuos separation of lipid particles from erythrocytes by means of laminar flow and acoustic standing wave forces. *Lab on a Chip.* 2004:20 - 22.

17.   Hawkes JJ, Limaye MS, Coakley WT. Filtration of bacteria and yeast by ultrasound-enhanced sedimentation. *Journal of Applied Microbiology.* 1997:39-47.

18.   Yoshioka K, Kawashima Y. Acoustic radiation pressure on a compressible sphere. *Acustica.* 1955:167 - 173.

19.   Lee CP, Wang TG. Acoustic radiation force on a bubble. *Journal of Acoustic Society of America.* 1993:1637-1640.

20.   Bruuns H. Acoustofluidics 7: The acoustic radiation force on small particles. *Lab on a Chip.* 2012:1014 - 1021.

21.   Gaida T, Doblhoff-Dier K, Strutzenberger O, et al. Selective retention of Viable Cells in Ultrasonic Resonance Field Devices. *Biotechnology Progress.* 2008:73-76.

22.   Benes E, Groschl M, Nowotny H, et al. Ultrasonic Separation of Suspended Particles. Paper presented at: Ultrasonics Symposium2001; Atlanta, GA.

23.   Dobloff-Dier O, Gaida T, Katinger H. A Novel Ultrasonic Resonance Field Device for the Retention of Animal Cells. *Biotechnology Progress.* 1994:428-432.

24.   Bosma R, van Spronsen WA, Tramper J, Wijffels RH. Ultrasound, a new separation technique to harvest microalgae. *Journal of Applied Phycology.* 2003:143-153.

25.   Tsutsui H, Ho C-M. Cell separation by non-inertial force fields in microfluidics systems. *Mechanics Research Communications.* 2009:92 - 103.

26.   Bohm H, Briarty L, Lowe K, Power B, Benes E, Davey M. Quantification of a Novel h - shaped Ultrasonic Resonator for Separation of Biomaterials Under Terrestrial Gravity and Microgravity Conditions. *Biotechnology and Bioengineering.* 2003:74 - 85.

27.   Johnson DA, Feke DL. Methodology for fractionating suspended particles using ultrasonic standing wave and divided flow fields. *Separations Technology.* 1955:251-258.

28.   Nilsson A, Petersson F, Jonsson H, Laurell T. Acoustic control of suspended particles in micro fluidic chips. *Lab on a chip.* 2003:131-135.

29.   Harris NR, Hill M, Beeby S, et al. A silicon microfluidic ultrasonic separator. *Sensors and Actuators.* 2003:425-434.

30.   Hill M, Wood RK. Modelling in the design of a flow-through ultrasonic separator. *Ultrasonics.* 2000:662-665.

31.   Hawkes JJ, Coakley TW, Groschl M, et al. Single half-wavelenght ultrasonic particle filter: Predictions of the transfer matrix ultrasonic resonator model and experimental filtration results. *Journal Acoustic Society of America.* 2002:1259-1266.

32.   Gorenflo VM, Smith L, Dedinsky B, Persson B, Piret JM. Scale-Up and Optimization of an Acoustic Filter for 200 L/day Perfusion of a CHO Cell Culture. *Biotechnology and Bioengineering.* 2002:438-444.

33.   Stolojanu V, Prakash A. Characterization of slurry systems by ultrasonic techniques. *Chemical Engineering Journal.* 2001:215-222.

34.   Coupland JN, McClements JD. Droplet size determination in food emulsions: comparison of ultrasonic and light scattering methods. *Journal of Food Engineering.* 2001:117 - 120.

35.   Challis RE, Povey MJ, Mather ML, Holmes AK. Ultrasound techniques for characterizing colloidal dispersions. *Reports on Progress in Physics.* 2005:1541-1637.

36.   Harker AH, Temple JA. Velocity and attenuation of ultrasound in suspensions of particles in fluids. *Journal of Applied Physics.* 1988:1576-1588.

37.   L.A. C. Acoustic force on a liquid droplet in an acoustic stationary wave. Vol 50. J. Acoust. Soc. Am.1971:157-163.

38.   Meinster R, Rodrique L. Ultrasonic Absorption and Velocity in Water Containing Algae in Suspension. *The Journal of the Acoustical Society of America.* 1960:556 - 559.

39.   Randall RH. *An Introduction to Acoustics.* Mineola: Dover Publications, Inc.; 2005.

40.   Hill M, Shen Y, Hawkes J. Modelling of layered resonators for ultrasonic separation. *Ultrasonics.* 2002:385-392.

41.   Ryll T, Dutina G, Reyes A, Gunson J, Krummen L, Etcheverry T. Performance of small-scale CHO Perfusion Cultures Using and Acoustic Cell filtration device for cell retention: Characterization of separation efficiency and impact of perfusion on product quality. *Biotechnology and Bioenegineering.* 2000:440 - 449.

42. Trampler F, Sonderhoff SA, Pui PW, Kilburn DG, Piret JM. Acoustic Cell Filter for High Density Perfusion Culture of Hybridoma Cells. *Nature Biotechnology.* 1994:281-284.

43. Raffel M, Willert C, Wereley ST, Kompenhans J. *Particle Image Velocimetry, A practical guide.* 2 nd Ed2007.

44. Bruus H. Acoustofluidics 7: The acoustic radiation force on small particles. *Lab on a Chip.* 2012;12(6):1014-1021.

45. Baker NV. SEGREGATION AND SEDIMENTATION OF RED BLOOD-CELLS IN ULTRASONIC STANDING WAVES. *Nature.* 1972;239(5372):398-&.

46. Bohm H, Briarty LG, Lowe KC, Power JB, Benes E, Davey MR. Quantification of a novel h-shaped ultrasonic resonator for separation of biomaterials under terrestrial gravity and microgravity conditions. *Biotechnology and Bioengineering.* 2003;82(1):74-85.

47. Lenshof A, Laurell T. Emerging Clinical Applications of Microchip-Based Acoustophoresis. *Jala.* 2011;16(6):443-449.

48. Radel S, McLoughlin AJ, Gherardini L, Doblhoff-Dier O, Benes E. Viability of yeast cells in well controlled propagating and standing ultrasonic plane waves. *Ultrasonics.* 2000;38(1-8):633-637.

49. Jacobsen F. *Fundamentals of general linear acoustics.* 2013.

50. Gould RK, Coakley WT, Grundy MA. UPPER SOUND PRESSURE LIMITS ON PARTICLE CONCENTRATION IN FIELDS OF ULTRASONIC STANDING-WAVE AT MEGAHERTZ FREQUENCIES. *Ultrasonics.* 1992;30(4):239-244.

51. Ilhan H, Savaroglu G. Temperature and Composition Dependence of Ultrasound Properties of Medical Nutrition Solutions Containing Carbohydrate, Protein, and Lipid. *Journal of Chemical and Engineering Data.* 2009;54(12):3281-3283.

52.   Johnson BL, Holland MR, Miller JG, Katz JI. Ultrasonic attenuation and speed of cornstarch suspensions. *J. Acoust. Soc. Am.* 2013:1399 - 1403.

53.   Fernandes BD, Dragone GM, Teixeira JA, Vicente AA. Light Regime Characterization in an Airlift Photobioreactor for Production of Microalgae with High Starch Content. *Applied Biochemistry and Biotechnology.* 2010;161(1-8):218-226.

54.   Challis RE, Povey MJW, Mather ML, Holmes AK. Ultrasound techniques for characterizing colloidal dispersions. *Reports on Progress in Physics.* 2005;68(7):1541-1637.

55.   Meinster R, Laurent R. Ultrasonic Absorption and Velocity in Water Containing Algae in Suspension. *The Journal of the Acoustical Society of America*1960: 556 - 559.

56.   Sweeley J. Ph.D. Dissertation. 2015.

57.   Hillebrand H, Dürselen C-D, Kirschtel D, Pollingher U, Zohary T. BIOVOLUME CALCULATION FOR PELAGIC AND BENTHIC MICROALGAE. *Journal of Phycology.* 1999;35(2):403-424.

58.   Gavish B, Gratton E, Hardy CJ. Adiabatic compressibility of globular proteins. *Proc. Natl. Sci.* 1983;80:750-754.

59.   Katz A, Avron M. DETERMINATION OF INTRACELLULAR OSMOTIC VOLUME AND SODIUM CONCENTRATION IN DUNALIELLA. *Plant Physiology.* 1985;78(4):817-820.

60.   King LV. On the acoustic radiation pressure on spheres. *Proceedings of the Royal Society of London. Series A-Mathematical and Physical Sciences.* 1934;147(861):212-240.

61.   Leong T, Johansson L, Juliano P, McArthur SL, Manasseh R. Ultrasonic Separation of Particulate Fluids in Small and Large Scale Systems: A Review. *Industrial & Engineering Chemistry Research.* 2013;52(47):16555-16576.

62.   Lenshof A, Evander M, Laurell T, Nilsson J. Acoustofluidics 5: Building microfluidic acoustic resonators. *Lab on a Chip.* 2012;12(4):684-695.

63.   Hawkes JJ, Limaye MS, Coakley WT. Filtration of bacteria and yeast by ultrasound-enhanced sedimentation. *Journal of Applied Microbiology.* 1997;82(1):39-47.

64.   Bosma R, van Spronsen WA, Tramper J, Wijffels RH. Ultrasound, a new separation technique to harvest microalgae. *Journal of Applied Phycology.* 2003;15(2-3):143-153.

65.   Boycott AE. Sedimentation of blood corpuscles. *Nature.* 1920;104:532-532.

66.   Choo CY, Tian Y, Kim WS, Blatter E, Conary J, Brady CP. High-level production of a monoclonal antibody in murine myeloma cells by perfusion culture using a gravity settler. *Biotechnology Progress.* 2007;23(1):225-231.

67.   Pohlscheidt M, Jacobs M, Wolf S, et al. Optimizing capacity utilization by large scale 3000 L perfusion in seed train bioreactors. *Biotechnology Progress.* 2013;29(1):222-229.

68.   Doblhoffdier O, Gaida T, Katinger H, Burger W, Groschl M, Benes E. A NOVEL ULTRASONIC RESONANCE FIELD DEVICE FOR THE RETENTION OF ANIMAL-CELLS. *Biotechnology Progress.* 1994;10(4):428-432.

69.   Haller MI, Khuriyakub BT. 1-3 COMPOSITES FOR ULTRASONIC AIR TRANSDUCERS. *Ieee 1992 Ultrasonics Symposium : Proceedings, Vols 1 and 2.* 1992:937-939.

70.   Hawkes JJ, Coakley WT. A continuous flow ultrasonic cell-filtering method. *Enzyme and Microbial Technology.* 1996;19(1):57-62.

71.   Urick RJ. A SOUND VELOCITY METHOD FOR DETERMINING THE
        COMPRESSIBILITY OF FINELY DIVIDED SUBSTANCES. *Journal of Applied
        Physics*. 1947;18(11):983-987.

72.   Benes E, Groschl M, Nowotny H, et al. Ultrasonic separation of suspended particles.
        2001 Ieee Ultrasonics Symposium Proceedings, Vols 1 and 2. 2001:649-659.

73.   Kilburn DG, Piret JM, Sonderhoff SA, Trampler F, Inventors; U.S. Patent Office
        ##5,626,767, assignee. Acoustic filter for separating and recycling suspended particles.
        1997.

74.   Wang Z, Feke D, Inventors; 2011/0262990, assignee. Acoustic device and methods
        thereof for separation and concentration. U.S. Patent Office Application 2011/0262990.
        2011.

75.   Thompson JK, Wilson JS, Inventors. Particle settler for use in cell culture. U.S. Patent
        #5'817,505. 1998.

76.   Nii S, Kikumoto S, Tokuyama H. Quantitative approach to ultrasonic emulsion
        separation. *Ultrasonics Sonochemistry*. 2009;16(1):145-149.

77.   Leong T, Johansson L, Juliano P, Mawson R, McArthur S, Manasseh R. Design
        parameters for the separation of fat from natural whole milk in an ultrasonic litre-scale
        vessel. *Ultrasonics Sonochemistry*. 2014;21(4):1289-1298.

78.   Trampler F, Sonderhoff SA, Pui PWS, Kilburn DG, Piret JM. ACOUSTIC CELL
        FILTER FOR HIGH-DENSITY PERFUSION CULTURE OF HYBRIDOMA CELLS.
        Bio-Technology. 1994;12(3):281-284.

79.   Pui PWS, Trampler F, Sonderhoff SA, Groeschl M, Kilburn DG, Piret JM. Batch and semicontinuous aggregation and sedimentation of hybridoma cells by acoustic resonance fields. *Biotechnology Progress.* 1995;11(2):146-152.

80.   Shirgaonkar IZ, Lanthier S, Kamen A. Acoustic cell filter: a proven cell retention technology for perfusion of animal cell cultures. *Biotechnology Advances.* 2004;22(6):433-444.

81.   Spengler JF, Jekel M, Christensen KT, Adrian RJ, Hawkes JJ, Coakley WT. Observation of yeast cell movement and aggregation in a small-scale MHz-ultrasonic standing wave field. *Bioseparation.* 2000;9(6):329-341.

82.   Spengler J, Jekel M. Ultrasound conditioning of suspensions - studies of streaming influence on particle aggregation on a lab- and pilot-plant scale. *Ultrasonics.* 2000;38(1-8):624-628.

83.   Richmond A, Cheng-Wu Z. Optimization of a flat plate glass reactor for mass production of Nannochloropsis sp outdoors. *Journal of Biotechnology.* 2001;85(3):259-269.

84.   Yao KM. THEORETICAL STUDY OF HIGH-RATE SEDIMENTATION. *Journal Water Pollution Control Federation.* 1970;42(2):218-&.

85.   Smith BT, Davis RH. Particle concentration using inclined sedimentation via sludge accumulation and removal for algae harvesting. *Chemical Engineering Science.* 2013;91:79-85.

86.   Henzler HJ. Continuous Fermentation with Animal Cells Part 2. Techniques and Methods of Cell Retention. *Chemie Ingenieur Technik.* 2012;84(9):1482-1496.

87.   Gaida T, DoblhoffDier O, Strutzenberger K, et al. Selective retention of viable cells in ultrasonic resonance field devices. *Biotechnology Progress.* 1996;12(1):73-76.

88.   Ryll T, Dutina G, Reyes A, Gunson J, Krummen L, Etcheverry T. Performance of small-scale CHO perfusion cultures using an acoustic cell filtration device for cell retention: Characterization of separation efficiency and impact of perfusion on product quality. *Biotechnology and Bioengineering.* 2000;69(4):440-449.

89.   Andrade M, Buiochi F, Adamowski J. Finite Element Analysis of a Piezoelectric Acoustic Levitator. *International Ultrasonic Symposium Proceedings.* 2008:1413 - 1416.

APPENDIX I

PERFORMANCE DATA

Flow Rate

Nannochloropsis oculata

EXPERIMENT 1

Flow Rate (mL·min⁻¹)	ORIGINAL Inlet O.D.	Diluted O.D.	Dilution Inlet	Diluted	FINAL Inlet	Diluted	Cell Concentration (cells·mL⁻¹) Inlet	Diluted	Filtration Efficiency
60	0.429	0.497	16	8.5	6.86	2.09	2.5E+09	7.7E+08	38%
50	0.429	0.426	16	8.5	6.86	4.22	2.5E+09	1.6E+09	47%
40	0.429	0.246	16	8.5	6.86	3.62	2.5E+09	1.3E+09	70%
30	0.429	0.178	16	8.5	6.86	2.09	2.5E+09	7.7E+08	78%
20	0.429	0.098	16	8.5	6.86	1.51	2.5E+09	5.6E+08	88%
Average	0.429				6.86		2.5E+09		
Standard Deviation	0.000				0.00		0.0E+00		
RelativeStandard Deviation	0%				0%		0%		

EXPERIMENT 2

Flow Rate (mL·min⁻¹)	ORIGINAL Inlet O.D.	Diluted O.D.	Dilution Inlet	Diluted	FINAL Inlet	Diluted	Cell Concentration (cells·mL⁻¹) Inlet	Diluted	Filtration Efficiency
60	0.321	0.375	16	11	5.14	4.13	1.9E+09	1.5E+09	20%
70	0.321	0.460	16	8.5	5.14	3.91	1.9E+09	1.4E+09	24%
60	0.321	0.353	16	8.5	5.14	3.00	1.9E+09	1.1E+09	42%
50	0.321	0.200	16	8.5	5.14	1.70	1.9E+09	6.3E+08	67%
40	0.321	0.101	16	8.5	5.14	0.86	1.9E+09	3.2E+08	83%
Average	0.321				5.14		1.9E+09		
Standard Deviation	0.000				0.00		0.0E+00		
RelativeStandard Deviation	0%				0%		0%		

EXPERIMENT 3

Flow Rate (mL·min⁻¹)	ORIGINAL Inlet O.D.	Diluted O.D.	Dilution Inlet	Diluted	FINAL Inlet	Diluted	Cell Concentration (cells·mL⁻¹) Inlet	Diluted	Filtration Efficiency
60	0.236	0.276	21	11	4.96	3.04	1.8E+09	1.1E+09	39%
50	0.236	0.375	21	11	4.96	4.13	1.8E+09	1.5E+09	17%
40	0.236	0.162	21	11	4.96	1.78	1.8E+09	6.6E+08	64%
30	0.236	0.217	21	11	4.96	2.39	1.8E+09	8.8E+08	52%
20	0.236	0.136	21	11	4.96	1.50	1.8E+09	5.5E+08	70%
Average	0.236				4.96		1.8E+09		
Standard Deviation	0.000				0.00		2.7E-07		
RelativeStandard Deviation	0%				0%		0%		

Saccharomyces cerevisiae

EXPERIMENT 1

Flow Rate (mL·min⁻¹)	ORIGINAL Inlet O.D.	Diluted O.D.	Dilution Inlet	Diluted	FINAL Inlet	Diluted	Cell Concentration (cells·mL⁻¹) Inlet	Diluted	Filtration Efficiency
80	0.221	0.292	16	8.5	3.54	2.48	2.1E+07	1.5E+07	30%
70	0.211	0.211	16	8.5	3.38	1.79	2.0E+07	1.1E+07	47%
60	0.191	0.177	16	8.5	3.06	1.50	1.8E+07	9.0E+06	51%
50	0.180	0.105	16	8.5	2.88	0.89	1.7E+07	5.4E+06	69%
40	0.178	0.094	16	8.5	2.85	0.80	1.7E+07	4.8E+06	72%
30	0.178	0.085	16	8.5	2.85	0.72	1.7E+07	4.3E+06	75%
20	0.178	0.572	16	1	2.85	0.57	1.7E+07	3.4E+06	80%
Average	0.191				3.06		1.8E+07		
Standard Deviation	0.018				0.29		1.7E+06		
RelativeStandard Deviation	9%				9%		9%		

EXPERIMENT 2

Flow Rate (mL·min⁻¹)	ORIGINAL Inlet O.D.	Diluted O.D.	Dilution Inlet	Diluted	FINAL Inlet	Diluted	Cell Concentration (cells·mL⁻¹) Inlet	Diluted	Filtration Efficiency
80	0.236	0.334	16	8.5	3.78	2.84	2.3E+07	1.7E+07	25%
70	0.232	0.303	16	8.5	3.71	2.58	2.2E+07	1.5E+07	31%
60	0.226	0.196	16	8.5	3.62	1.67	2.2E+07	1.0E+07	54%
50	0.204	0.140	16	8.5	3.26	1.19	2.0E+07	7.1E+06	64%
40	0.216	0.120	16	8.5	3.46	1.02	2.1E+07	6.1E+06	70%
30	0.211	0.117	16	8.5	3.38	0.99	2.0E+07	6.0E+06	71%
20	0.203	0.114	16	8.5	3.25	0.97	1.9E+07	5.8E+06	70%
Average	0.218				3.49		2.1E+07		
Standard Deviation	0.013				0.21		1.3E+06		
RelativeStandard Deviation	6%				6%		6%		

EXPERIMENT 3

Flow Rate (mL·min⁻¹)	ORIGINAL Inlet O.D.	Diluted O.D.	Dilution Inlet	Diluted	FINAL Inlet	Diluted	Cell Concentration (cells·mL⁻¹) Inlet	Diluted	Filtration Efficiency
80	0.222	0.292	16	8.5	3.55	2.48	2.1E+07	1.5E+07	30%
70	0.256	0.211	16	8.5	4.10	1.79	2.5E+07	1.1E+07	56%
60	0.231	0.177	16	8.5	3.70	1.50	2.2E+07	9.0E+06	59%
50	0.215	0.105	16	8.5	3.44	0.89	2.1E+07	5.4E+06	74%
40	0.218	0.094	16	8.5	3.49	0.80	2.1E+07	4.8E+06	77%
30	0.212	0.085	16	8.5	3.39	0.72	2.0E+07	4.3E+06	79%
20	0.215	0.572	16	1	3.44	0.57	2.1E+07	3.4E+06	83%
Average	0.224				3.59		2.2E+07		
Standard Deviation	0.015				0.25		1.5E+06		
RelativeStandard Deviation	7%				7%		7%		

Concentration								
Saccharomyces cerevisiae								

DATA POINT 1

Test 1	ORIGINAL		Dilution		FINAL		Cell Concentration (cells·mL^{-1})		
	Inlet O.D.	Diluted O.D.	Inlet	Diluted	Inlet	Diluted	Inlet	Diluted	Filtration Efficiency
	0.441	0.110	16	8.5	7.06	0.94	4.2E+07	5.6E+06	87%
	0.429	0.078	16	8.5	6.86	0.66	4.1E+07	4.0E+06	90%
	0.433	0.173	16	8.5	6.93	1.47	4.2E+07	8.8E+06	79%
Average	0.434	0.120			6.949	1.023	4.2E+07		85%
Standard Deviation	0.005	0.039			0.080	0.335	5.9E+05		5%
RelativeStandard Deviation	1%	33%			1%	33%	1%		6%

Test 2	ORIGINAL		Dilution		FINAL		Cell Concentration (cells·mL^{-1})		
	Inlet O.D.	Diluted O.D.	Inlet	Diluted	Inlet	Diluted	Inlet	Diluted	Filtration Efficiency
	0.393	0.184	16	8.5	6.29	1.56	3.8E+07	9.4E+06	75%
	0.401	0.196	16	8.5	6.42	1.67	3.8E+07	1.0E+07	74%
	0.394	0.173	16	8.5	6.30	1.47	3.8E+07	8.8E+06	77%
Average	0.396	0.184			6.336	1.567	3.8E+07		75%
Standard Deviation	0.004	0.009			0.057	0.080	4.2E+05		1%
RelativeStandard Deviation	1%	5%			1%	5%	1%		1%

Test 3	ORIGINAL		Dilution		FINAL		Cell Concentration (cells·mL^{-1})		
	Inlet O.D.	Diluted O.D.	Inlet	Diluted	Inlet	Diluted	Inlet	Diluted	Filtration Efficiency
	0.410	0.200	16	8.5	6.56	1.70	3.9E+07	1.0E+07	74%
	0.404	0.199	16	8.5	6.46	1.69	3.9E+07	1.0E+07	74%
	0.387	0.146	16	8.5	6.19	1.24	3.7E+07	7.4E+06	80%
Average	0.400	0.182			6.405	1.544	3.8E+07		76%
Standard Deviation	0.010	0.025			0.156	0.214	1.1E+06		3%
RelativeStandard Deviation	2%	14%			2%	14%	3%		4%
Average							3.9E+07		79%
Standard Deviation							7.2E+05		3%

DATA POINT 2

Test 1	ORIGINAL		Dilution		FINAL		Cell Concentration (cells·mL^{-1})		
	Inlet O.D.	Diluted O.D.	Inlet	Diluted	Inlet	Diluted	Inlet	Diluted	Filtration Efficiency
	0.375	0.079	8.5	8.5	3.19	0.67	1.9E+07	4.0E+06	79%
	0.358	0.072	8.5	8.5	3.04	0.61	1.8E+07	3.7E+06	80%
	0.363	0.096	8.5	8.5	3.09	0.82	1.9E+07	4.9E+06	74%
Average	0.365	0.082			3.105	0.700	1.9E+07		77%
Standard Deviation	0.007	0.010			0.074	0.086	4.5E+05		3%
RelativeStandard Deviation	2%	12%			2%	12%	2%		4%

Test 2	ORIGINAL		Dilution		FINAL		Cell Concentration (cells·mL^{-1})		
	Inlet O.D.	Diluted O.D.	Inlet	Diluted	Inlet	Diluted	Inlet	Diluted	Filtration Efficiency
	0.376	0.076	8.5	8.5	3.20	0.65	1.9E+07	3.9E+06	80%
	0.371	0.079	8.5	8.5	3.15	0.67	1.9E+07	4.0E+06	79%
	0.364	0.076	8.5	8.5	3.09	0.65	1.9E+07	3.9E+06	79%
Average	0.370	0.077			3.148	0.655	1.9E+07		79%
Standard Deviation	0.005	0.001			0.042	0.012	3.1E+05		0%
RelativeStandard Deviation	1%	2%			1%	2%	2%		1%

Test 3	ORIGINAL		Dilution		FINAL		Cell Concentration (cells·mL^{-1})		
	Inlet O.D.	Diluted O.D.	Inlet	Diluted	Inlet	Diluted	Inlet	Diluted	Filtration Efficiency
	0.364	0.066	8.5	8.5	3.09	0.56	1.9E+07	3.4E+06	82%
	0.359	0.075	8.5	8.5	3.05	0.64	1.8E+07	3.8E+06	79%
	0.368	0.083	8.5	8.5	3.13	0.71	1.9E+07	4.2E+06	77%
Average	0.364	0.075			3.091	0.635	1.9E+07		79%
Standard Deviation	0.004	0.007			0.031	0.059	2.3E+05		2%
RelativeStandard Deviation	1%	9%			1%	9%	1%		2%
Average							1.9E+07		79%
Standard Deviation							3.3E+05		2%

3

Test 1	ORIGINAL		Dilution		FINAL		Cell Concentration (cells·mL^{-1})		
	Inlet O.D.	Diluted O.D.	Inlet	Diluted	Inlet	Diluted	Inlet	Diluted	Filtration Efficiency
	0.166	0.062	8.5	8.5	1.41	0.53	8.5E+06	3.2E+06	63%
	0.172	0.048	8.5	8.5	1.46	0.41	8.8E+06	2.4E+06	72%
	0.173	0.053	8.5	8.5	1.47	0.45	8.8E+06	2.7E+06	69%
Average	0.170	0.054			1.448	0.462	8.7E+06		68%
Standard Deviation	0.003	0.006			0.026	0.049	1.9E+05		4%
RelativeStandard Deviation	2%	11%			2%	11%	2%		6%

	ORIGINAL		Dilution		FINAL		Cell Concentration (cells·mL^{-1})		
	Inlet O.D.	Diluted O.D.	Inlet	Diluted	Inlet	Diluted	Inlet	Diluted	Filtration Efficiency

	ORIGINAL Inlet O.D.	Diluted O.D.	Dilution Inlet	Diluted	FINAL Inlet	Diluted	Cell Concentration (cells·mL⁻¹) Inlet	Diluted	Filtration Efficiency
Test 2	0.176	0.052	8.5	8.5	1.50	0.44	9.0E+06	2.7E+06	70%
	0.171	0.045	8.5	8.5	1.45	0.38	8.7E+06	2.3E+06	74%
	0.166	0.055	8.5	8.5	1.41	0.47	8.5E+06	2.8E+06	67%
Average	0.171	0.051			1.454	0.431	8.7E+06		70%
Standard Deviation	0.004	0.004			0.035	0.036	2.6E+05		3%
RelativeStandard Deviation	2%	8%			2%	8%	3%		4%

	ORIGINAL Inlet O.D.	Diluted O.D.	Dilution Inlet	Diluted	FINAL Inlet	Diluted	Cell Concentration (cells·mL⁻¹) Inlet	Diluted	Filtration Efficiency
Test 3	0.171	0.055	8.5	8.5	1.45	0.47	8.7E+06	2.8E+06	68%
	0.162	0.064	8.5	8.5	1.38	0.54	8.3E+06	3.3E+06	60%
	0.158	0.053	8.5	8.5	1.34	0.45	8.1E+06	2.7E+06	66%
Average	0.164	0.057			1.391	0.487	8.3E+06		65%
Standard Deviation	0.005	0.005			0.046	0.041	3.4E+05		3%
RelativeStandard Deviation	3%	8%			3%	8%	4%		5%
Average							8.6E+06		68%
Standard Deviation							2.6E+05		3%

DATA POINT 4

	ORIGINAL Inlet O.D.	Diluted O.D.	Dilution Inlet	Diluted	FINAL Inlet	Diluted	Cell Concentration (cells·mL⁻¹) Inlet	Diluted	Filtration Efficiency
Test 1	0.178	0.063	4	4	0.71	0.25	4.3E+06	1.5E+06	65%
	0.178	0.060	4	4	0.71	0.24	4.3E+06	1.4E+06	66%
	0.178	0.068	4	4	0.71	0.27	4.3E+06	1.6E+06	62%
Average	0.178	0.064			0.712	0.255	4.3E+06		64%
Standard Deviation	0.000	0.003			0.000	0.013	0.0E+00		2%
RelativeStandard Deviation	0%	5%			0%	5%	0%		3%

	ORIGINAL Inlet O.D.	Diluted O.D.	Dilution Inlet	Diluted	FINAL Inlet	Diluted	Cell Concentration (cells·mL⁻¹) Inlet	Diluted	Filtration Efficiency
Test 2	0.191	0.065	8.5	8.5	1.62	0.55	9.7E+06	3.3E+06	66%
	0.188	0.069	8.5	8.5	1.60	0.59	9.6E+06	3.5E+06	63%
	0.183	0.070	8.5	8.5	1.56	0.60	9.3E+06	3.6E+06	62%
Average	0.187	0.068			1.592	0.578	9.6E+06		64%
Standard Deviation	0.003	0.002			0.028	0.018	2.1E+05		2%
RelativeStandard Deviation	2%	3%			2%	3%	2%		3%
Average							6.9E+06		64%
Standard Deviation							1.0E+05		1%

DATA POINT 5

	ORIGINAL Inlet O.D.	Diluted O.D.	Dilution Inlet	Diluted	FINAL Inlet	Diluted	Cell Concentration (cells·mL⁻¹) Inlet	Diluted	Filtration Efficiency
Test 1	0.159	0.083	1	1	0.16	0.08	9.5E+05	5.0E+05	48%
	0.151	0.085	1	1	0.15	0.09	9.1E+05	5.1E+05	44%
	0.158	0.093	1	1	0.16	0.09	9.5E+05	5.6E+05	41%
Average	0.156	0.087			0.156	0.087	9.4E+05		44%
Standard Deviation	0.004	0.004			0.004	0.004	2.6E+04		3%
RelativeStandard Deviation	2%	5%			2%	5%	3%		6%

	ORIGINAL Inlet O.D.	Diluted O.D.	Dilution Inlet	Diluted	FINAL Inlet	Diluted	Cell Concentration (cells·mL⁻¹) Inlet	Diluted	Filtration Efficiency
Test 2	0.162	0.079	1	1	0.16	0.08	9.7E+05	4.7E+05	51%
	0.154	0.070	1	1	0.15	0.07	9.2E+05	4.2E+05	55%
	0.152	0.059	1	1	0.15	0.06	9.1E+05	3.5E+05	61%
Average	0.156	0.069			0.156	0.069	9.4E+05		56%
Standard Deviation	0.004	0.008			0.004	0.008	3.2E+04		4%
RelativeStandard Deviation	3%	12%			3%	12%	3%		7%

	ORIGINAL Inlet O.D.	Diluted O.D.	Dilution Inlet	Diluted	FINAL Inlet	Diluted	Cell Concentration (cells·mL⁻¹) Inlet	Diluted	Filtration Efficiency
Test 3	0.157	0.068	1	1	0.16	0.07	9.4E+05	4.1E+05	57%
	0.148	0.061	1	1	0.15	0.06	8.9E+05	3.7E+05	59%
	0.146	0.067	1	1	0.15	0.07	8.8E+05	4.0E+05	54%
Average	0.150	0.065			0.150	0.065	9.0E+05		57%
Standard Deviation	0.005	0.003			0.005	0.003	3.5E+04		2%
RelativeStandard Deviation	3%	5%			3%	5%	4%		3%
Average							9.2E+05		52%
Standard Deviation							3.1E+04		3%

Nannochloropsis oculata

	ORIGINAL Inlet O.D.	Diluted O.D.	Dilution Inlet	Diluted	FINAL Inlet	Diluted	Cell Concentration (cells·mL⁻¹) Inlet	Diluted	Filtration Efficiency
Test 1	0.240	0.117	21	11	5.04	1.29	3.0E+08	7.7E+07	74%
	0.243	0.104	21	11	5.10	1.14	3.1E+08	6.9E+07	78%
	0.241	0.123	21	11	5.06	1.35	3.0E+08	8.1E+07	73%
Average	0.241	0.115			5.068	1.261	3.0E+08	7.6E+07	75%

DATA POINT 1									
Standard Deviation	0.001	0.008			0.026	0.087	1.9E+06	6.4E+06	2%
RelativeStandard Deviation	1%	7%			1%	7%	1%	8%	2%
	ORIGINAL		Dilution		FINAL		Cell Concentration (cells·mL^{-1})		
	Inlet O.D.	Diluted O.D.	Inlet	Diluted	Inlet	Diluted	Inlet	Diluted	Filtration Efficiency
Test 2	0.200	0.183	21	11	4.20	2.01	1.6E+08	7.4E+07	52%
	0.243	0.104	21	11	5.10	1.14	1.9E+08	4.2E+07	78%
	0.241	0.123	21	11	5.06	1.35	1.9E+08	5.0E+07	73%
Average	0.228	0.137			4.788	1.503	1.8E+08	5.6E+07	68%
Standard Deviation	0.020	0.034			0.416	0.370	1.9E+07	1.7E+07	11%
RelativeStandard Deviation	9%	25%			9%	25%	11%	30%	16%
Average							1.6E+08		71%
Standard Deviation							6.9E+06		6%

DATA POINT 2									
	ORIGINAL		Dilution		FINAL		Cell Concentration (cells·mL^{-1})		
	Inlet O.D.	Diluted O.D.	Inlet	Diluted	Inlet	Diluted	Inlet	Diluted	Filtration Efficiency
Test 2	0.097	0.153	25	8.5	2.43	1.30	9.0E+07	4.8E+07	46%
	0.100	0.157	25	8.5	2.50	1.33	9.3E+07	4.9E+07	47%
	0.100	0.154	25	8.5	2.50	1.31	9.3E+07	4.8E+07	48%
Average	0.099	0.155			4.788	1.503	9.2E+07	4.9E+07	47%
Standard Deviation	0.002	0.002			0.416	0.370	1.6E+06	6.5E+05	11%
RelativeStandard Deviation	2%	1%			9%	25%	2%	1%	16%
Average							9.2E+07		47%
Standard Deviation							1.6E+06		11%

DATA POINT 3									
	ORIGINAL		Dilution		FINAL		Cell Concentration (cells·mL^{-1})		
	Inlet O.D.	Diluted O.D.	Inlet	Diluted	Inlet	Diluted	Inlet	Diluted	Filtration Efficiency
Test 2	0.106	0.084	12	14	1.27	1.18	4.7E+07	4.4E+07	8%
	0.106	0.057	12	14	1.27	0.80	4.7E+07	3.0E+07	37%
	0.100	0.062	12	14	1.20	0.87	4.4E+07	3.2E+07	28%
Average	0.104	0.068			4.788	1.503	4.6E+07	3.5E+07	24%
Standard Deviation	0.003	0.014			0.416	0.370	1.5E+06	7.4E+06	11%
RelativeStandard Deviation	3%	21%			9%	25%	3%	21%	16%
Average							4.6E+07		24%
Standard Deviation							1.5E+06		11%

	Power								
	Polyamide Particles								

DATA POINT 1

Test 1

	ORIGINAL		Dilution		FINAL		Particle Concentration (particles·mL⁻¹)		Filtration Efficiency
	Inlet O.D.	Diluted O.D.	Inlet	Diluted	Inlet	Diluted	Inlet	Diluted	
	0.364	0.274	16	16	5.82	4.38	3.7E+07	2.8E+07	25%
	0.329	0.263	16	16	5.26	4.21	3.4E+07	2.7E+07	20%
	0.325	0.297	16	16	5.20	4.75	3.3E+07	3.0E+07	9%
Average	0.339	0.278			5.429	4.448	3.5E+07	2.8E+07	18%
Standard Deviation	0.018	0.014			0.280	0.227	2.2E+06	1.8E+06	7%
Relative Standard Deviation	5%	5%			5%	5%	6%	6%	38%

Test 2

	ORIGINAL		Dilution		FINAL		Particle Concentration (particles·mL⁻¹)		Filtration Efficiency
	Inlet O.D.	Diluted O.D.	Inlet	Diluted	Inlet	Diluted	Inlet	Diluted	
	0.371	0.336	16	16	5.94	5.38	3.8E+07	3.4E+07	9%
	0.380	0.318	16	16	6.08	5.09	3.9E+07	3.3E+07	16%
	0.335	0.293	16	16	5.36	4.69	3.4E+07	3.0E+07	13%
Average	0.362	0.316			5.792	5.051	3.7E+07	3.2E+07	13%
Standard Deviation	0.019	0.018			0.311	0.282	2.4E+06	2.2E+06	3%
Relative Standard Deviation	5%	6%			5%	6%	7%	7%	22%

Test 3

	ORIGINAL		Dilution		FINAL		Particle Concentration (particles·mL⁻¹)		Filtration Efficiency
	Inlet O.D.	Diluted O.D.	Inlet	Diluted	Inlet	Diluted	Inlet	Diluted	
	0.366	0.337	16	16	5.86	5.39	3.7E+07	3.5E+07	8%
	0.355	0.336	16	16	5.68	5.38	3.6E+07	3.4E+07	5%
	0.346	0.327	16	16	5.54	5.23	3.5E+07	3.3E+07	5%
Average	0.356	0.333			5.691	5.333	3.6E+07	3.4E+07	6%
Standard Deviation	0.008	0.004			0.131	0.072	1.0E+06	5.6E+05	1%
Relative Standard Deviation	2%	1%			2%	1%	3%	2%	19%

		Power (W)	*Filtration Efficiency*
Average		1.9	12%
Standard Deviation		0.7	4%

DATA POINT 2

Test 1

	ORIGINAL		Dilution		FINAL		Particle Concentration (particles·mL⁻¹)		Filtration Efficiency
	Inlet O.D.	Diluted O.D.	Inlet	Diluted	Inlet	Diluted	Inlet	Diluted	
	0.357	0.262	16	16	5.71	4.19	3.7E+07	2.7E+07	27%
	0.331	0.207	16	16	5.30	3.31	3.4E+07	2.1E+07	37%
	0.290	0.198	16	16	4.64	3.17	3.0E+07	2.0E+07	32%
Average	0.326	0.222			5.216	3.557	3.3E+07	2.3E+07	32%
Standard Deviation	0.028	0.028			0.441	0.453	3.5E+06	3.5E+06	4%
RelativeStandard Deviation	8%	13%			8%	13%	10%	16%	14%

Test 2

	ORIGINAL		Dilution		FINAL		Particle Concentration (particles·mL⁻¹)		Filtration Efficiency
	Inlet O.D.	Diluted O.D.	Inlet	Diluted	Inlet	Diluted	Inlet	Diluted	
	0.341	0.174	16	16	5.46	2.78	3.5E+07	1.8E+07	49%
	0.286	0.158	16	16	4.58	2.53	2.9E+07	1.6E+07	45%
	0.256	0.157	16	16	4.10	2.51	2.6E+07	1.6E+07	39%

DATA POI

	Inlet O.D.	Diluted O.D.	Inlet	Diluted	Inlet	Diluted	Inlet	Diluted	Filtration Efficiency
Average	0.294	0.163			4.709	2.608	3.0E+07	1.7E+07	44%
Standard Deviation	0.035	0.008			0.563	0.125	4.4E+06	9.8E+05	4%
RelativeStandard Deviation	12%	5%			12%	5%	15%	6%	10%

	ORIGINAL		Dilution		FINAL		Particle Concentration (particles·mL^{-1})		
Test 3	Inlet O.D.	Diluted O.D.	Inlet	Diluted	Inlet	Diluted	Inlet	Diluted	Filtration Efficiency
	0.328	0.240	16	16	5.25	3.84	3.4E+07	2.5E+07	27%
	0.288	0.193	16	16	4.61	3.09	2.9E+07	2.0E+07	33%
	0.234	0.188	16	16	3.74	3.01	2.4E+07	1.9E+07	20%
Average	0.283	0.207			4.533	3.312	2.9E+07	2.1E+07	26%
Standard Deviation	0.039	0.023			0.616	0.375	4.8E+06	2.9E+06	5%
RelativeStandard Deviation	14%	11%			14%	11%	17%	14%	21%

		Power (W)	Filtration Efficiency
Average		4.1	34%
Standard Deviation		1.2	5%

DATA POINT 3

	ORIGINAL		Dilution		FINAL		Particle Concentration (particles·mL^{-1})		
Test 1	Inlet O.D.	Diluted O.D.	Inlet	Diluted	Inlet	Diluted	Inlet	Diluted	Filtration Efficiency
	0.232	0.034	16	16	3.71	0.54	2.4E+07	3.5E+06	85%
	0.214	0.026	16	16	3.42	0.42	2.2E+07	2.7E+06	88%
	0.144	0.052	16	16	2.30	0.83	1.5E+07	5.3E+06	64%
Average	0.197	0.037			3.147	0.597	2.0E+07	3.8E+06	79%
Standard Deviation	0.038	0.011			0.607	0.174	4.8E+06	1.4E+06	11%
RelativeStandard Deviation	19%	29%			19%	29%	24%	36%	14%

	ORIGINAL		Dilution		FINAL		Particle Concentration (particles·mL^{-1})		
Test 2	Inlet O.D.	Diluted O.D.	Inlet	Diluted	Inlet	Diluted	Inlet	Diluted	Filtration Efficiency
	0.228	0.067	16	16	3.65	1.07	2.3E+07	6.9E+06	71%
	0.187	0.075	16	16	2.99	1.20	1.9E+07	7.7E+06	60%
	0.164	0.073	16	16	2.62	1.17	1.7E+07	7.5E+06	55%
Average	0.193	0.072			3.088	1.147	2.0E+07	7.3E+06	62%
Standard Deviation	0.026	0.003			0.424	0.054	3.3E+06	4.3E+05	6%
RelativeStandard Deviation	14%	5%			14%	5%	17%	6%	10%

	ORIGINAL		Dilution		FINAL		Particle Concentration (particles·mL^{-1})		
Test 3	Inlet O.D.	Diluted O.D.	Inlet	Diluted	Inlet	Diluted	Inlet	Diluted	Filtration Efficiency
	0.286	0.147	16	16	4.58	2.35	2.9E+07	1.5E+07	49%
	0.277	0.121	16	16	4.43	1.94	2.8E+07	1.2E+07	56%
	0.212	0.113	16	16	3.39	1.81	2.2E+07	1.2E+07	47%
Average	0.258	0.127			4.133	2.032	2.6E+07	1.3E+07	51%
Standard Deviation	0.033	0.015			0.527	0.232	4.1E+06	1.8E+06	4%
RelativeStandard Deviation	13%	11%			13%	11%	16%	14%	8%

		Power (W)	Filtration Efficiency
Average		5.9	64%
Standard Deviation		0.8	7%

	ORIGINAL		Dilution		FINAL		Particle Concentration (particles·mL^{-1})		

132

		ORIGINAL		Dilution		FINAL		Particle Concentration (particles·mL^{-1})		
		Inlet O.D.	Diluted O.D.	Inlet	Diluted	Inlet	Diluted	Inlet	Diluted	Filtration Efficiency
DATA POINT 4	Test 1	0.331	0.052	16	16	5.30	0.83	3.4E+07	5.3E+06	84%
		0.313	0.073	16	16	5.01	1.17	3.2E+07	7.5E+06	77%
		0.282	0.425	16	16	4.51	0.43	2.9E+07	2.7E+06	91%
	Average	0.309	0.183			4.939	0.808	3.2E+07	5.2E+06	84%
	Standard Deviation	0.020	0.171			0.324	0.304	2.5E+06	2.4E+06	6%
	RelativeStandard Deviation	7%	93%			7%	38%	8%	46%	7%
		ORIGINAL		Dilution		FINAL		Particle Concentration (particles·mL^{-1})		
		Inlet O.D.	Diluted O.D.	Inlet	Diluted	Inlet	Diluted	Inlet	Diluted	Filtration Efficiency
	Test 2	0.360	0.732	16	1	5.76	0.73	3.7E+07	4.7E+06	87%
		0.289	1.152	16	1	4.62	1.15	3.0E+07	7.4E+06	75%
		0.223	1.124	16	1	3.57	1.12	2.3E+07	7.2E+06	68%
	Average	0.291	1.003			4.651	1.003	3.0E+07	6.4E+06	77%
	Standard Deviation	0.056	0.192			0.895	0.192	7.0E+06	1.5E+06	8%
	RelativeStandard Deviation	19%	19%			19%	19%	24%	23%	10%
		ORIGINAL		Dilution		FINAL		Particle Concentration (particles·mL^{-1})		
		Inlet O.D.	Diluted O.D.	Inlet	Diluted	Inlet	Diluted	Inlet	Diluted	Filtration Efficiency
	Test 3	0.325	0.849	16	1	5.20	0.85	3.3E+07	5.4E+06	84%
		0.271	0.629	16	1	4.34	0.63	2.8E+07	4.0E+06	85%
		0.246	0.301	16	1	3.94	0.30	2.5E+07	1.9E+06	92%
	Average	0.281	0.593			4.491	0.593	2.9E+07	3.8E+06	87%
	Standard Deviation	0.033	0.225			0.527	0.225	4.1E+06	1.8E+06	4%
	RelativeStandard Deviation	12%	38%			12%	38%	14%	47%	4%
								Power (W)		*Filtration Efficiency*
	Average							7.4		83%
	Standard Deviation							0.9		6%
		ORIGINAL		Dilution		FINAL		Particle Concentration (particles·mL^{-1})		
		Inlet O.D.	Diluted O.D.	Inlet	Diluted	Inlet	Diluted	Inlet	Diluted	Filtration Efficiency
DATA POINT 5	Test 1	0.294	0.089	16	16	4.70	1.42	3.0E+07	9.1E+06	70%
		0.260	0.066	16	16	4.16	1.06	2.7E+07	6.8E+06	75%
		0.233	0.079	16	16	3.73	1.26	2.4E+07	8.1E+06	66%
	Average	0.262	0.078			4.197	1.248	2.7E+07	8.0E+06	70%
	Standard Deviation	0.025	0.009			0.399	0.151	3.1E+06	1.2E+06	3%
	RelativeStandard Deviation	10%	12%			10%	12%	12%	15%	5%
								Power (W)		*Filtration Efficiency*
	Average							12.7		70%
	Standard Deviation							0.5		3%
Saccharomyces cerevisiae										
		ORIGINAL		Dilution		FINAL		Cell Concentration (cells·mL^{-1})		
		Inlet O.D.	Diluted O.D.	Inlet	Diluted	Inlet	Diluted	Inlet	Diluted	Filtration Efficiency
	Test 1	0.441	0.110	16	8.5	7.06	0.94	4.2E+07	5.6E+06	87%
		0.429	0.078	16	8.5	6.86	0.66	4.1E+07	4.0E+06	90%
		0.433	0.173	16	8.5	6.93	1.47	4.2E+07	8.8E+06	79%
	Average	0.434	0.120			6.949	1.023	4.2E+07	6.1E+06	85%

DATA POINT 1

	ORIGINAL		Dilution		FINAL		Cell Concentration (cells·mL⁻¹)		Filtration Efficiency
Standard Deviation	0.005	0.039			0.080	0.335	5.9E+05	2.5E+06	5%
RelativeStandard Deviation	1%	33%			1%	33%	1%	40%	6%

	ORIGINAL		Dilution		FINAL		Cell Concentration (cells·mL⁻¹)		
	Inlet O.D.	Diluted O.D.	Inlet	Diluted	Inlet	Diluted	Inlet	Diluted	Filtration Efficiency
Test 2	0.393	0.184	16	8.5	6.29	1.56	3.8E+07	9.4E+06	75%
	0.401	0.196	16	8.5	6.42	1.67	3.8E+07	1.0E+07	74%
	0.394	0.173	16	8.5	6.30	1.47	3.8E+07	8.8E+06	77%
Average	0.396	0.184			6.336	1.567	3.8E+07	9.4E+06	75%
Standard Deviation	0.004	0.009			0.057	0.080	4.2E+05	5.9E+05	1%
RelativeStandard Deviation	1%	5%			1%	5%	1%	6%	1%

	ORIGINAL		Dilution		FINAL		Cell Concentration (cells·mL⁻¹)		
	Inlet O.D.	Diluted O.D.	Inlet	Diluted	Inlet	Diluted	Inlet	Diluted	Filtration Efficiency
Test 3	0.410	0.200	16	8.5	6.56	1.70	3.9E+07	1.0E+07	74%
	0.404	0.199	16	8.5	6.46	1.69	3.9E+07	1.0E+07	74%
	0.387	0.146	16	8.5	6.19	1.24	3.7E+07	7.4E+06	80%
Average	0.400	0.182			6.405	1.544	3.8E+07	9.3E+06	76%
Standard Deviation	0.010	0.025			0.156	0.214	1.1E+06	1.6E+06	3%
RelativeStandard Deviation	2%	14%			2%	14%	3%	17%	4%

							Power (W)		Filtration Efficiency
Average							6.5		79%
Standard Deviation							1.6		3%

DATA POINT 2

	ORIGINAL		Dilution		FINAL		Cell Concentration (cells·mL⁻¹)		
	Inlet O.D.	Diluted O.D.	Inlet	Diluted	Inlet	Diluted	Inlet	Diluted	Filtration Efficiency
Test 1	0.409	0.130	16	16	6.54	2.08	3.9E+07	1.2E+07	68%
	0.405	0.144	16	16	6.48	2.30	3.9E+07	1.4E+07	64%
	0.391	0.129	16	16	6.26	2.06	3.8E+07	1.2E+07	67%
Average	0.402	0.134			6.427	2.149	3.9E+07	1.3E+07	67%
Standard Deviation	0.008	0.007			0.123	0.110	9.1E+05	8.1E+05	2%
RelativeStandard Deviation	2%	5%			2%	5%	2%	6%	2%

	ORIGINAL		Dilution		FINAL		Cell Concentration (cells·mL⁻¹)		
	Inlet O.D.	Diluted O.D.	Inlet	Diluted	Inlet	Diluted	Inlet	Diluted	Filtration Efficiency
Test 2	0.378	0.149	16	16	6.05	2.38	3.6E+07	1.4E+07	61%
	0.416	0.135	16	16	6.66	2.16	4.0E+07	1.3E+07	68%
	0.399	0.151	16	16	6.38	2.42	3.8E+07	1.4E+07	62%
Average	0.398	0.145			6.363	2.320	3.8E+07	1.4E+07	63%
Standard Deviation	0.016	0.007			0.249	0.114	1.8E+06	8.4E+05	3%
RelativeStandard Deviation	4%	5%			4%	5%	5%	6%	5%

							Power (W)		Filtration Efficiency
Average							4.0		65%
Standard Deviation							0.9		2%

	ORIGINAL		Dilution		FINAL		Cell Concentration (cells·mL⁻¹)	

Test 1	Inlet O.D.	Diluted O.D.	Inlet	Diluted	Inlet	Diluted	Inlet	Diluted	Filtration Efficiency
	0.393	0.205	16	16	6.29	3.28	3.8E+07	2.0E+07	48%
	0.396	0.187	16	16	6.34	2.99	3.8E+07	1.8E+07	53%
	0.394	0.217	16	16	6.30	3.47	3.8E+07	2.1E+07	45%
Average	0.394	0.203			6.309	3.248	3.8E+07	1.9E+07	49%
Standard Deviation	0.001	0.012			0.020	0.197	1.5E+05	1.4E+06	3%
RelativeStandard Deviation	0%	6%			0%	6%	0%	7%	7%

		Power (W)		Filtration Efficiency
Average		1.8		49%
Standard Deviation		0.6		3%

DATA POINT 4

Test 1	ORIGINAL		Dilution		FINAL		Cell Concentration (cells·mL⁻¹)		
	Inlet O.D.	Diluted O.D.	Inlet	Diluted	Inlet	Diluted	Inlet	Diluted	Filtration Efficiency
	0.421	0.128	16	8.5	6.74	1.09	4.0E+07	6.5E+06	84%
	0.419	0.168	16	8.5	6.70	1.43	4.0E+07	8.6E+06	79%
	0.411	0.144	16	8.5	6.58	1.22	3.9E+07	7.3E+06	81%
Average	0.417	0.147			6.672	1.247	4.0E+07	7.5E+06	81%
Standard Deviation	0.004	0.016			0.069	0.140	5.1E+05	1.0E+06	2%
RelativeStandard Deviation	1%	11%			1%	11%	1%	14%	3%

Test 2	ORIGINAL		Dilution		FINAL		Cell Concentration (cells·mL⁻¹)		
	Inlet O.D.	Diluted O.D.	Inlet	Diluted	Inlet	Diluted	Inlet	Diluted	Filtration Efficiency
	0.400	0.163	16	8.5	6.40	1.39	3.8E+07	8.3E+06	78%
	0.402	0.170	16	8.5	6.43	1.45	3.9E+07	8.7E+06	78%
	0.403	0.180	16	8.5	6.45	1.53	3.9E+07	9.2E+06	76%
Average	0.402	0.171			6.427	1.454	3.9E+07	8.7E+06	77%
Standard Deviation	0.001	0.007			0.020	0.059	1.5E+05	4.4E+05	1%
RelativeStandard Deviation	0%	4%			0%	4%	0%	5%	1%

Test 3	ORIGINAL		Dilution		FINAL		Cell Concentration (cells·mL⁻¹)		
	Inlet O.D.	Diluted O.D.	Inlet	Diluted	Inlet	Diluted	Inlet	Diluted	Filtration Efficiency
	0.397	0.185	16	8.5	6.35	1.57	3.8E+07	9.4E+06	75%
	0.410	0.187	16	8.5	6.56	1.59	3.9E+07	9.5E+06	76%
	0.399	0.184	16	8.5	6.38	1.56	3.8E+07	9.4E+06	76%
Average	0.402	0.185			6.432	1.575	3.9E+07	9.5E+06	76%
Standard Deviation	0.006	0.001			0.091	0.011	6.7E+05	7.8E+04	0%
RelativeStandard Deviation	1%	1%			1%	1%	2%	1%	0%

		Power (W)		Filtration Efficiency
Average		9.7		78%
Standard Deviation		0.9		1%

Nannochloropsis oculata - UEIS

Test 1	ORIGINAL		Dilution		FINAL		Cell Concentration (cells·mL⁻¹)		
	Inlet O.D.	Diluted O.D.	Inlet	Diluted	Inlet	Diluted	Inlet	Diluted	Filtration Efficiency
	0.153	0.260	21	11	3.21	2.86	1.2E+08	1.1E+08	11%
	0.201	0.261	21	11	4.22	2.87	1.6E+08	1.1E+08	32%
	0.201	0.288	21	11	4.22	3.17	1.6E+08	1.2E+08	25%

	Inlet O.D.	Diluted O.D.			Inlet	Diluted	Inlet	Diluted	Filtration Efficiency
Average	0.185	0.270			3.885	2.966	1.4E+08	1.1E+08	23%
Standard Deviation	0.028	0.016			0.582	0.175	2.2E+07	6.5E+06	11%
RelativeStandard Deviation	15%	6%			15%	6%	15%	6%	47%

						Power (W)			*Filtration Efficiency*
Average						2.5			23%
andard Deviation						0.2			11%

DATA POINT 2

	ORIGINAL		Dilution		FINAL		Cell Concentration (cells·mL^{-1})		
Test 1	Inlet O.D.	Diluted O.D.	Inlet	Diluted	Inlet	Diluted	Inlet	Diluted	Filtration Efficiency
	0.153	0.167	21	11	3.21	1.84	1.2E+08	6.8E+07	43%
	0.187	0.183	21	11	3.93	2.01	1.5E+08	7.4E+07	49%
	0.187	0.255	21	11	3.93	2.81	1.5E+08	1.0E+08	29%
Average	0.176	0.202			3.689	2.218	1.4E+08	8.2E+07	40%
Standard Deviation	0.020	0.047			0.412	0.516	1.5E+07	1.9E+07	10%
RelativeStandard Deviation	11%	23%			11%	23%	11%	23%	26%

						Power (W)			*Filtration Efficiency*
Average						3.5			40%
andard Deviation						0.4			10%

DATA POINT 3

	ORIGINAL		Dilution		FINAL		Cell Concentration (cells·mL^{-1})		
Test 2	Inlet O.D.	Diluted O.D.	Inlet	Diluted	Inlet	Diluted	Inlet	Diluted	Filtration Efficiency
	0.240	0.117	21	11	5.04	1.29	1.9E+08	4.8E+07	74%
	0.243	0.104	21	11	5.10	1.14	1.9E+08	4.2E+07	78%
	0.241	0.123	21	11	5.06	1.35	1.9E+08	5.0E+07	73%
Average	0.241	0.115			5.068	1.261	1.9E+08	4.7E+07	75%
Standard Deviation	0.001	0.008			0.026	0.087	1.2E+06	4.0E+06	2%
RelativeStandard Deviation	1%	7%			1%	7%	1%	8%	2%

	ORIGINAL		Dilution		FINAL		Cell Concentration (cells·mL^{-1})		
Test 3	Inlet O.D.	Diluted O.D.	Inlet	Diluted	Inlet	Diluted	Inlet	Diluted	Filtration Efficiency
	0.200	0.183	21	11	4.20	2.01	1.6E+08	7.4E+07	52%
	0.243	0.104	21	11	5.10	1.14	1.9E+08	4.2E+07	78%
	0.241	0.123	21	11	5.06	1.35	1.9E+08	5.0E+07	73%
Average	0.228	0.137			4.788	1.503	1.8E+08	5.6E+07	68%
Standard Deviation	0.020	0.034			0.416	0.370	1.9E+07	1.7E+07	11%
RelativeStandard Deviation	9%	25%			9%	25%	11%	30%	16%

	ORIGINAL		Dilution		FINAL		Cell Concentration (cells·mL^{-1})		
Test 4	Inlet O.D.	Diluted O.D.	Inlet	Diluted	Inlet	Diluted	Inlet	Diluted	Filtration Efficiency
	0.175	0.149	21	11	3.68	1.64	1.4E+08	6.1E+07	55%
	0.166	0.098	21	11	3.49	1.08	1.3E+08	4.0E+07	69%
	0.156	0.074	21	11	3.28	0.81	1.2E+08	3.0E+07	75%
Average	0.166	0.107			3.479	1.177	1.3E+08	4.4E+07	67%
Standard Deviation	0.008	0.031			0.163	0.344	7.4E+06	1.6E+07	8%
RelativeStandard Deviation	5%	29%			5%	29%	6%	36%	12%

								Power (W)		*Filtration Efficiency*
	Average							5.5		70%
	andard Deviation							1.4		7%

DATA POINT 4

		ORIGINAL		Dilution		FINAL		Cell Concentration (cells·mL^{-1})		
		Inlet O.D.	Diluted O.D.	Inlet	Diluted	Inlet	Diluted	Inlet	Diluted	Filtration Efficiency
Test 1		0.153	0.082	21	11	3.21	0.90	1.2E+08	3.3E+07	72%
		0.156	0.074	21	11	3.28	0.81	1.2E+08	3.0E+07	75%
		0.156	0.079	21	11	3.28	0.87	1.2E+08	3.2E+07	73%
Average		0.155	0.078			3.255	0.862	1.2E+08	3.2E+07	74%
Standard Deviation		0.002	0.004			0.036	0.044	1.3E+06	1.6E+06	2%
RelativeStandard Deviation		1%	5%			1%	5%	1%	5%	2%

								Power (W)		*Filtration Efficiency*
	Average							10.0		74%
	andard Deviation							1.5		2%

DATA POINT 5

		ORIGINAL		Dilution		FINAL		Cell Concentration (cells·mL^{-1})		
		Inlet O.D.	Diluted O.D.	Inlet	Diluted	Inlet	Diluted	Inlet	Diluted	Filtration Efficiency
Test 1		0.153	0.094	21	11	3.21	1.03	1.2E+08	3.8E+07	68%
		0.166	0.098	21	11	3.49	1.08	1.3E+08	4.0E+07	69%
		0.166	0.100	21	11	3.49	1.10	1.3E+08	4.1E+07	68%
Average		0.162	0.097			3.395	1.071	1.3E+08	4.0E+07	68%
Standard Deviation		0.008	0.003			0.158	0.034	5.8E+06	1.2E+06	1%
RelativeStandard Deviation		5%	3%			5%	3%	5%	3%	1%

								Power (W)		*Filtration Efficiency*
	Average							8.0		68%
	andard Deviation							1.0		1%

Nannochloropsis oculata - "U" shape UES harvesting with an ATL division

DATA POINT 1

		ORIGINAL		Dilution		FINAL		Cell Concentration (cells·mL^{-1})		
		Inlet O.D.	Diluted O.D.	Inlet	Diluted	Inlet	Diluted	Inlet	Diluted	Filtration Efficiency
Test 1		0.241	0.201	31	31	7.47	6.23	2.8E+08	2.3E+08	17%
		0.248	0.206	31	31	7.69	6.39	2.8E+08	2.4E+08	17%
		0.248	0.206	31	31	7.69	6.39	2.8E+08	2.4E+08	17%
Average		0.246	0.204			7.616	6.334	2.8E+08	2.3E+08	17%
Standard Deviation		0.003	0.002			0.102	0.073	4.6E+06	3.3E+06	0%
Relative Standard Deviation		1%	1%			1%	1%	2%	1%	1%

		ORIGINAL		Dilution		FINAL		Cell Concentration (cells·mL^{-1})		
		Inlet O.D.	Diluted O.D.	Inlet	Diluted	Inlet	Diluted	Inlet	Diluted	Filtration Efficiency
Test 2		0.256	0.178	31	31	7.94	5.52	2.9E+08	2.0E+08	30%
		0.230	0.177	31	31	7.13	5.49	2.6E+08	2.0E+08	23%
		0.226	0.158	31	31	7.01	4.90	2.6E+08	1.8E+08	30%
Average		0.237	0.171			7.357	5.301	2.7E+08	2.0E+08	28%
Standard Deviation		0.013	0.009			0.412	0.285	1.9E+07	1.3E+07	3%
Relative Standard Deviation		6%	5%			6%	5%	7%	7%	12%

		ORIGINAL		Dilution		FINAL		Cell Concentration (cells·mL^{-1})		

Test 3	Inlet O.D.	Diluted O.D.	Inlet	Diluted	Inlet	Diluted	Inlet	Diluted	Filtration Efficiency
	0.236	0.170	31	31	7.32	5.27	2.7E+08	1.9E+08	28%
	0.230	0.169	31	31	7.13	5.24	2.6E+08	1.9E+08	27%
	0.218	0.149	31	31	6.76	4.62	2.5E+08	1.7E+08	32%
Average	0.228	0.163			7.068	5.043	2.6E+08	1.9E+08	29%
Standard Deviation	0.007	0.010			0.232	0.300	1.1E+07	1.4E+07	2%
Relative Standard Deviation	3%	6%			3%	6%	4%	7%	8%

DATA POINT 2

Test 3	Inlet O.D.	Diluted O.D.	Inlet	Diluted	Inlet	Diluted	Inlet	Diluted	Filtration Efficiency
	0.236	0.170	31	31	7.32	5.27	2.7E+08	1.9E+08	28%
	0.230	0.169	31	31	7.13	5.24	2.6E+08	1.9E+08	27%
	0.218	0.149	31	31	6.76	4.62	2.5E+08	1.7E+08	32%
Average	0.228	0.163			7.068	5.043	2.6E+08	1.9E+08	29%
Standard Deviation	0.007	0.010			0.232	0.300	1.1E+07	1.4E+07	2%
Relative Standard Deviation	3%	6%			3%	6%	4%	7%	8%

		Power (W)	Filtration Efficiency
Average		2.0	24%
Standard Deviation		0.2	2%

Test 1	ORIGINAL		Dilution		FINAL		Cell Concentration (cells·mL^{-1})		
	Inlet O.D.	Diluted O.D.	Inlet	Diluted	Inlet	Diluted	Inlet	Diluted	Filtration Efficiency
	0.237	0.155	31	31	7.35	4.81	2.7E+08	1.8E+08	35%
	0.231	0.160	31	31	7.16	4.96	2.6E+08	1.8E+08	31%
	0.239	0.140	31	31	7.41	4.34	2.7E+08	1.6E+08	41%
Average	0.236	0.152			7.306	4.702	2.7E+08	1.7E+08	36%
Standard Deviation	0.003	0.008			0.105	0.263	4.8E+06	1.2E+07	4%
Relative Standard Deviation	1%	6%			1%	6%	2%	7%	12%

Test 2	ORIGINAL		Dilution		FINAL		Cell Concentration (cells·mL^{-1})		
	Inlet O.D.	Diluted O.D.	Inlet	Diluted	Inlet	Diluted	Inlet	Diluted	Filtration Efficiency
	0.245	0.159	31	31	7.60	4.93	2.8E+08	1.8E+08	35%
	0.227	0.150	31	31	7.04	4.65	2.6E+08	1.7E+08	34%
	0.241	0.177	31	31	7.47	5.49	2.8E+08	2.0E+08	27%
Average	0.238	0.162			7.368	5.022	2.7E+08	1.9E+08	32%
Standard Deviation	0.008	0.011			0.239	0.348	1.1E+07	1.6E+07	4%
Relative Standard Deviation	3%	7%			3%	7%	4%	8%	12%

Test 3	ORIGINAL		Dilution		FINAL		Cell Concentration (cells·mL^{-1})		
	Inlet O.D.	Diluted O.D.	Inlet	Diluted	Inlet	Diluted	Inlet	Diluted	Filtration Efficiency
	0.231	0.173	31	31	7.16	5.36	2.6E+08	2.0E+08	25%
	0.238	0.161	31	31	7.38	4.99	2.7E+08	1.8E+08	32%
	0.237	0.162	31	31	7.35	5.02	2.7E+08	1.9E+08	32%
Average	0.235	0.165			7.295	5.125	2.7E+08	1.9E+08	30%
Standard Deviation	0.003	0.005			0.096	0.169	4.3E+06	7.6E+06	3%
Relative Standard Deviation	1%	3%			1%	3%	2%	4%	11%

		Power (W)	Filtration Efficiency
Average		5.2	32%
Standard Deviation		0.6	4%

Test 1	ORIGINAL		Dilution		FINAL		Cell Concentration (cells·mL^{-1})		
	Inlet O.D.	Diluted O.D.	Inlet	Diluted	Inlet	Diluted	Inlet	Diluted	Filtration Efficiency
	0.222	0.116	31	31	6.88	3.60	2.5E+08	1.3E+08	48%
	0.213	0.140	31	31	6.60	4.34	2.4E+08	1.6E+08	34%

<table>
<thead>
<tr><th rowspan="2"></th><th colspan="2">ORIGINAL</th><th colspan="2">Dilution</th><th colspan="2">FINAL</th><th colspan="2">Cell Concentration (cells·mL^{-1})</th><th rowspan="2">Filtration Efficiency</th></tr>
<tr><th>Inlet O.D.</th><th>Diluted O.D.</th><th>Inlet</th><th>Diluted</th><th>Inlet</th><th>Diluted</th><th>Inlet</th><th>Diluted</th></tr>
</thead>
<tbody>
<tr><td></td><td>0.189</td><td>0.125</td><td>31</td><td>31</td><td>5.86</td><td>3.88</td><td>2.2E+08</td><td>1.4E+08</td><td>34%</td></tr>
<tr><td>Average</td><td>0.208</td><td>0.127</td><td></td><td></td><td>6.448</td><td>3.937</td><td>2.4E+08</td><td>1.5E+08</td><td>39%</td></tr>
<tr><td>Standard Deviation</td><td>0.014</td><td>0.010</td><td></td><td></td><td>0.432</td><td>0.307</td><td>2.0E+07</td><td>1.4E+07</td><td>6%</td></tr>
<tr><td>Relative Standard Deviation</td><td>7%</td><td>8%</td><td></td><td></td><td>7%</td><td>8%</td><td>8%</td><td>10%</td><td>17%</td></tr>
<tr><td></td><td colspan="2" align="center">ORIGINAL</td><td colspan="2" align="center">Dilution</td><td colspan="2" align="center">FINAL</td><td colspan="2" align="center">Cell Concentration (cells·mL^{-1})</td><td>Filtration Efficiency</td></tr>
<tr><td>Test 2</td><td>Inlet O.D.</td><td>Diluted O.D.</td><td>Inlet</td><td>Diluted</td><td>Inlet</td><td>Diluted</td><td>Inlet</td><td>Diluted</td><td></td></tr>
<tr><td></td><td>0.225</td><td>0.098</td><td>31</td><td>31</td><td>6.98</td><td>3.04</td><td>2.6E+08</td><td>1.1E+08</td><td>56%</td></tr>
<tr><td></td><td>0.191</td><td>0.104</td><td>31</td><td>31</td><td>5.92</td><td>3.22</td><td>2.2E+08</td><td>1.2E+08</td><td>46%</td></tr>
<tr><td></td><td>0.196</td><td>0.143</td><td>31</td><td>31</td><td>6.08</td><td>4.43</td><td>2.2E+08</td><td>1.6E+08</td><td>27%</td></tr>
<tr><td>Average</td><td>0.204</td><td>0.115</td><td></td><td></td><td>6.324</td><td>3.565</td><td>2.3E+08</td><td>1.3E+08</td><td>43%</td></tr>
<tr><td>Standard Deviation</td><td>0.015</td><td>0.020</td><td></td><td></td><td>0.465</td><td>0.618</td><td>2.1E+07</td><td>2.8E+07</td><td>12%</td></tr>
<tr><td>Relative Standard Deviation</td><td>7%</td><td>17%</td><td></td><td></td><td>7%</td><td>17%</td><td>9%</td><td>21%</td><td>28%</td></tr>
<tr><td></td><td></td><td></td><td></td><td></td><td></td><td colspan="2" align="center">*Power (W)*</td><td></td><td>*Filtration Efficiency*</td></tr>
<tr><td>Average</td><td></td><td></td><td></td><td></td><td></td><td></td><td>7.2</td><td></td><td>41%</td></tr>
<tr><td>Standard Deviation</td><td></td><td></td><td></td><td></td><td></td><td></td><td>0.6</td><td></td><td>9%</td></tr>
</tbody>
</table>

DATA POINT 3

<table>
<thead>
<tr><th rowspan="2">Test 1</th><th colspan="2">ORIGINAL</th><th colspan="2">Dilution</th><th colspan="2">FINAL</th><th colspan="2">Cell Concentration (cells·mL^{-1})</th><th rowspan="2">Filtration Efficiency</th></tr>
<tr><th>Inlet O.D.</th><th>Diluted O.D.</th><th>Inlet</th><th>Diluted</th><th>Inlet</th><th>Diluted</th><th>Inlet</th><th>Diluted</th></tr>
</thead>
<tbody>
<tr><td></td><td>0.206</td><td>0.108</td><td>31</td><td>31</td><td>6.39</td><td>3.35</td><td>2.4E+08</td><td>1.2E+08</td><td>48%</td></tr>
<tr><td></td><td>0.226</td><td>0.121</td><td>31</td><td>31</td><td>7.01</td><td>3.75</td><td>2.6E+08</td><td>1.4E+08</td><td>46%</td></tr>
<tr><td></td><td>0.209</td><td>0.108</td><td>31</td><td>31</td><td>6.48</td><td>3.35</td><td>2.4E+08</td><td>1.2E+08</td><td>48%</td></tr>
<tr><td>Average</td><td>0.214</td><td>0.112</td><td></td><td></td><td>6.624</td><td>3.482</td><td>2.5E+08</td><td>1.3E+08</td><td>47%</td></tr>
<tr><td>Standard Deviation</td><td>0.009</td><td>0.006</td><td></td><td></td><td>0.273</td><td>0.190</td><td>1.2E+07</td><td>8.6E+06</td><td>1%</td></tr>
<tr><td>Relative Standard Deviation</td><td>4%</td><td>5%</td><td></td><td></td><td>4%</td><td>5%</td><td>5%</td><td>7%</td><td>2%</td></tr>
<tr><td></td><td></td><td></td><td></td><td></td><td></td><td colspan="2" align="center">*Power (W)*</td><td></td><td>*Filtration Efficiency*</td></tr>
<tr><td>Average</td><td></td><td></td><td></td><td></td><td></td><td></td><td>8.2</td><td></td><td>47%</td></tr>
<tr><td>Standard Deviation</td><td></td><td></td><td></td><td></td><td></td><td></td><td>0.7</td><td></td><td>1%</td></tr>
</tbody>
</table>

DATA POINT 4

<table>
<thead>
<tr><th rowspan="2">Test 1</th><th colspan="2">ORIGINAL</th><th colspan="2">Dilution</th><th colspan="2">FINAL</th><th colspan="2">Cell Concentration (cells·mL^{-1})</th><th rowspan="2">Filtration Efficiency</th></tr>
<tr><th>Inlet O.D.</th><th>Diluted O.D.</th><th>Inlet</th><th>Diluted</th><th>Inlet</th><th>Diluted</th><th>Inlet</th><th>Diluted</th></tr>
</thead>
<tbody>
<tr><td></td><td>0.228</td><td>0.129</td><td>31</td><td>31</td><td>7.07</td><td>4.00</td><td>2.6E+08</td><td>1.5E+08</td><td>43%</td></tr>
<tr><td></td><td>0.235</td><td>0.130</td><td>31</td><td>31</td><td>7.29</td><td>4.03</td><td>2.7E+08</td><td>1.5E+08</td><td>45%</td></tr>
<tr><td></td><td>0.209</td><td>0.108</td><td>31</td><td>31</td><td>6.48</td><td>3.35</td><td>2.4E+08</td><td>1.2E+08</td><td>48%</td></tr>
<tr><td>Average</td><td>0.224</td><td>0.122</td><td></td><td></td><td>6.944</td><td>3.792</td><td>2.6E+08</td><td>1.4E+08</td><td>45%</td></tr>
<tr><td>Standard Deviation</td><td>0.011</td><td>0.010</td><td></td><td></td><td>0.341</td><td>0.314</td><td>1.5E+07</td><td>1.4E+07</td><td>2%</td></tr>
<tr><td>Relative Standard Deviation</td><td>5%</td><td>8%</td><td></td><td></td><td>5%</td><td>8%</td><td>6%</td><td>10%</td><td>5%</td></tr>
<tr><td>Test 2</td><td colspan="2" align="center">ORIGINAL</td><td colspan="2" align="center">Dilution</td><td colspan="2" align="center">FINAL</td><td colspan="2" align="center">Cell Concentration (cells·mL^{-1})</td><td>Filtration Efficiency</td></tr>
<tr><td></td><td>Inlet O.D.</td><td>Diluted O.D.</td><td>Inlet</td><td>Diluted</td><td>Inlet</td><td>Diluted</td><td>Inlet</td><td>Diluted</td><td></td></tr>
<tr><td></td><td>0.206</td><td>0.111</td><td>31</td><td>31</td><td>6.39</td><td>3.44</td><td>2.4E+08</td><td>1.3E+08</td><td>46%</td></tr>
<tr><td></td><td>0.207</td><td>0.107</td><td>31</td><td>31</td><td>6.42</td><td>3.32</td><td>2.4E+08</td><td>1.2E+08</td><td>48%</td></tr>
<tr><td></td><td>0.183</td><td>0.127</td><td>31</td><td>31</td><td>5.67</td><td>3.94</td><td>2.1E+08</td><td>1.5E+08</td><td>31%</td></tr>
<tr><td>Average</td><td>0.199</td><td>0.115</td><td></td><td></td><td>6.159</td><td>3.565</td><td>2.3E+08</td><td>1.3E+08</td><td>42%</td></tr>
<tr><td>Standard Deviation</td><td>0.011</td><td>0.009</td><td></td><td></td><td>0.344</td><td>0.268</td><td>1.6E+07</td><td>1.2E+07</td><td>8%</td></tr>
</tbody>
</table>

DATA POINT 5

	ORIGINAL		Dilution		FINAL		Cell Concentration (cells·mL⁻¹)		
	Inlet O.D.	Diluted O.D.	Inlet	Diluted	Inlet	Diluted	Inlet	Diluted	Filtration Efficiency
Relative Standard Deviation	6%	8%			6%	8%	7%	9%	19%

	Power (W)	Filtration Efficiency
Average	15.0	44%
Standard Deviation	0.9	5%

DATA POINT 6

	ORIGINAL		Dilution		FINAL		Cell Concentration (cells·mL⁻¹)		
	Inlet O.D.	Diluted O.D.	Inlet	Diluted	Inlet	Diluted	Inlet	Diluted	Filtration Efficiency
Test 1	0.341	0.317	16	8	5.46	2.54	2.0E+08	9.4E+07	54%
	0.434	0.434	16	8	6.94	3.47	2.6E+08	1.3E+08	50%
	0.348	0.348	16	8	5.57	2.78	2.1E+08	1.0E+08	50%
Average	0.374	0.366			5.989	2.931	2.2E+08	1.1E+08	51%
Standard Deviation	0.042	0.049			0.677	0.396	3.1E+07	1.8E+07	2%
Relative Standard Deviation	11%	14%			11%	14%	14%	17%	3%

	Power (W)	Filtration Efficiency
Average	10.1	51%
Standard Deviation	1.5	2%

Performance Comparison

a) Vertical UES harvesting chamber without internal ATL

Test	ORIGINAL			Dilution			FINAL			Cell Concentration (cells·mL^{-1})			Filtration Efficiency	Concentration Factor
	Inlet O.D.	Concentrated O.D.	Diluted O.D.	Inlet	Concentrated	Diluted	Inlet	Concentrated	Diluted	Inlet	Concentrated	Diluted		
	0.365	0.496	0.495	16	32	8	5.84	15.87	3.96	2.2E+08	5.9E+08	1.5E+08	32%	2.7
	0.367	0.580	0.460	16	32	8	5.87	18.56	3.68	2.2E+08	6.9E+08	1.4E+08	37%	3.2
	0.321	0.521	0.505	16	32	8	5.14	16.67	4.04	1.9E+08	6.2E+08	1.5E+08	21%	3.2
Average	0.351	0.532	0.487				5.616	17.035	3.893	2.1E+08	6.3E+08	1.4E+08	30%	3.0
Standard Deviation	0.021	0.035	0.019				0.340	1.127	0.154	1.5E+07	5.1E+07	7.0E+06	7%	0.2
Relative Standard Deviation	6%	7%	4%				6%	7%	4%	7%	8%	5%	22%	0.1

b) U" shape UES harvesting with an ATL division

Test	ORIGINAL			Dilution			FINAL			Cell Concentration (cells·mL^{-1})			Filtration Efficiency	Concentration Factor
	Inlet O.D.	Concentrated O.D.	Diluted O.D.	Inlet	Concentrated	Diluted	Inlet	Concentrated	Diluted	Inlet	Concentrated	Diluted		
	0.360	0.698	0.386	16	32	8	5.76	22.34	3.09	2.1E+08	8.3E+08	1.1E+08	46%	3.9
	0.354	0.659	0.360	16	32	8	5.66	21.09	2.88	2.1E+08	7.8E+08	1.1E+08	49%	3.7
	0.367	0.607	0.485	16	32	8	5.87	19.42	3.88	2.2E+08	7.2E+08	1.4E+08	34%	3.3
Average	0.360	0.655	0.410				5.765	20.949	3.283	2.1E+08	7.8E+08	1.2E+08	43%	3.6
Standard Deviation	0.005	0.037	0.054				0.085	1.193	0.431	3.9E+06	5.4E+07	2.0E+07	7%	0.2
Relative Standard Deviation	1%	6%	13%				1%	6%	13%	2%	7%	16%	15%	0.1

c) Inclined UES without an intermediate ATL - Countercurrent feed

Test	ORIGINAL			Dilution			FINAL			Cell Concentration (cells·mL^{-1})			Filtration Efficiency	Concentration Factor
	Inlet O.D.	Concentrated O.D.	Diluted O.D.	Inlet	Concentrated	Diluted	Inlet	Concentrated	Diluted	Inlet	Concentrated	Diluted		
	0.338	0.277	0.381	16	31	8.5	5.41	8.59	3.24	2.0E+08	3.2E+08	1.2E+08	40%	1.6
	0.311	0.254	0.270	16	31	8.5	4.98	7.87	2.30	1.8E+08	2.9E+08	8.5E+07	54%	1.6
	0.325	0.451	0.309	16	31	8.5	5.20	13.98	2.63	1.9E+08	5.2E+08	9.7E+07	49%	2.7
Average	0.325	0.327	0.320				5.195	10.147	2.720	1.9E+08	3.8E+08	1.0E+08	48%	2.0
Standard Deviation	0.011	0.088	0.046				0.176	2.726	0.391	8.0E+06	1.2E+08	1.8E+07	6%	0.5
Relative Standard Deviation	3%	27%	14%				3%	27%	14%	4%	33%	18%	12%	0.3

c) Inclined UES without an intermediate ATL - Concurrent feed

Test	ORIGINAL			Dilution			FINAL			Cell Concentration (cells·mL^{-1})			Filtration Efficiency	Concentration Factor
	Inlet O.D.	Concentrated O.D.	Diluted O.D.	Inlet	Concentrated	Diluted	Inlet	Concentrated	Diluted	Inlet	Concentrated	Diluted		
	0.393	0.288	0.511	16	31	8.5	6.29	8.93	4.34	2.3E+08	3.3E+08	1.6E+08	31%	1.4
	0.382	0.201	0.581	16	31	8.5	6.11	6.23	4.94	2.3E+08	2.3E+08	1.8E+08	19%	1.0
	0.375	0.235	0.571	16	31	8.5	6.00	7.29	4.85	2.2E+08	2.7E+08	1.8E+08	19%	1.2
Average	0.383	0.241	0.554				6.133	7.481	4.712	2.3E+08	2.8E+08	1.7E+08	23%	1.2
Standard Deviation	0.007	0.036	0.031				0.119	1.110	0.263	5.4E+06	5.0E+07	1.2E+07	6%	0.2
Relative Standard Deviation	2%	15%	6%				2%	15%	6%	2%	18%	7%	24%	0.1

d) Inclined cell settler

Test	ORIGINAL			Dilution			FINAL			Cell Concentration (cells·mL^{-1})			Filtration Efficiency	Concentration Factor
	Inlet O.D.	Concentrated O.D.	Diluted O.D.	Inlet	Concentrated	Diluted	Inlet	Concentrated	Diluted	Inlet	Concentrated	Diluted		
	0.256	0.196	0.231	21	31	21	5.38	6.08	4.85	2.0E+08	2.2E+08	1.8E+08	10%	1.1
	0.253	0.195	0.228	21	31	21	5.31	6.05	4.79	2.0E+08	2.2E+08	1.8E+08	10%	1.1
	0.249	0.210	0.225	21	31	21	5.23	6.51	4.73	1.9E+08	2.4E+08	1.7E+08	10%	1.2
Average	0.253	0.096	0.228				5.306	2.976	4.788	2.0E+08	2.3E+08	1.8E+08	10%	1.2
Standard Deviation	0.003	0.000	0.002				0.060	0.000	0.051	2.7E+06	9.6E+06	2.3E+06	0%	0.1
Relative Standard Deviation	1%	0%	1%				1%	0%	1%	1%	4%	1%	1%	0.1

d) UEIS - our design

Test	ORIGINAL Inlet O.D.	ORIGINAL Concentrated O.D.	ORIGINAL Diluted O.D.	Dilution Inlet	Dilution Concentrated	Dilution Diluted	FINAL Inlet	FINAL Concentrated	FINAL Diluted	Cell Conc. Inlet	Cell Conc. Concentrated	Cell Conc. Diluted	Filtration Efficiency	Concentration Factor
	0.240	0.440	0.117	21	183	11	5.04	80.52	1.29	1.9E+08	3.0E+09	4.8E+07	74%	16.0
	0.243	0.169	0.104	21	183	11	5.10	30.93	1.14	1.9E+08	1.1E+09	4.2E+07	78%	6.1
	0.241	0.204	0.123	21	183	11	5.06	37.33	1.35	1.9E+08	1.4E+09	5.0E+07	73%	7.4
Average	0.241	0.271	0.115				5.068	49.593	1.261	1.9E+08	1.8E+09	4.7E+07	75%	9.8
Standard Deviation	0.001	0.120	0.008				0.026	22.024	0.087	1.2E+06	1.0E+09	4.0E+06	2%	4.4
Relative Standard Deviation	1%	44%	7%				1%	44%	7%	1%	54%	8%	2%	0.4

Test	ORIGINAL Inlet O.D.	ORIGINAL Concentrated O.D.	ORIGINAL Diluted O.D.	Dilution Inlet	Dilution Concentrated	Dilution Diluted	FINAL Inlet	FINAL Concentrated	FINAL Diluted	Cell Conc. Inlet	Cell Conc. Concentrated	Cell Conc. Diluted	Filtration Efficiency	Concentration Factor
	0.200	0.440	0.183	21	183	11	4.20	80.52	2.01	1.6E+08	3.0E+09	7.4E+07	52%	19.2
	0.243	0.169	0.104	21	183	11	5.10	30.93	1.14	1.9E+08	1.1E+09	4.2E+07	78%	6.1
	0.241	0.204	0.123	21	183	11	5.06	37.33	1.35	1.9E+08	1.4E+09	5.0E+07	73%	7.4
Average	0.228	0.271	0.137				4.788	49.593	1.503	1.8E+08	1.8E+09	5.6E+07	68%	10.9
Standard Deviation	0.020	0.120	0.034				0.416	22.024	0.370	1.9E+07	1.0E+09	1.7E+07	11%	5.9
Relative Standard Deviation	9%	44%	25%				9%	44%	25%	11%	54%	30%	16%	0.5

Test	ORIGINAL Inlet O.D.	ORIGINAL Concentrated O.D.	ORIGINAL Diluted O.D.	Dilution Inlet	Dilution Concentrated	Dilution Diluted	FINAL Inlet	FINAL Concentrated	FINAL Diluted	Cell Conc. Inlet	Cell Conc. Concentrated	Cell Conc. Diluted	Filtration Efficiency	Concentration Factor
	0.175	0.440	0.149	21	183	11	3.68	80.52	1.64	1.4E+08	3.0E+09	6.1E+07	55%	21.9
	0.166	0.169	0.098	21	183	11	3.49	30.93	1.08	1.3E+08	1.1E+09	4.0E+07	69%	8.9
	0.156	0.204	0.074	21	183	11	3.28	37.33	0.81	1.2E+08	1.4E+09	3.0E+07	75%	11.4
Average	0.166	0.271	0.107				3.479	49.593	1.177	1.3E+08	1.8E+09	4.4E+07	67%	14.1
Standard Deviation	0.008	0.120	0.031				0.163	22.024	0.344	7.4E+06	1.0E+09	1.6E+07	8%	5.6
Relative Standard Deviation	5%	44%	29%				5%	44%	29%	6%	54%	36%	12%	0.4
Average													70%	11.6
Standard Deviation													5%	2.2
Relative Standard Deviation													10%	0.5

APPENDIX II

Drawings of Different Devices

Manufacturing Drawings

Chamber Drawing

Chamber Manufacturing Drawing

Top Endcap Drawing

2 X Ø7/16 - 1/4" MPT
Ø.20 - thru all
4 X Ø1/8 thru all
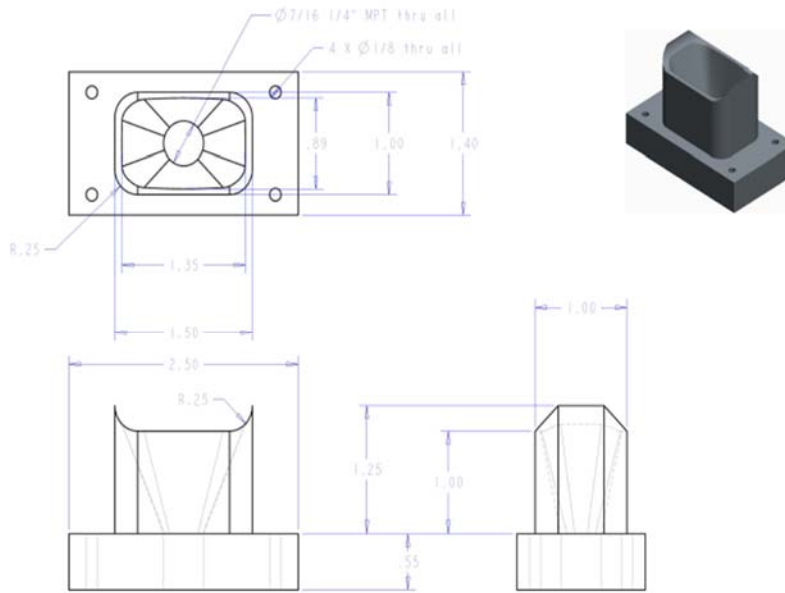.24
1.00
1.40
.6678
.973T
1.26
1.50
2.50
R.30
R.25
.95
.70
.50
.55
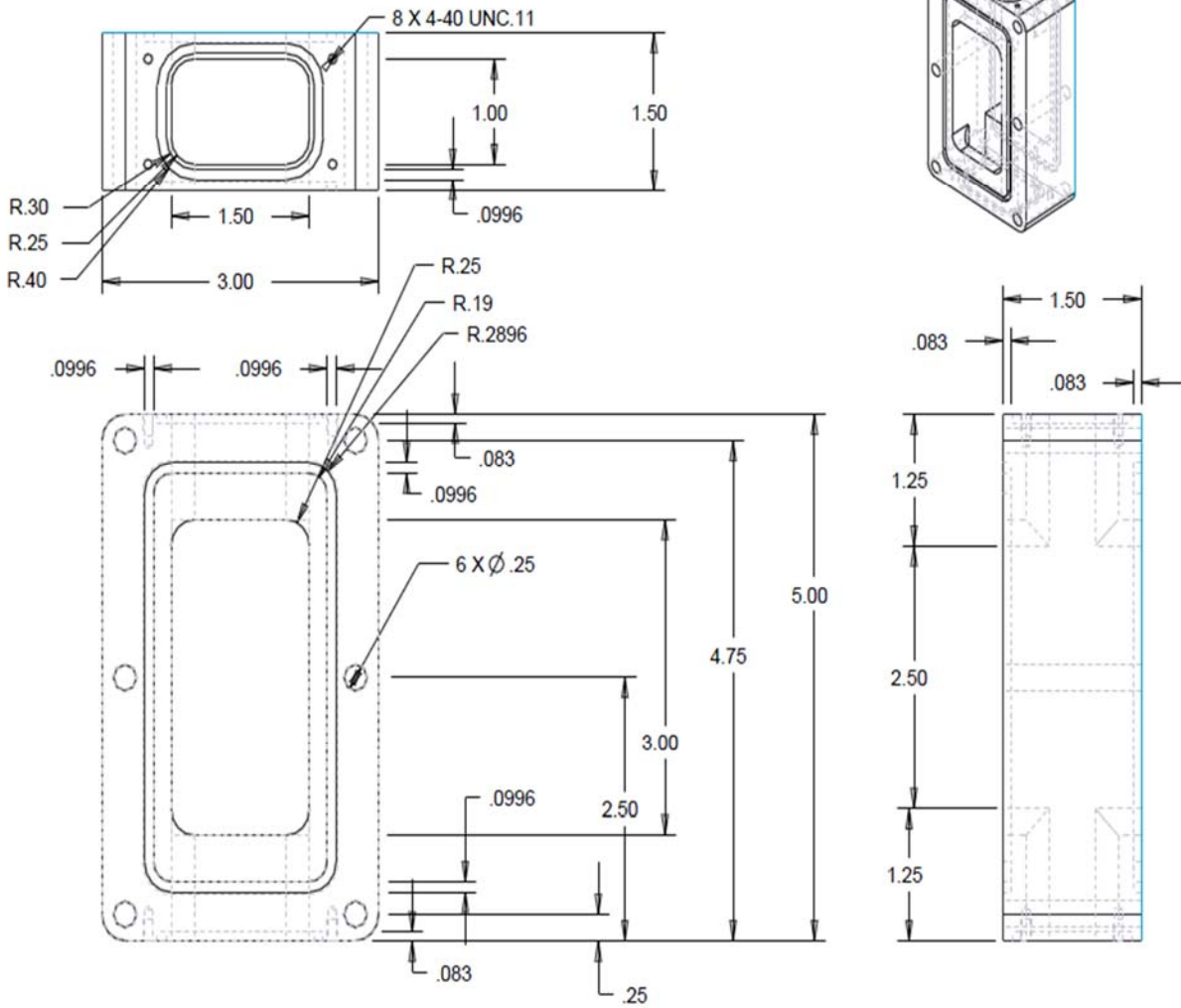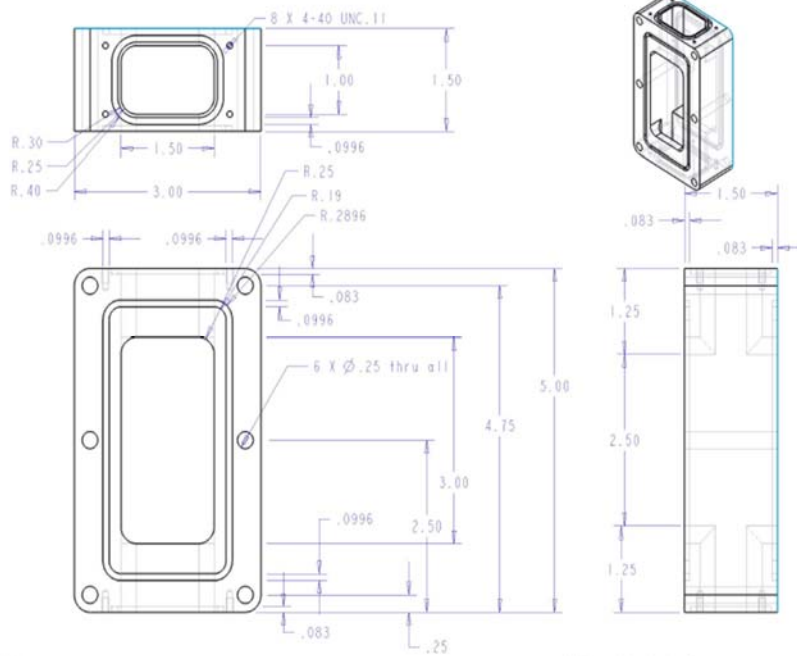
Double Hole End Cap
Scale: 1.0
CSU Mechanical Engineering - Senior Design - Solix

All units in inches
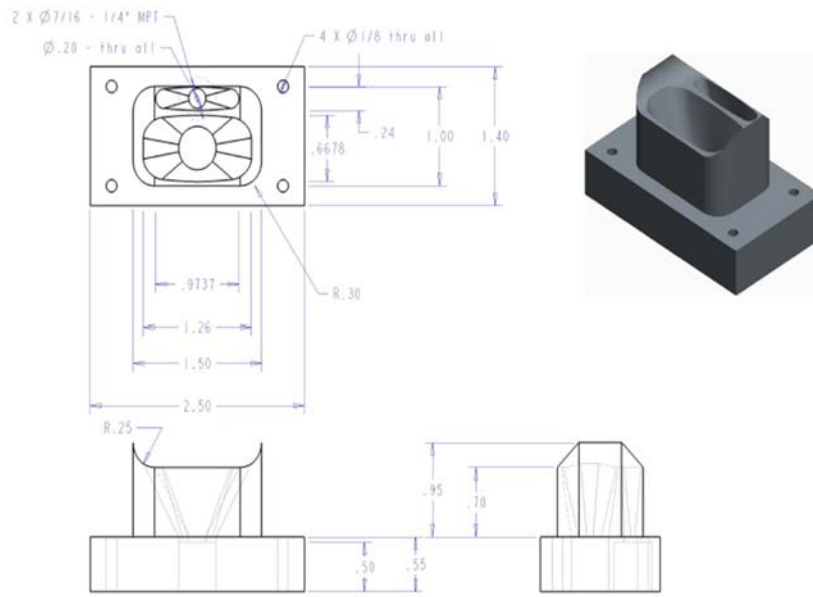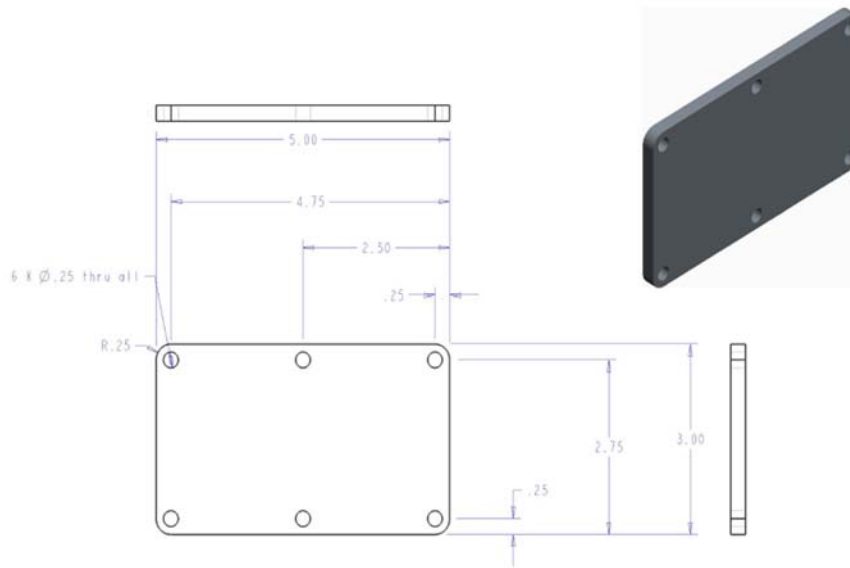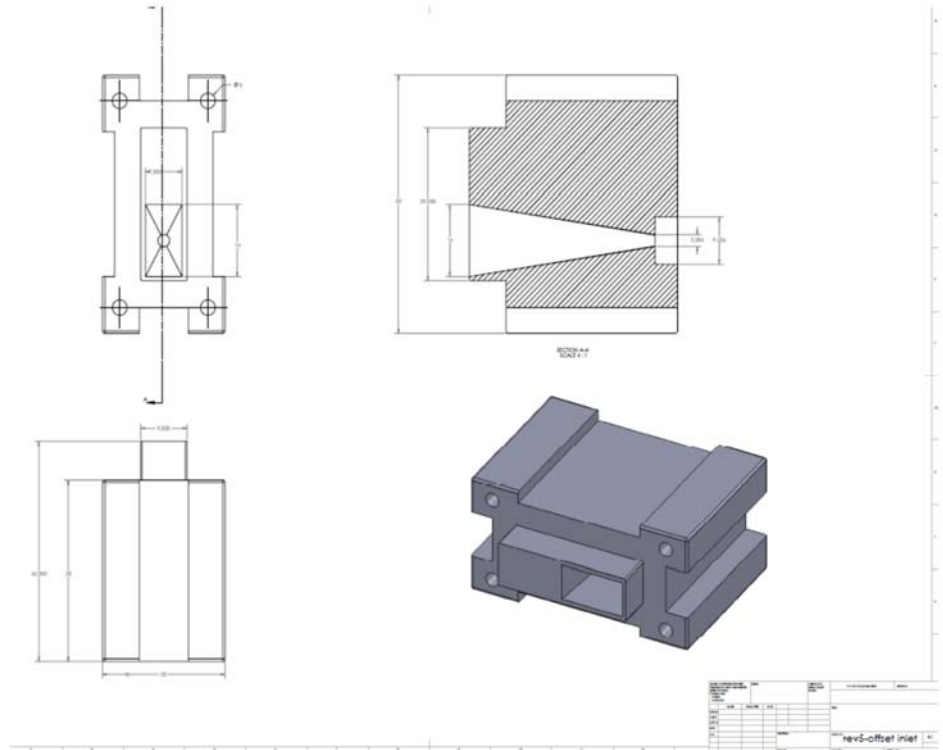All tolerances +0.005/-0.0 unless otherwise noted
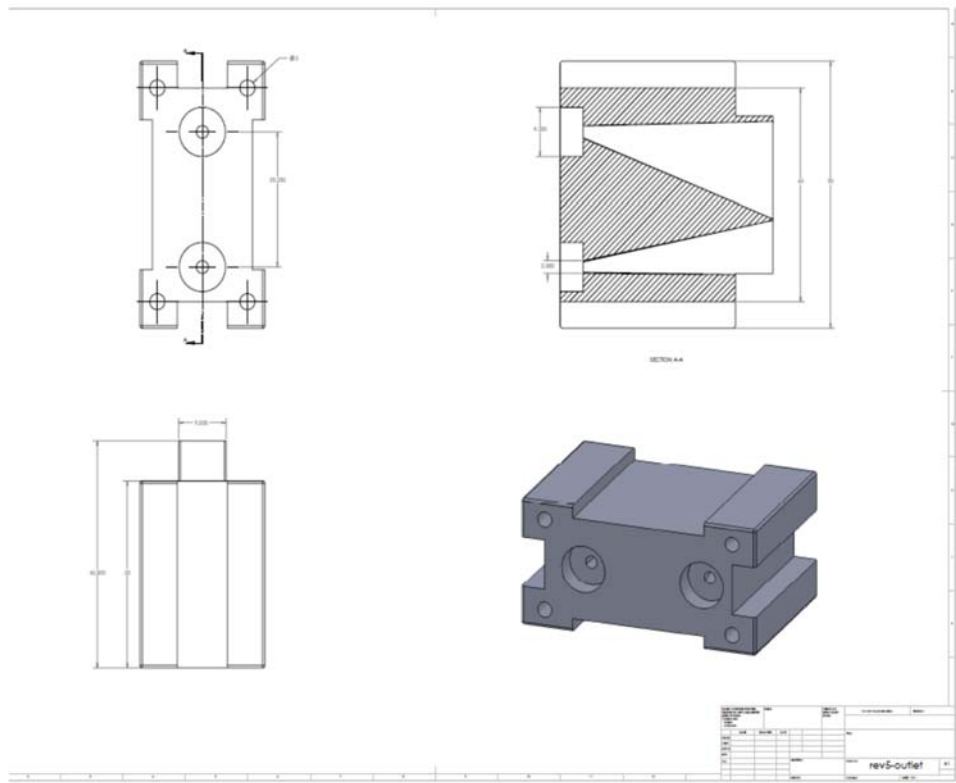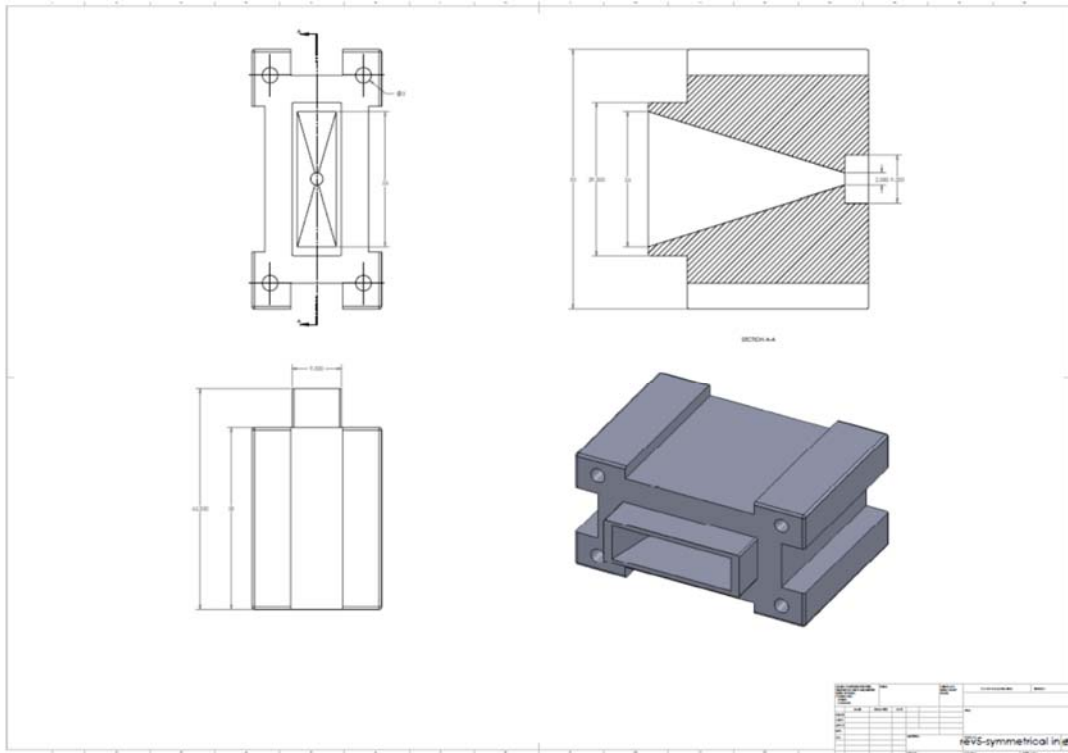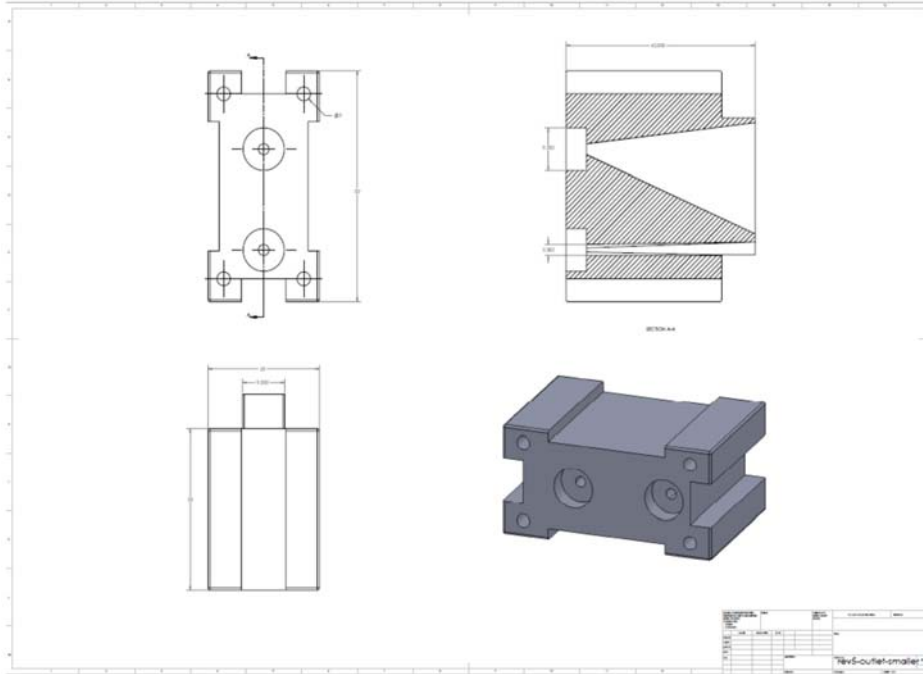Material: 6061 Aluminum

Bottom Endcap Drawing

5.00
4.75
2.50
.25
6 X Ø.25 thru all
R.25
2.75
3.00
.25

End Plate
Scale: 0.5
CSU Mechanical Engineering - Senior Design - Solix

All units in inches
All tolerances +0.005/-0.0 unless otherwise note
Material: 6061 Aluminum

Endplate Drawing
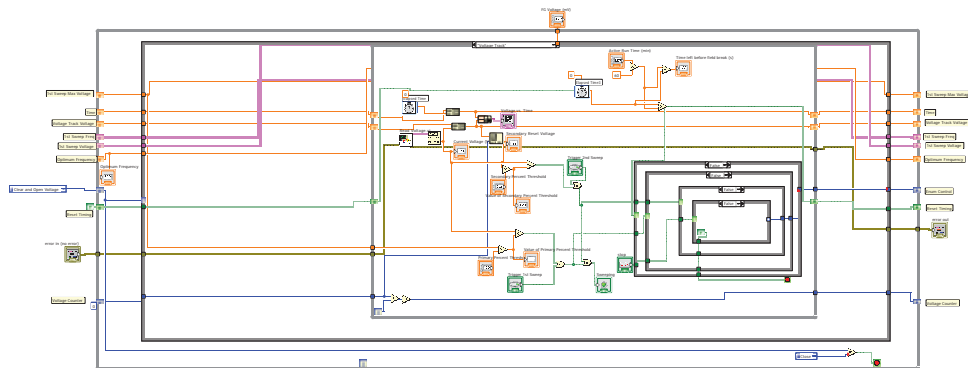
Horizontal h-Device end cap

Horizontal h-Device

"rev5-outlet-smaller"

"rev5-symmetrical inlet"
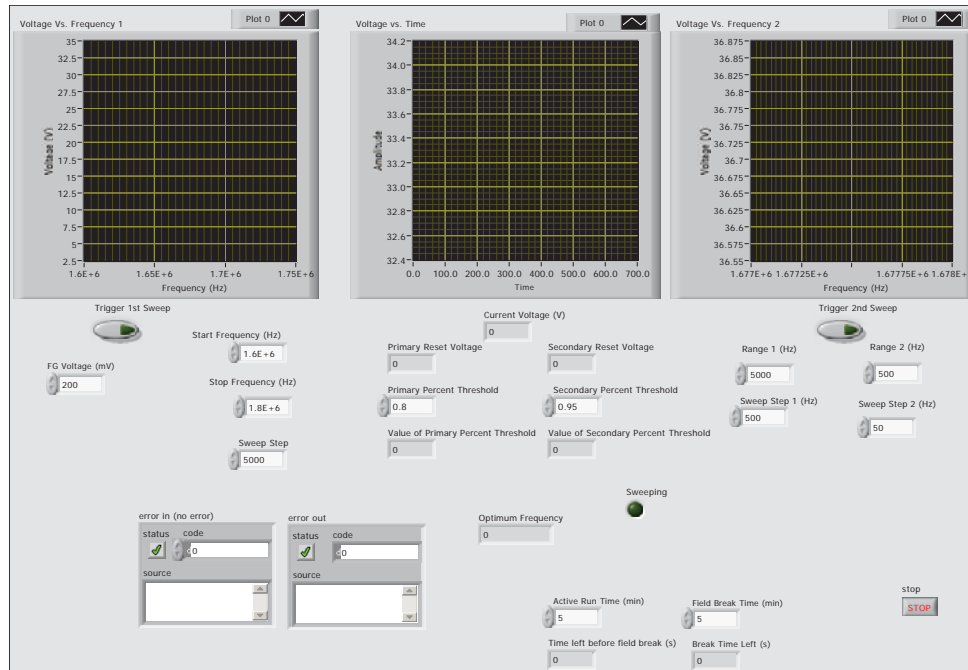
APPENDIX III

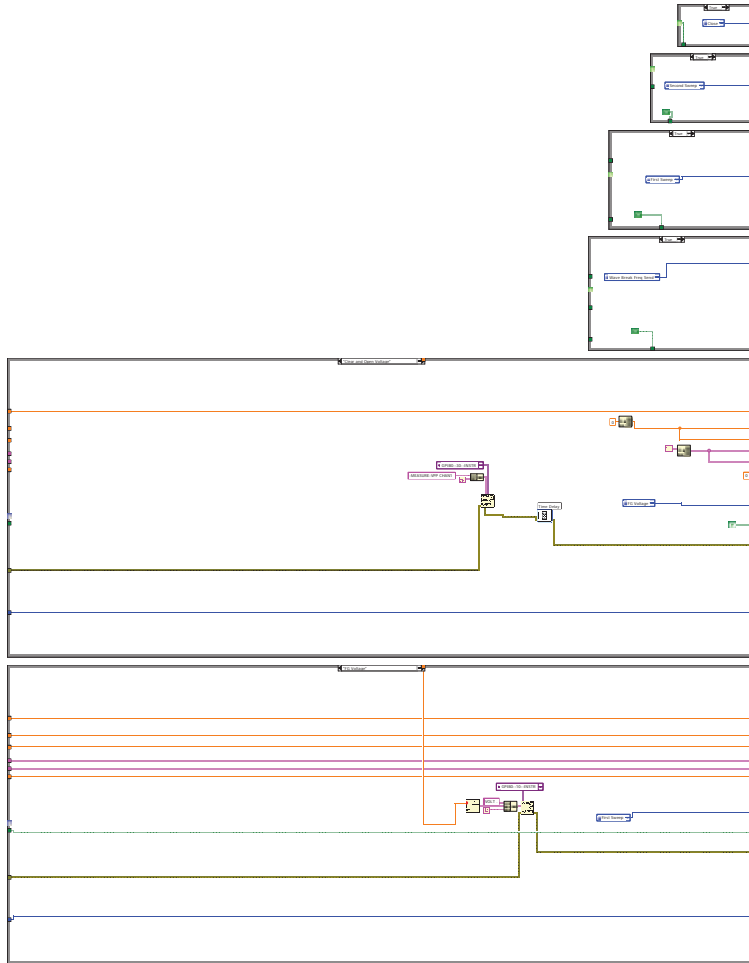**Frequency Tracking Algorithm Code**

State Machine with wave break.vi
U:\LabView\LabView\State Machine with wave break.vi
Last modified on 11/13/2012 at 8:36 PM
Printed on 10/12/2014 at 5:09 PM

Page 1

State Machine with wave break.vi

| Voltage Vs. Frequency 1 | Plot 0 | | Voltage vs. Time | Plot 0 | | Voltage Vs. Frequency 2 | Plot 0 |

Trigger 1st Sweep

Start Frequency (Hz)
1.6E+6

FG Voltage (mV)
200

Stop Frequency (Hz)
1.8E+6

Sweep Step
5000

Current Voltage (V)
0

Primary Reset Voltage
0

Secondary Reset Voltage
0

Primary Percent Threshold
0.8

Secondary Percent Threshold
0.95

Value of Primary Percent Threshold
0

Value of Secondary Percent Threshold
0

Trigger 2nd Sweep

Range 1 (Hz)
5000

Range 2 (Hz)
500

Sweep Step 1 (Hz)
500

Sweep Step 2 (Hz)
50

Sweeping

error in (no error)
status code
0
source

error out
status code
0
source

Optimum Frequency
0

Active Run Time (min)
5

Field Break Time (min)
5

stop
STOP

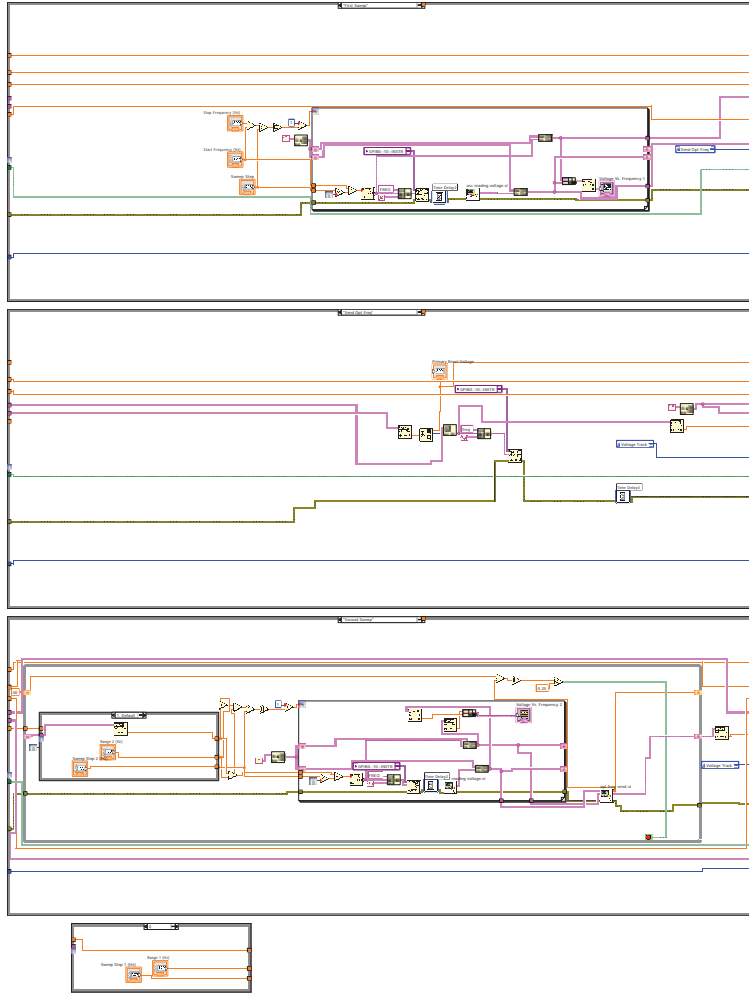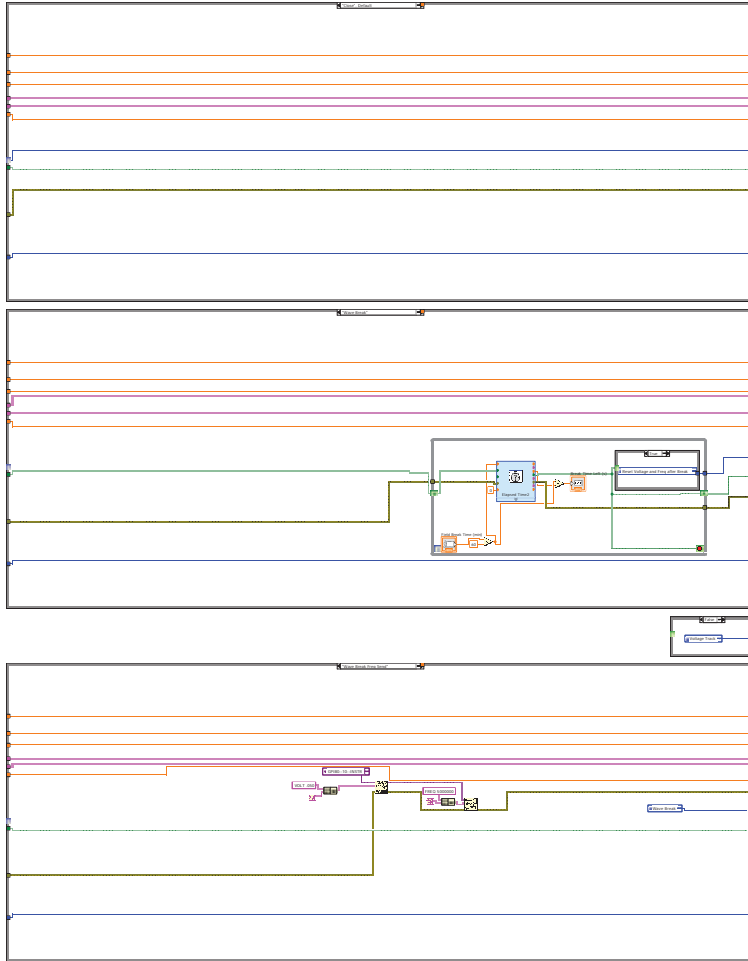Time left before field break (s)
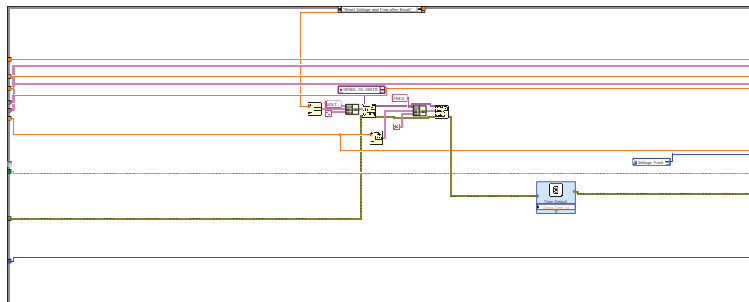0

Break Time Left (s)
0

150

State Machine with wave break.vi
U:\LabView\LabView\State Machine with wave break.vi
Last modified on 11/13/2012 at 8:36 PM
Printed on 10/12/2014 at 5:09 PM

State Machine with wave break.vi
U:\LabView\LabView\State Machine with wave break.vi
Last modified on 11/13/2012 at 8:36 PM
Printed on 10/12/2014 at 5:09 PM

State Machine with wave break.vi
U:\LabView\LabView\State Machine with wave break.vi
Last modified on 11/13/2012 at 8:36 PM
Printed on 10/12/2014 at 5:09 PM

State Machine with wave break.vi
U:\LabView\LabView\State Machine with wave break.vi
Last modified on 11/13/2012 at 8:36 PM
Printed on 10/12/2014 at 5:09 PM

Time Delay5
Time Delay
Inserts a time delay into the calling VI.

This Express VI is configured as follows:

Delay Time: 1 s

Elapsed Time3
Elapsed Time
Indicates the amount of time that has elapsed since the specified start time.

This Express VI is configured as follows:

Time Target: 1 s
Auto Reset: Off

Elapsed Time2
Elapsed Time
Indicates the amount of time that has elapsed since the specified start time.

Time Delay4
Time Delay
Inserts a time delay into the calling VI.

This Express VI is configured as follows:

Delay Time: 0.25 s

State Machine with wave break.vi
U:\LabView\LabView\State Machine with wave break.vi
Last modified on 11/13/2012 at 8:36 PM
Printed on 10/12/2014 at 5:09 PM

Time Delay3
Time Delay
Inserts a time delay into the calling VI.

This Express VI is configured as follows:

Delay Time: 0.15 s

Elapsed Time
Elapsed Time
Indicates the amount of time that has elapsed since the specified start time.

This Express VI is configured as follows:

Time Target: 1 s
Auto Reset: Off

Time Delay2
Time Delay
Inserts a time delay into the calling VI.

This Express VI is configured as follows:

Delay Time: 0.15 s

Time Delay
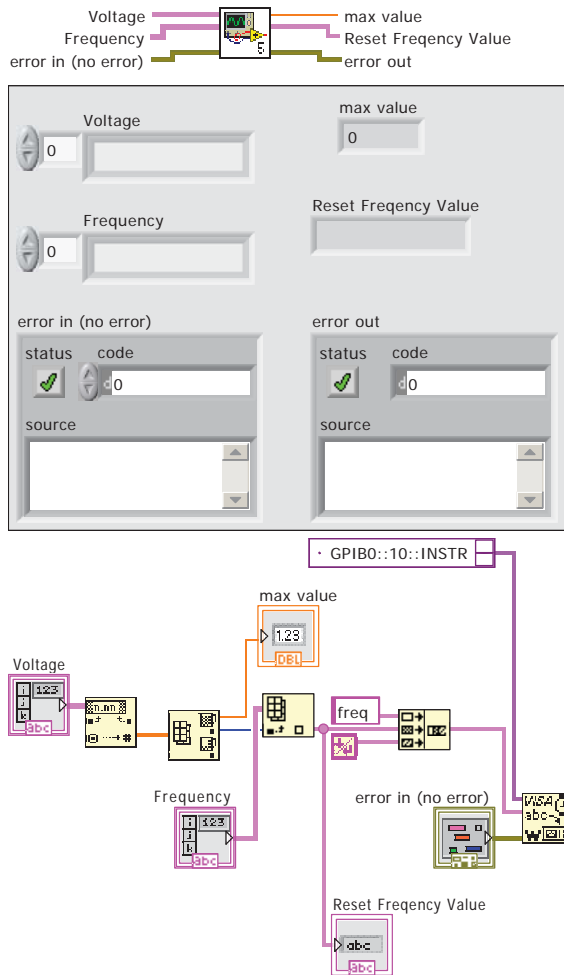Time Delay
Inserts a time delay into the calling VI.

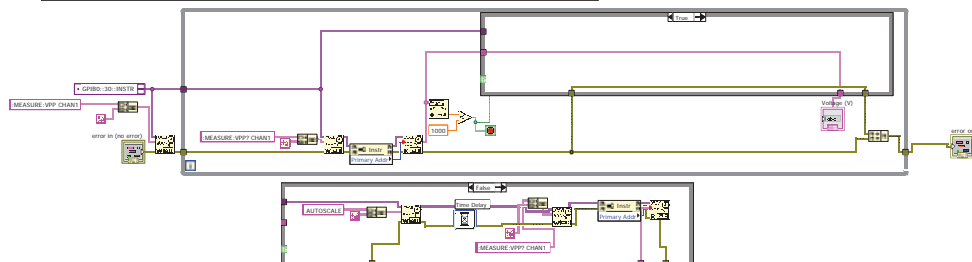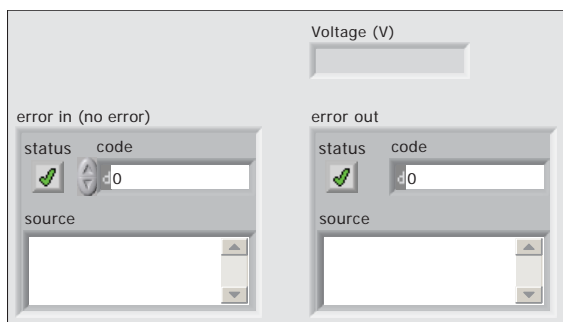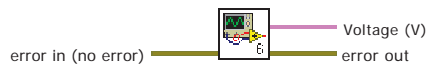This Express VI is configured as follows:

Delay Time: 1 s

155

opt freq send.vi
U:\LabView\LabView\opt freq send.vi
Last modified on 11/13/2012 at 8:36 PM
Printed on 10/12/2014 at 5:12 PM

opt freq send.vi

156

osc reading voltage.vi
U:\LabView\LabView\osc reading voltage.vi
Last modified on 11/13/2012 at 8:36 PM
Printed on 10/12/2014 at 5:11 PM

osc reading voltage.vi

Voltage (V)

error in (no error)   error out

Voltage (V)

error in (no error)   error out

status   code   status   code
            d 0   d 0

source   source

Time Delay
Time Delay
Inserts a time delay into the calling VI.

This Express VI is configured as follows:

Delay Time: 5 s

157

Read Voltage.vi
U:\LabView\LabView\Read Voltage.vi
Last modified on 11/13/2012 at 8:36 PM
Printed on 10/12/2014 at 5:10 PM

Read Voltage.vi

Current Voltage

error in (no error) ———— error out

error in (no error)	error out
status code	status code
✔ 0	✔ 0
source	source
	Current Voltage

· GPIB0::30::INSTR

:MEASURE:VPP? CHAN1

Primary Addr

Current Voltage

error in (no error)

error out

158